Spring 5-5-2023

The Influence of Heat and Mass Transfer on the Setting Rate of Adhesives Between Porous Substrates

Mubarak Mohammed Khlewee

THE INFLUENCE OF HEAT AND MASS TRANSFER ON THE SETTING RATE OF ADHESIVES BETWEEN POROUS SUBSTRATES

By

Mubarak Mohammed Khlewee

B.S. Southern Technical University, 2011

M.S. University of Maine, 2017

A DISSERTATION

Submitted in Partial Fulfillment of the

Requirement for the Degree of

Doctor of Philosophy

(in Chemical Engineering)

The Graduate School

The University of Maine

May 2023

Advisory Committee:

Dr. Douglas W. Bousfield, Professor of Chemical & Biomedical Engineering, Co-Advisor

Dr. William J. DeSisto, Professor of Chemical & Biomedical Engineering, Co-Advisor

Dr. Albert Co, Associate Professor of Chemical & Biomedical Engineering

Dr. Mehdi Tajvidi, Associate Professor of Renewable Nanomaterials

Dr. John Roper, Consultant

THE INFLUENCE OF HEAT AND MASS TRANSFER ON THE SETTING RATE OF ADHESIVES BETWEEN POROUS SUBSTRATES

By Mubarak Mohammed Khlewee

Dissertation Co-Advisors: Dr. Douglas W. Bousfield and Dr. William J. DeSisto

An Abstract of the Dissertation Presented
in Partial Fulfillment of the Requirements for the
Degree of Doctor of Philosophy
(in Chemical Engineering)
May 2023

The dynamic penetration of fluid into a porous media where other changes are occurring such as temperature or concentration is of interest to a number of situations. However, little experimental and theoretical analysis of this situation is found in the literature where most of the previously published works have studied the penetration with constant physical properties, where there is no change of the fluid as it enters the pores. This situation is important in the setting of adhesives in porous medium such as in the setting of hot melt and water-based adhesives in the production of paper based packaging. The controlled penetration of the adhesive is important to obtain rapid setting rates and good bond strength. However, the degree of penetration depth of adhesives into systems like paper was limited to cross-sectional images and no quantitative method is well established in the literature. The analysis of these images is difficult especially if there is an interaction between the adhesive and the pores inside the porous mediums. In addition, little has been published on the rate of adhesive setting and final bond strength as a function of fundamental parameters such as pore size distribution, adhesive properties, and process parameters such as pressure and temperature.

Experiments were designed to understand the extent of penetration of hot melt and water-based adhesives into several porous coated and uncoated papers. Methods to characterize penetration depth were developed and compared: one method, based on silicone oil absorption, was found to be accurate and convenient. Tests were performed to determine the penetration depth as a function of the characteristics of the paper such as the pore size distribution, porosity, permeability, and other parameters such as paper temperature, adhesive temperature or concentration, contact pressure and time. Paper surfaces were modified by a range of coatings that have different porosities and pore sizes, and contact angles; these surfaces were characterized with a range of techniques.

The results of the setting of hot melt adhesive show that more penetration when the paper is hot and less penetration when the latex level increases in the coating layer due to the reduced permeability. For the range of pigments used in this study, the influence of the pigment size particle on the penetration depth was minor. Mechanical testing confirmed that more penetration leads to stronger bond strength. The water-based adhesive on the other hand, at various solids contents, was applied to the paper surfaces in a press as well varying press pressures and times. Similar to the setting of the hot melt adhesive, the results showed more penetration when the paper is uncoated and less penetration when the latex level increased in the coating layer. The significant finding here is that the different press pressures and times and solids contents of adhesive did not significantly change the degree of penetration depth for the same type of paper used. Various other tests indicate that this result is due to the adhesive that is able to clog pores and stop flowing. This clogging mechanism can be related to the dewatering of the adhesive inside the pore space in which the adhesive increases in viscosity as water leaves into the paper fibers. This finding was supported by the mechanical Instron testing that showed similar loads for the samples that have the same

penetration depths except for the sample that has a higher latex level which is due to the strong coating layer that needs higher force to peel. Reducing the adhesive amount and changing the paper type were other examples that confirmed these two mechanisms. The green bond strength was also obtained for all samples using the roll press test. The green bond strength was low compared to the final bond strength of the same sample.

Various models were developed to predict the penetration of the adhesive as a function of the fundamental parameters. A model based on the unsteady-state flow of a polymer into a pore that includes dynamic heat or mass transfer is developed using a finite element method-based model (COMSOL Multiphysics 5.5) and compared to a modified Lucas-Washburn equation where the viscosity was a function of temperature (hot melt adhesive) or concentration (water-based adhesive). In addition, a model was developed based on Darcy's law to describe the penetration accounting for changes in fluid properties and account for different layers of pore space and the limited supply of adhesive. These models consider the change of viscosity of the fluid as it enters the pore structure. These models were compared to the experimental results and some simple experiments. Good agreement within a reasonable range for different papers, pressing times and pressures, paper temperatures, and adhesive solids contents is obtained. For the dynamic heat transfer model, a new dimensionless group called D* is proposed that can help predict if cooling in the pore is important or not: if $D^* > 1000$, cooling is not expected to occur and large penetration happens. For the dynamic mass transfer model on the other hand, another dimensionless group called Z* is proposed to determine if solvent diffusion is important or not. When this group is large, over 5×10^6, diffusion is minimal and large penetration happens.

The net outcome of this research is to provide a better understanding of the dynamic behavior during the process of penetration of adhesives into various porous surfaces as well as in

specifying the key parameters that mostly affect the rate of setting, the depth of penetration, and the strength of green and final bond in a flow that involves temperature and concentration changes. To our knowledge, this is the first attempt at trying to predict the dynamic penetration of an adhesive into a porous structure in this manner where it will advance the knowledge and help the industry overcome this type of problem. In addition, this should be the first time where the model is compared directly to experiments where most of the parameters are well-known.

ACKNOWLEDGEMENTS

First and foremost, I would like to offer my greatest thanks to my advisors Dr. Douglas W. Bousfield and Dr. William J. DeSisto for their constant support, invaluable encouragement, excellent guidance, and patience throughout the journey of my study. This work would not exist without their guidance and belief in me. I would also like to express my deepest gratitude to my graduate committee namely Dr. Albert Co, Dr. Mehdi Tajvidi, and Dr. John Roper for their time and valuable contributions to this research.

I wish to thank the entire staff of the Process Development Center for their training and help with various instruments, answering questions, and willingness to provide help. Additionally, I am very grateful to Dr. Emma Perry for her support and assistance with the microscopy analysis. Many thanks go to Dr. Tajvidi's lab for allowing me to use their instruments and facilitate running some experiments. Furthermore, I offer thanks to Angel Hildreth and Cathy Dunn for help putting up and processing orders and needs for the lab during the whole years of my study.

I would also like to express my sincere appreciation to the industrial sponsors of the Paper Surface Science Program at the University of Maine for all of their support, contributions, and discussions given in our meetings held each semester. I acknowledge the Ministry of Oil and Dhi Qar Oil Company in Iraq for their acceptance to come and complete my Ph.D. degree at UMaine. Many thanks go to them.

Lastly, this dissertation would not have been possible without the help and love of my parents who have given me endless courage, unwavering support, and unconditional love. I greatly thank my mother who has given her most wonderful years to take care of me. Most of all, I will be forever grateful for the support and encouragement provided by my lovely wife throughout the journey of my academic career. Her encouragement and indispensable love made possible what I am now. I

would also like to thank my brothers and sisters for their support, love, and care for my life. To my little ones (starting from the oldest), (Mohammed, Ridha, and Zainalabideen), you always bring calm and positive energy to my life. Your smiley faces are making every day full of happiness and joy.

TABLE OF CONTENTS

LIST OF TABLES

LIST OF FIGURES

CHAPTER 1: INTRODUCTION

1.1 Motivation

The flow of a liquid in a porous media is important in many industrial processes. When flow is influenced by concentration and temperature changes, the viscosity of the liquid in the pore may change. However, little experimental and theoretical analysis of this situation is found in the literature. For example, in the gluing of wood, adhesive penetrates the pores of the wood and changes composition, as water is removed, but analysis of this situation is limited (Mendoza et al. 2012). The changes exhibit in fluid composition as it penetrates the porous medium (i.e. paper) control the setting rate and process performance where both heat and mass transfer play a major role (Songok et al. 2016; Ribeiro et al. 2007; Baggio et al. 1997; Ding et al. 2017).

Incorporating temperature and concentration changes during the unsteady-state penetration of liquid adhesives into a porous media is a new study that should contribute to providing new and unique details where there is an obvious lack of articles in both modeling and setting of adhesives that have discussed these types of problems. Solving and understanding the dynamic behavior of the penetration of adhesives has not been covered yet to the extent that can be understood well, especially when having parameters dependent on each other such as the temperature and concentration dependency of viscosity. These dynamic details likely play a major role in the setting of adhesives.

In the setting of liquid adhesives in wood and paper systems, the degree of penetration of the adhesive into a porous media is known to contribute to the setting rate and the strength of the final bond. The impact of different parameters on the green and final bond strength is not well understood. For example, for a hot melt glue, the cooling of the glue as it penetrates the porous

media likely changes the viscosity of the glue and how deep the glue penetrates the substrate. The analysis of this dynamic situation is lacking in the literature.

The experimental methods in most of the previously published literature were focused on "fiber tear" after a bond is formed. The fiber tear method does not explain the reasons behind a strong or a weak bond where it does not provide details about the dynamic data. Fiber tear is a quick and easy test that is an indicator of the final adhesion strength. The limitation of tests that measure the peeling force after a glue-setting event is another motivating goal that pushes towards developing a new type of test that should be useful in predicting good dynamic data and be achievable in future investigations.

To the author's best knowledge, none of the previously published articles have described modeling of the adhesive penetration to quantify the setting event. While much is reported on the penetration of coatings and ink into paper, adhesives are unique in that a temperature or concentration change may occur during penetration.

Finally, this dissertation should provide a valuable technique for solving problems that require temperature and concentration changes during the process of adhesive penetration. The prediction of penetration should help clarify the important process and material parameters. Moreover, developing new experimental methods will help improve our understanding of the penetration of adhesives and the dynamics of the event. Additionally, the finite element method-based model (COMSOL Multiphysics 5.5) will bring more knowledge and understanding to this area since to the author best's knowledge it is going to be the first-time investment of this software in the setting of adhesives.

1.2 Literature Review

1.2.1 Introduction

Adhesion problems are hard to predict and understand. Adhesives are typically considered highly viscous liquids that change physically or chemically during a setting step. Obtaining strongly bonded joints using hot melt glue or water-based glue systems depends on the type of adhesive, type of porous media, and conditions at which gluing processes carry out. Adhesives as chemical products differ in their setting processes. Thermosetting adhesives require cooling to set allowing the polymer to cool between two surfaces. Water-based adhesives are rereferred to as cold-setting adhesives and are set by the removal or drying of water from the joint (Ninness et al. 2011). An example of thermosetting adhesives is ethylene-vinyl acetate (McBride 1994), while polyvinyl acetate (Ventresca et al. 2019) is an example of cold-setting adhesives. Many different types of adhesives are known worldwide and have been used frequently in joining two surfaces together such as polyurethane, epoxies, etc. Starch has been used as an adhesive in wood-based panels and packaging such as corrugated paperboard (Daub et al. 1990; Wang et al. 2011; Zhang et al. 2015). Metals have also been bonded using adhesives to form joints of aluminum, steel, carbon fiber, etc.

The main focus in most of the previously published literature was to obtain a strong bond strength between bonded surfaces, so different techniques and materials have been explored to overcome adhesion failures. The formulations of hot melt and water-based adhesives, and substrates joints, combined with the pressing pressure, temperature, and time were different from one process to another and are based on the materials used and the operating conditions applied.

1.2.2 Hot Melt Adhesives

Hot melt glues are a common type of system that requires heat to set. A wide range of polymers has been used for hot melt adhesives such as Ethylene-Vinyl Acetate (EVA) Copolymer, Alkyl Acrylate Ethylene Copolymer, Ethylene Butyl Acrylate (EBBA), Polyamide Polymers as well as Amorphous Poly Alpha Olefins (McBride 1994; Komornicki et al. 1991; Simons 1996; Ahmed 2001).

Temperature plays a major role during setting events in which adhesive mechanical properties can be changed as temperature changes, and as a sequence, failure modes will be changed too (Na et al. 2018). The time needed to cool the polymer from the application temperature to some value below the glass transition temperature determines the setting time. Green bond strength is important to hold the product in place when production time is short. The final bond strength is also the key measure of the performance of the adhesive.

The disadvantages of hot melt glues are the high temperature involved; these temperatures require special equipment and materials. However, high temperatures help in decreasing the adhesive viscosity due to the viscosity dependency of temperature allowing good penetration. The decrease in the adhesive viscosity results in an increase in the degree of penetration into the porous media.

1.2.3 Water-Based Adhesives

Aqueous glues are widely used alternatives to hot melt glues because of their costs and ease of use. (Houtman et al. 2007) have used water-based acrylic pressure-sensitive adhesives PSAs. (Forsyth 2004) has listed waterborne adhesives that have been used for labeling as follows: dextrines, starch based-jelly gums, ice-proof caseins, non-caseins, polyvinyl alcohols, and

formulated vinyl acetate ethylene copolymers (Vale's), PVAc's and acrylics. (Bashford 1993) has listed all possible water-based adhesives that are used for bottle labels, snack food, confectionery packaging, coffee laminations, diaper bag laminates, meat and cheese structures, condiments and liquid packaging, and graphic art laminations.

The chemistries of the aqueous glues have been described in some past articles. For example, in (Houtman et al. 2007), a list of monomers used to synthesize water-based adhesives was presented as follows: soft monomers (n-butyl acrylate), functional monomers (acrylic acid), medium monomers (ethyl acrylate), and hard monomers (vinyl acetate). While in (Bashford 1993), the chemical types of adhesives were as follows: one and two component styrene butadiene rubber, one and two component acrylic, one and two component polyether urethane, and two component polyester urethane.

The aqueous glues set due to the loss of water, depositing the polymer in the joint. The rate of setting links to the drying rate, but water can also leave by absorption into the wood or paper fibers. When latex is used, as water leaves, the polymer forms a continuous film in the joint. While this is a common process and system, little theoretical work has been reported in the open literature on the parameters that control the setting rate and the final bond strength.

1.2.4 Surface Tension and Contact Angle Measurements

There have been many different approaches used to determine the surface free energy and its components using contact angle measurement approaches. The measurements were based on a capillary rise based on the Washburn equation, dynamic contact angle measurements according to the Wilhelmy-plate principle, and sessile drop measurements. The contact angles were measured using various pure liquids and different approaches such as the Zisman approach, the equation of

state, the harmonic mean equation, the geometric mean equation, and the acid–base approach to estimate the surface free energy of wood. Wood surface properties were examined using various liquid standards with different polarities (α-bromonaphthalene, formamide, ethylene glycol, glycerol, and water) for purpose of measuring wood wettability and wood surface free energy and its components (Kúdela 2014); (Piao et al. 2010); (Rodrı´guez-Valverde et al. 2002); (Jennings et al. 2006); (Meijer et al. 2000); (Gindl et al. 2004); (Gindl et al. 2001); (Gindl et al. 2002); (Gardner 1996); and (Gunnells et al. 1994).

The contact angle measurements are usually done using more than one probe liquid. Based on the three controlling parameters γ_s^{LW} (Lifshitz-van der Waals), γ_s+ (Lewis acid-base electron-acceptor), and γ_s- (Lewis acid-base electron-donor) of a polar solid, there is a need for three different liquids (γ_L^{LW}, γ_L+, and γ_L-) to calculate the polar solid parameters using contact angle measurements (Oss et al. 1988).

The mercury porosimetry technique is an excellent method to characterize wood surfaces where it can provide useful information that can be implied in the understanding of wood contact angle and surface free energy (Moura et al. 2005) and (Zauer et al. 2014). The only drawback of the Mercury intrusion porosimetry technique is that it assumes perfectly aligned cylindrical pores and the pores may not be all in a cylindrical shape in general.

1.2.5 Metal Systems

Metals are not porous and likely that literature is not important. However, this system has been studied by many researchers by looking at the effect of temperature and humidity (Na et al. 2018), the amounts of glue applied, overlap lengths, and treatments (Koricho et al. 2016), the pre-treatment processes, adhesive layer thicknesses, and overlap lengths (Manohar et al. 2019). In

addition, finite element analyses of metal joints have also been studied by many such as (Chiminelli et al. 2019).

1.2.6 Wood Systems

Failure modes (types) have been the focus of many previously published literature where they have been introduced in percentage and classified into two types: adhesive and cohesive failure modes (Bachtiar et al. 2017). The effect of water-based glue spread levels on the tensile shear strength was little and did not alter the performance of adhesive for both adhesive spread levels, 250 and 500 g/m^2 (Hashim et al. 2011). This paper did not study flow dynamics where they were most interested in measuring bond strength. Both adhesive layer thickness and overlap length contribute to performing strong or weak bond strength in glued joints (Tannert et al. 2012). Both experimental and numerical investigations done in this paper have not performed penetration analysis. Performing experimental and numerical analysis on penetration may lead to an understanding of why overlap lengths can strengthen joints while adhesive layer thicknesses cannot. (Gadhave et al. 2017) published a review on the performance of starch as an adhesive. Starch-based adhesives can help in getting excellent strength performance in gluing wooden joints; however, the major problem is that they have poor and limited water resistance. This review can be a good guide when thinking about blending starch with other resins during gluing events.

1.2.7 Penetration into Porous Materials

The penetration of fluid into a capillary or porous material is of interest in many situations, but this phenomenon seems to be important to understand the adhesive setting. The Lucas-Washburn equation, which is still used today, was able to combine the capillary pressure generated

by the free surface in the pore with the equation that describes the flow in a tube, to predict the rate of capillary rise (Fries et al. 2008a, 2008b; Hamraoui et al. 2002; Li et al. 2015). Others have built on this model to include complex pore shapes and the interconnection of pores. For example, (Bousfield et al. 2004) developed a three dimensional model that connects pores of various sizes with constrictions to predict fluid uptake.

Penetration into a porous media is found to influence and change coating parameters (Ding et al. 2017). This study did not involve temperature and concentration changes during the process of penetration. Absorption into porous media may also be influenced by cohesion and adhesion forces (Gane et al. 2000). The process was isothermal in which one droplet was allowed to touch the porous substrate without considering concentration changes. Others have represented the porous media with various geometric approximations to predict the penetration of liquids (Blunt et al. 1995) and (Thompson 2002). The substrate thickness affects the process of penetration (Alleborn et al. 2007). These studies were steady-state and did not account for changes in the fluid properties inside the pore.

The rate of penetration into a porous media at times can be controlled by a filtercake that forms on top of the surface as particles in a suspension are captured (Xiang et al. 2004). This situation seems to be the case for the setting of inks on coating layers. In the setting of water-based adhesives on a coating layer, there is the potential that this mechanism also plays a role in the setting rate.

Some limited work is reported that takes into account the change in the permeability of the paper in various layers after contact with a fluid. (Bousfield et al. 2016) modeled the depth of penetration of starch solutions prepared at various solids into a porous web. The potential that the permeability of the paper changes after contact with water due to fiber swelling explained some of

the results. For water-based adhesives, the fibers likely do take up water and swell upon contact with the glue, but the literature is not clear if this is important.

(Meijer 2005) published a review on the interfacial aspects of wood coatings research. The author discussed coatings penetration into wood pores, wood surface energy calculations, and finally adhesion between wood and coatings. The author found that the degree of coating penetration into wood capillaries is controlled by coating flow as well as the anatomical wood structure where the viscosity changes result from water and/or solvent diffusion through the cell walls is the main factor that plays a major role during the penetration process.

A study on penetration of water-borne, solvent-borne coatings (paint primers and wood stain base-coats), high solids, and hybrid systems into four different wood species was performed by (Bulcke et al. 2003) in which both confocal scanning laser microscope (CSLM) and image analysis methods were used. The key influencing parameters that affect penetration are each resin type, resin weight, and viscosity.

The results obtained from the Scanning Electron Microscope (SEM) showed different penetration depths for different adhesives (Bachtiar et al. 2017). The reason why these penetration depths are different between these adhesives has not been discussed.

Some other works have considered general fluid flow in various porous mediums. In these past works, fluid flow and heat and/or mass transport phenomena were solved using governing equations (momentum, energy, and mass transport equations). A steady flow of a viscous incompressible fluid was studied in a channel with porous walls (Babaelahi et al. 2010). An unsteady flow of incompressible electrically conducting fluid with heat and mass transfer was studied in two vertical porous plates (Raghunath et al. 2020). The heat and mass transfer phenomenon was studied in an unsteady boundary layer flow of viscous incompressible fluid over

a stretching sheet through porous media taking into account the presence of wall suction (Husnain et al. 2012). A flow of two viscous incompressible fluids separated by a cylindrical interface with heat and mass transfer across the interface was studied through a porous medium (Awasthi et al. 2013). An unsteady flow of a viscous fluid with heat transfer was studied in a horizontal annulus of a composite porous medium (Nasir et al. 2012). A laminar steady and unsteady incompressible fluid flow with heat transfer was studied in a spatially periodic array of porous square rods in which a computational unit cell scale model was used (Alshare et al. 2010). In other studies that included modeling, (Elhalwagy et al. 2017) modeled heat and mass transfer in conjugate fluid/porous domains. A fluid flow with heat and mass transfer in engineered spaces was modeled in which both macroscopic and microscopic models were coupled (Chen et al. 2007). A coupled incompressible fluid flow and heat or mass transport in porous media was modeled by (Younes 2003).

Although these studies are important in the fields of fluid flow and transport phenomenon, none of them has considered the flow of adhesives into paper systems that are the main focus of the current research project. Based on this fact, the current work will be a new study that differs from the above works in both the type of fluid that will be used and the systems that will represent the porous medium. As a result of that, the influencing parameters as well as the operating conditions will also be different in both current and previous studies.

1.2.8 Adhesive Penetration and Bonding

The substrate pore size is expected to play a major role in bond strength. (Dadvar et al. 2015). This work indicates that, for hot melt glues, a high impression force and large pores should increase the penetration of the glue into the pore structure and increase adhesion.

A few studies have used models to predict the penetration of adhesives into the wood. (Hammerquist et al. 2018). The pressure-driven adhesive penetration was used in realistic wood structures, however, no heat and/or mass transfer was studied during penetration in this article. Simulations of the flow of various adhesives into hardwood (beech samples) revealed that the penetration depth was largely affected by either the hardening process or low amounts of adhesive applied, starved bond line (Mendoza et al. 2012). In this study, the adhesive viscosity was modeled as a function of time and concentration. More than six major assumptions were made to the model adopted by this study. Due to the high assumptions made already in this work, a comparative study can be difficult but is not impossible.

The analysis of adhesive bond lines after or during penetration is important in determining and measuring adhesive penetration depths. Adhesive penetration depths can be measured using various imaging techniques. Both scanning electron microscopy and confocal laser scanning microscopy are the two famous techniques used among others. The other techniques used to measure the penetration depth of adhesives into the wood are the micro X-ray computed tomography by (Paris et al. 2015), synchrotron radiation X-ray tomographic microscopy by (Hass et al. 2012), epi-fluorescence microscope by (Sernek et al. 1999), confocal laser scanning microscopy by (Xing et al. 2005), fluorescence and electron microscopy by (Meijer et al. 1998), Chemical-State X-Ray Microscopy by (Buckley et al. 2002), and UV-microscopy by (Gindl et al. 2002).

A review of adhesive penetration into the wood was done by (Kamke et al. 2007). Good adhesive bond performance is dependent on the degree of penetration of the adhesive into the wood structure. In this review, adhesive penetration can occur in three different levels of scale that are nano-penetration (penetration into cell wall), micro-penetration (penetration into cell lumens and

pits), and macro-penetration (penetration through process-induced cracks). The wood-related parameters that affected penetration were permeability and surface energy. The other parameters that also affected penetration were the molecular weight distribution, viscosity, solids content, additives, open assembly time, pressing time, temperature, consolidation pressure, and surface tension of the adhesive liquid phase. The cohesive strength, covalent bonding, and secondary chemical bonding are other parameters that had a large impact on adhesive bond performance compared to the penetration itself. Since paper is of interest in this thesis, the next sections will present some recent studies on paper coatings and adhesive penetration into different porous substrates.

1.2.9 Paper Coatings

Paper and paperboard coatings are commonly used to increase the printing properties of paper and improve its appearance. (Lepoutre 1989) listed the key points for the basic relationship of materials. Paper coatings that were applied as an aqueous suspension contained pigments such as clay and calcium carbonate and binders such as latex or starch. Little is stated concerning the adhesive setting with no further details that are: the adhesion and coating strength can be controlled by the interaction that exists between pigment and binder surfaces in the coating suspension and: the coating void fraction and contact angle control the aqueous glue's setting rate. With regard to penetration, ink penetration was given as an example of fluid penetration into porous coating layers.

The pore size and porosity of a coating layer were found to be controlled by various parameters (Dahlstrom et al. 2012). Decreasing the binder level is known to increase the pore space. Pigment size often controls the pore size. Pigments with a steep particle size distribution

will increase the porosity of the coating. While the ability to glue two coated surfaces together likely depends on the coating porosity, this has not been clearly demonstrated in the literature.

1.2.10 Paper Systems

In the production of corrugated paperboard, modified starch is used as a water-based glue that needs to be set rapidly in the production step (Daub et al. 1990). The article found that the two main paper properties that had an obvious impact on the pin adhesion strength were the absorption coefficient and the bonding strength of the paper. No models were developed to describe the setting rate or bond development. (Daub et al. 1990) also studied paper properties that influence penetration and glueability processes. They observed that higher absorption coefficients led to a lower corrugated board pin adhesion strength. A correlation was noticed between the pin adhesion strength and the surface temperatures of the paper in the single facer at moisture contents of 6% to 7%. The outcomes listed above were given without further descriptions.

Among all of the five binders used in the coating layer, the polyvinyl acetate homopolymer (PVAc) gave the best performance followed by the vinyl acetate ethylene copolymer (VAE) (Farwaha et al. 2012). The fast setting of glue was achieved using PVAc since PVAc can help in providing more open spots in the coating structure leading to a faster dewatering of the glue. The time needed to develop a green tack in a glued layer is between 30 seconds to 2 minutes and that is based on dewatering achievements. The authors deduced that the failure mode occurs in the weaker spots if they sit next to the stronger green tack of the glue.

The degree of penetration of the glue into the double-coated paperboard was found to influence the bond strength (Ninness et al. 2011). The glued samples were evaluated after 1 and 2 hours of setting time using the fiber tear method when performing the aqueous glue tests. It was

found that as more glues penetrate down to the coating/fiber interface, the bond strength increases linearly. Confocal laser scanning microscopy (CLSM) was the best compared to scanning electron mapping (SEM) and optical microscopy in determining quantitively the extent of penetration into coating layers. The authors here have not shown enough reasons behind failure modes as well as behind various penetration depths.

In the gluing of coated paperboard, the coating layer is known to influence the results. The type and amount of latex in the coating are known to influence the final bond strength of both water-based and hot melt glues (Ventresca et al. 2019). Increasing the binder level promotes adhesion strength in both pigment and glue systems, regardless of the type of binder. The adhesion strength of the hot melt glue specimen was measured manually by peeling samples apart after 1 minute of cooling. On the other hand, the fiber tear method was accomplished after 30 and 120 minutes for the aqueous glue specimen.

Based on the works discussed above on paper adhesions, one can conclude that the works done previously did not explain and discuss the reasons and/or mechanisms that different latex influence the bonding where it could be one latex generates a different pore space. The pore structure has not been characterized by looking deeply into pore sizes, porosities, and absorption properties. The above works did not include any “modeling" or do any fundamental analysis of these systems. In addition, the final fiber tear results may be caused by the binder generating a strong coating layer, and not really relate to the setting rate. While the work above is impressive, a better understanding of the material and process parameters that lead to green and final bond strength is important to help troubleshoot operations, design new systems, and help understand the coating layer properties that influence the setting.

1.2.11 Summary of Literature

Several studies have attempted to understand adhesion as described earlier in the previous sections. To summarize what was mentioned above:

1. Adhesives were only compared based on their ability to form strongly bonded joints. The reasons behind failure modes have not been clearly described and understood.
2. Most publications report the final bond strength in various systems by looking at fiber tear without looking deeply at the phenomena that affect the formation process of the bonds.
3. In wood adhesion and paper, penetration into the pores of the adhesive is important, but little is reported on what controls this penetration.
4. Few publications have studied the influence of some parameters during glue events such as thicknesses of the adhesives, overlap lengths, humidity, and temperature changes. However, few have linked experimental data to modeling results investing these parameters.
5. The dynamic behavior involving both temperature and concentration changes during glue processes has not been considered in various models.
6. The degree of penetration of adhesives into porous mediums was measured using image analyses, however, there were fewer explanations as to why penetration stopped and the adhesive solidified.
7. The effects of major forces such as capillary effects, pressure changes, viscous forces, and pore size distribution have been reported. However, models to predict adhesive setting based on these is lacking in the literature.

8. Many articles have studied the penetration of a fluid into porous materials in which various parameters were discussed, but nothing has been described where the viscosity changes as the fluid penetrates the pores.
9. Linking all parameters into several well developed and controlled dimensionless groups has not been done by any of the previous efforts. All key parameters are linked together through different dimensionless groups in the current research project.

1.3 Structure of Thesis

The organization of this thesis is discussed below. The literature review that consists of various systems, adhesives, and materials properties is discussed in Chapter 1. Chapter 2 presents results and discussions for unsteady isothermal penetration of polymer into a single capillary where the results of the finite element model are compared to the predictions of the modified Lucas-Washburn equation for various polymer viscosities and conditions. The remaining chapters are either published or potentially published papers with a literature review included. Chapter 3 first contains modeling of unsteady non-isothermal penetration of polymer into a single capillary using the finite element method where the modeling results are given in terms of several dimensionless groups generated from different parameters and compared to the results of the modified Lucas-Washburn equation. Second, the experimental results obtained from pressing a polyethylene film at various temperatures against a paper that has a CNF layer for two pressing times are compared to Darcy's law predictions (Khlewee, M., Al-Gharrawi, M. and Bousfield, D., "Modeling the penetration of polymer into paper during extrusion coating." Journal of Coatings Technology and Research 19(1), pp. 25-34 (2021). Chapter 4 focuses on comparing four novel methods developed in the laboratory and scanning electron microscopy for penetration depth determination at different

conditions (Khlewee, M., DeSisto, W. and Bousfield, D., “Comparison of methods to characterize the penetration of hot melt adhesive into paper.” Nordic Pulp & Paper Research Journal (2022).

Chapter 5 reports experimental penetration depth results obtained from the silicone oil method for various bonded coated and uncoated samples at different paper temperatures and press pressures using hot melt adhesive (submitted to Industrial & Engineering Chemistry Research Journal). The model predictions are compared to the experimental ones using the modified Darcy’s law accounting for the multi-layer system with finite adhesive quantity using the viscosity of the adhesive that corresponds to the expected temperature of the adhesive obtained from an energy balance. The mechanical tester Instron is also used to measure the final bond strength. Chapter 6 addresses the setting of water-based adhesive in various uncoated and coated papers using the carver press tester and the roll press tester (potential published paper). This chapter uses the silicone oil method to measure adhesive penetration depths. The modified Darcy’s law is also used in this chapter as well as the filtercake equation. This chapter shows a section that handles the modeling of water diffusion through pore walls where the results of modeling are compared in terms of various dimensionless groups. The mechanical tester is used as well to measure the green and final bond strength. Chapter 7 concludes the thesis's key observations and contains suggestions and recommendations for future work.

CHAPTER 2: MODELING THE UNSTEADY ISOTHERMAL POLYMER PENETRATION INTO A SINGLE CAPILLARY

2.1 Introduction

The flowing of fluid into a porous media is of interest in many industries. Understanding the path that the fluids follow and the rate of flow when passing through a porous material has been studied for decades. The influence of the medium such as the pore size distribution can be included in the calculations. Incorporating heat or mass transfer is important in the modeling of these processes. There is a large body of literature looking at the interaction of a fluid with porous media in steady-state flows that also involve steady-state heat or mass transfer. Temperature and concentration changes accompanying the process of penetration of liquid adhesives into a porous media have not been published in the literature to our knowledge.

Here the results of the finite element method base model (COMSOL Multiphysics 5.5) were compared with the Lucas-Washburn equation that describes the penetration of a fluid into a single capillary. The modeling results obtained from the penetration of isothermal liquid into a porous medium were discussed through two cases that are either pressure or surface tension driven the flow. In order to reduce the number of parameters, the simulation results were given in terms of several dimensionless groups that have been generated. The net outcome of this theoretical work is to provide insight into the key parameters that affect the process of penetration of liquid adhesives into medium pores.

While a simple cylindrical pore is the subject of the model, the learning gained should help understand the complex flow inside a porous media. The reason behind choosing this simple geometry in the current research project is that this is a first-time study that handles adhesives penetration problems during the unsteady-state flow, and the focus was to start someplace before

going any further steps in complexity. Also, we may not need that complex of a model to answer the questions about how much penetration occurs that links to bond strength.

2.2 Model Set-Up

A commercial finite element code (COMSOL Multiphysics 5.5) was used to model 2D axisymmetric flow into a single capillary. The steps taken to set up the model are described as follows: in the physics section, two phase flow-level set method and laminar flow physics were chosen. The level-set method solves the Navier-Stokes equations for the conservation of momentum and the continuity equation for the conservation of mass for two fluids separated by a free surface; the interface position is tracked by solving a transport equation for the level-set function that keeps track of what liquid is in what region of the simulation.

The input parameters were selected to model the dynamic flow of a fluid into the fine capillary, taking into account the surface tension forces at the interface and the fluid properties of the two phases. The problem was an unsteady-state. In the software, the selection "global definitions" allows various parameters to be defined and the values inserted. Here parameters such as surface tension, contact angle, and fluid properties can be defined. The geometry is simple where two rectangles were selected to represent the pore and the inlet region to the pore: rectangles are actually cylinders in the r-z coordinate system if they touch the axisymmetric line.

The material tree is used to assign air physical properties to the single capillary and adhesive properties to the inlet region where the parameters are listed in the parameter section. Air was assumed to be in the empty cylinder-shaped pore and an adhesive region was placed at the inlet to the pore. Also, there is an option in this tree that can be used to create an analytical function to assign the viscosity to be a constant or a function of temperature or concentration. The next trees

are the physics trees where the boundary and initial conditions are set. In the laminar flow physics section after we neglected both gravity and inertia terms, we added two boundaries that were the inlet and the outlet to which we assigned the inlet and the outlet pressure. In the level set section, we added five boundaries that were the initial value of air, the initial value of adhesive, the initial interface, the inlet, and the outlet. In this tree, the fluid parameter scales from zero to one, where zero is air and one represents the adhesive. The wetted wall boundary was added to the Multiphysics tree where both the slip length and the contact angle values are adjusted. The surface tension value was inserted into the surface tension branch under the "two-phase flow-level set" section in the same Multiphysics tree. The final tree is the mesh tree where we can specify the number of elements (besides others) that needs to be accounted for in the computational steps. The geometry, boundary, and initial conditions are depicted in Figure 2.1 whereas a mesh selection window is shown in Figure 2.2.

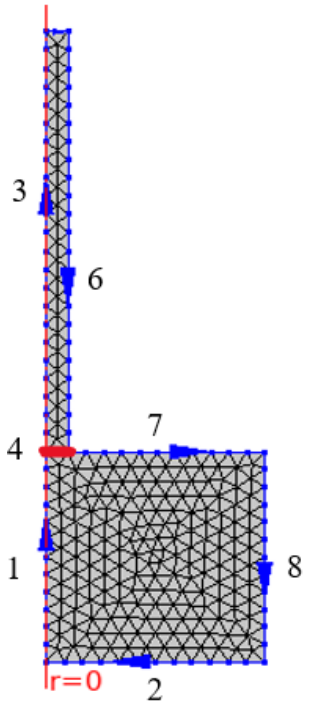

Figure 2.1. Single pore geometry in axisymmetric coordinate meshed system.

The boundaries shown in Figure 2.1 define as follows:

- 1, 2, 7, and 8 represent the adhesive region.
- 1 and 3 are the axisymmetric conditions for all equations.
- 6 is the capillary wall with no-slip conditions.
- For the fluid flow, no-slip boundary conditions are used along walls 6 and 7.
- 2 and 8 are the inlet boundaries for the adhesive.
- At the top, not labeled, is the outlet condition.
- 4 is the initial meniscus that separates air from the liquid. The meniscus between two immiscible fluids moves at a rate that is set by a balance between the wall adhesion, the surface tension, and the contact angle between the fluid interface and the wall. This boundary motion also depends on a parameter in the level-set method call the slip length, which is represented by either f or β symbols in the model. Slip length is needed to allow the three phase contact point at the wall, near the boundary, to move and yet maintain the no-slip condition of the fluid at the boundary.

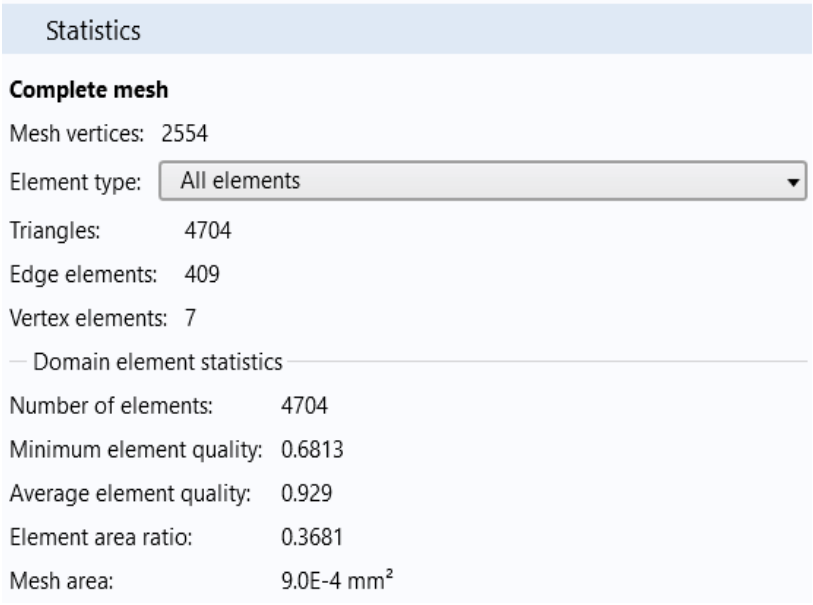

Figure 2.2. Normal mesh statistic for case in Figure 2.1.

The size of the inlet region of the capillary (boundaries 1,2,7, and 8) is not important, but if it is too small, extra resistance to flow is generated and too large, extra mesh is generated which slows down the calculation. The initial conditions are not important when inertial terms are neglected. As time progresses, the adhesive flows into the capillary and the meniscus position increases as a function of time.

2.3 Lucas-Washburn Equation

The penetration of a fluid into a capillary is approximated by the well-known Lucas-Washburn equation. This penetration is derived by using the capillary pressure generated in a tube due to a liquid with a specific contact angle given by the LaPlace equation and the steady-state flow in a tube using the Hagen-Poiseuille equation. This equation has been verified by numerous experiments over the years and is valid for typical situations related to paper interacting with a fluid. The typical form of the Lucas-Washburn equation that neglects gravity is

$$L = \sqrt{\frac{\gamma\, R\, t\, cos(\theta)}{2\,\mu}} \qquad (2.1)$$

Where γ is surface tension, R is capillary radius, t is time, θ is contact angle of fluid with solid, and μ is viscosity. When an external pressure is added to the capillary pressure due to some external pressure such as a pressure nip, then the modified equation is

$$L = \sqrt{\frac{R^2\, t}{4\,\mu}\left(\frac{2\,\gamma\, cos(\theta)}{R} + \Delta P\right)} \qquad (2.2)$$

Where ΔP is pressure applied to the fluid. If penetration depth is scaled with radius L^*=L/R, contact angle with a reference contact angle of 90° θ^*=θ/θr where r in contact angle expression is some reference angle, time with surface tension, radius, and viscosity t* = t γ/A R, and pressure with surface tension and radius ΔP* = ΔP R/γ, then the new equation in dimensionless variables is

$$L^* = \sqrt{\frac{t^*}{2}\left(cos(\theta^*) + \frac{\Delta P^*}{2}\right)} \qquad (2.3)$$

This equation we call the modified Lucas-Washburn equation comes from balancing the viscous resistance of flow in a tube with the pressure driving the flow. If dimensionless pressure is larger than one, the surface tension influence is minimized, and the equation reduces to unsteady pressure driven flow into a tube. It is expected in most industrial cases, the capillary pressure will be small compared to the pressure pulse.

The scale of interest for the penetration of adhesive into paper is a pore size that is around 5 μm in diameter. The contact angle is set to 45°. The viscosity of the adhesive can have a large range depending on the type of adhesive of interest. Some water-based adhesives may have viscosities in the range of 0.01-0.1 Pa s. Hot melt glues, depending on the temperature, may have values that are on the order of 10 Pa s. The applied pressure in a rolling nip depends on the mechanical system, but often situations like this may produce pressures on the order of 1 MPa. The surface tension of the adhesive likely would be in the range of 0.03-0.05 N/m. In the case of adhesives that see a pressure nip, it is assumed that capillary driven flow will be minimal.

2.4 Results and Discussion

To validate the finite element model, the isothermal flow into a capillary was described. Both inertia and gravity terms were neglected based on past work and the scale of the non-dimensional groups involved. Table 2.1 presents the parameters assumed for the model.

Table 2.1. Model Parameters.

Parameters	Value
γ, Surface Tension (N/m)	0.05
ρ, Adhesive Density (Kg/m^3)	1110
θ, Contact Angle (degree)	45
R, Pore Radius (μm)	5
μ, Dynamic Viscosity (Pa s)	various
f, Minimum Element Length Factor, Slip Length, (unitless)	1

Applying pressure helped in an increase in the penetration depth and amount because when pressure is applied to the inlet, the pressure will drive flow into the capillary besides surface tension forces. Here, using the same parameters listed in Table 2.1, several inlet pressure values were signed into the inlet boundary (boundaries 2 and 8) to record the influence of the pressure changes on the penetration depth and to compare with the theory (Modified Lucas-Washburn equation).

There are two parameters in the software that exhibited a significant influence on the results that are the slip length (β) on the wetted wall and the mesh size. Therefore, for the full range of parameters, the normal mesh at small times and the slip length factor (f =1) were used because this parameter had little influence on the results compared to β.

When plotted in dimensionless terms, the value of the viscosity should be scaled into time and the results should not depend on the viscosity used. However, at a viscosity of near water, 0.001 Pa s, the model underpredicted the Lucas-Washburn equation and the other viscosity cases

as shown in Figure 2.3. The behavior seen in 0.001 Pa s case is due to short time scales. This case represents where the meniscus shape does not have time to adjust to the contact angle imposed. The high rate of penetration for the low viscosity case disrupts the time scale needed to establish a curved meniscus that leads to this result.

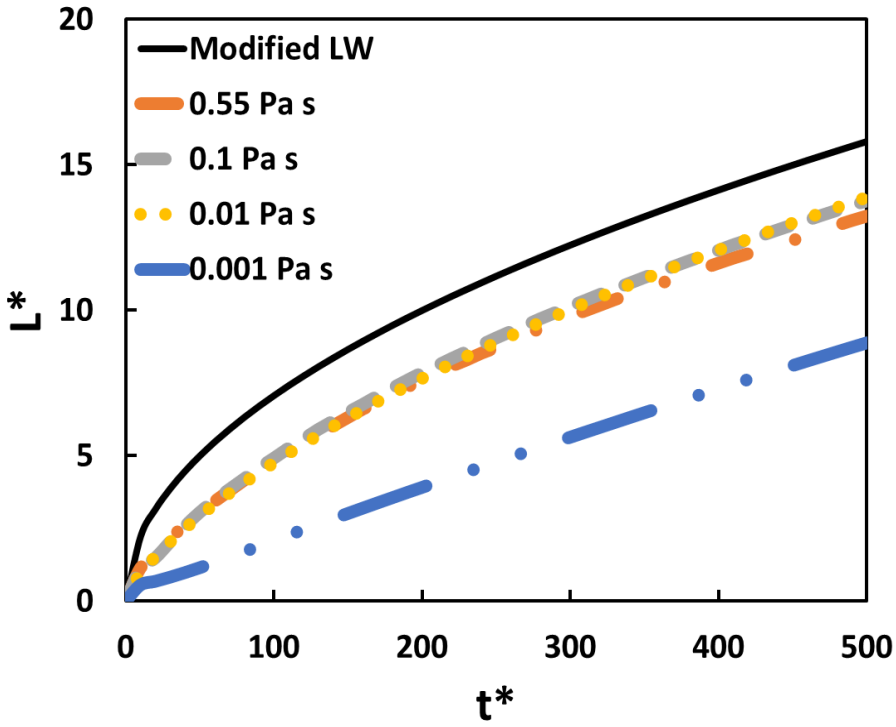

Figure 2.3. Effect of liquid viscosity changes on the penetration depth at $\Delta P^*=0$.

Figure 2.4 shows the velocity distribution for the low and high values of liquid viscosity. The velocity was high for the low viscosity liquid as expected and the real time was 0.05 ms. For the high viscosity liquid, the velocity was low and the curvature at the meniscus had time to adjust. Figure 2.5 shows the fluid position in the capillary. For the low viscosity, the meniscus was not curved as expected.

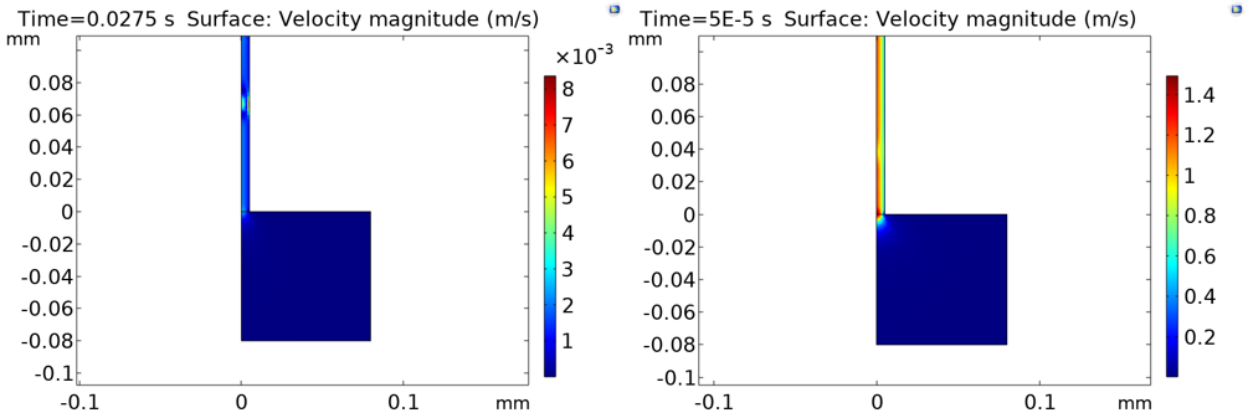

Figure 2.4. Velocity distribution for a liquid viscosity of 0.55 Pa s (left) and 0.001 Pa s (right), ΔP*=0.

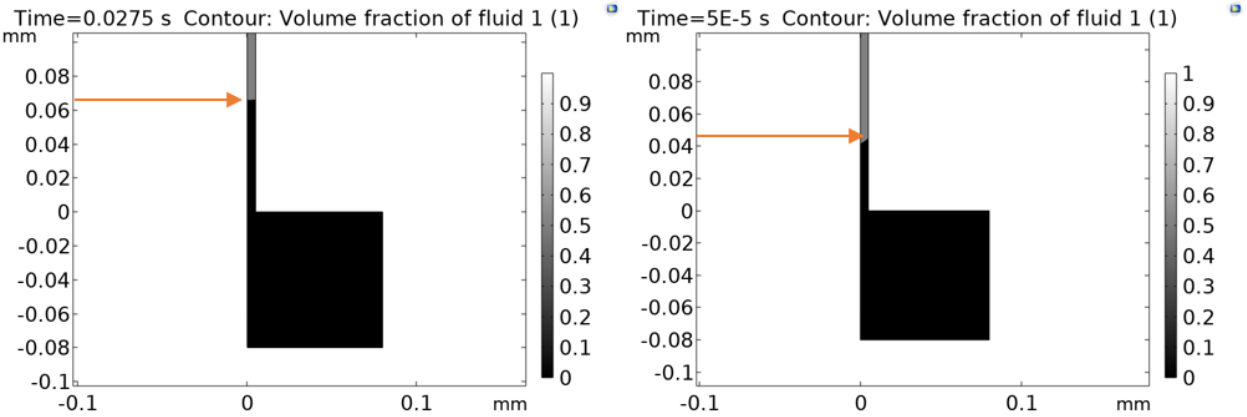

Figure 2.5. The advancement of the meniscus into the capillary for a viscosity of 0.55 Pa s (left) and 0.001 Pa s (right), ΔP*=0.

The inlet dimensionless pressure started to show an influence on the results when it was over unity. The effect was obvious compared to the cases described above where now the imposed pressure is responsible for the flow over the surface tension. Increasing the inlet dimensionless pressure value to 50 increased penetration as expected and shown in Figure 2.6. The change in the results was noticeable with ΔP*=50 where the L* jumped from 13.9 to 117.5 with about an 88% increase when the ΔP* increased from 0 to 50 for the 0.01 Pa s viscosity modeling results. It can be seen also that the viscosity of 0.001 Pa s is now adjusting back following the same trend as others compared to the case of ΔP*= 0 where it behaved differently. This means that at this high

pressure level, the time scale issues no longer have an impact on the meniscus adjustment where this pressure limit handled this issue successfully and helped the low viscous adhesive to penetrate deeper into the capillary compared to the high viscous ones.

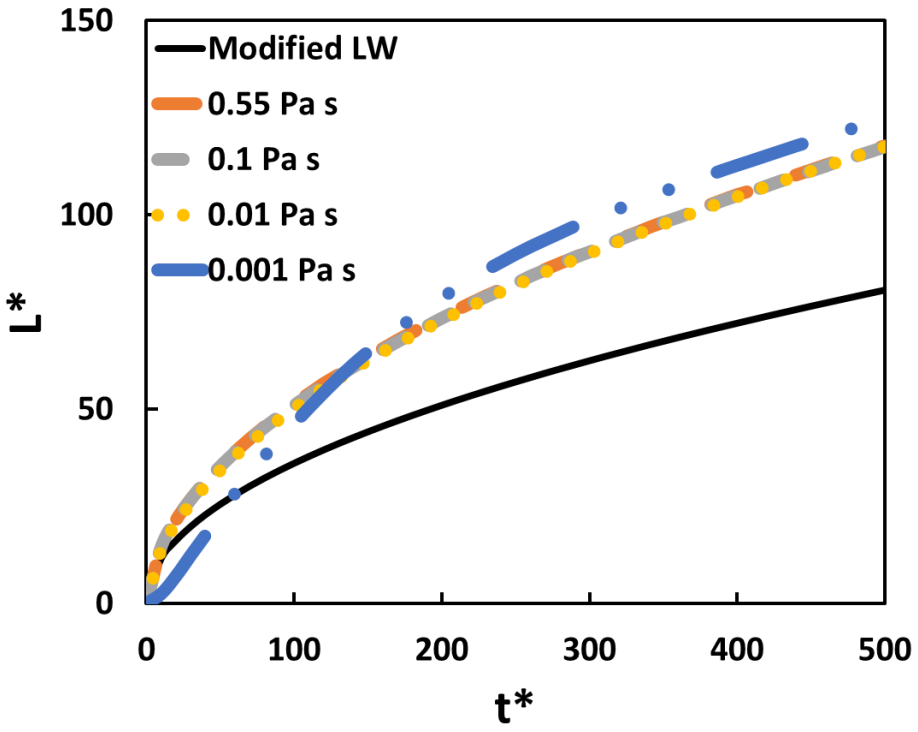

Figure 2.6. Effect of liquid viscosity changes on the penetration depth at ΔP*=50.

The three surface plots given below explain the behavior shown in Figure 2.6 regarding the 0.001 Pa s viscosity case. Figures 2.7, 2.8, and 2.9 are the velocity, pressure, and depth distributions taken from the early stages of the run time at ΔP*=50. As we can see that the velocity is still high for the case of 0.001 Pa s compared to 0.55 Pa s, however, the pressure distribution can explain the results clearly. In Figure 2.8 and at the same depth in the capillary, the pressure distribution was uniform for both viscosities and it was about 4×10^5 Pa. Despite the short run time that is associated with the 0.001 Pa s, we can tell that the increased pressure was able to drive more adhesive into the capillary faster compared to the other cases where the time scales were high, but the viscosity was high as well to force the adhesive to penetrate deeper into the capillary.

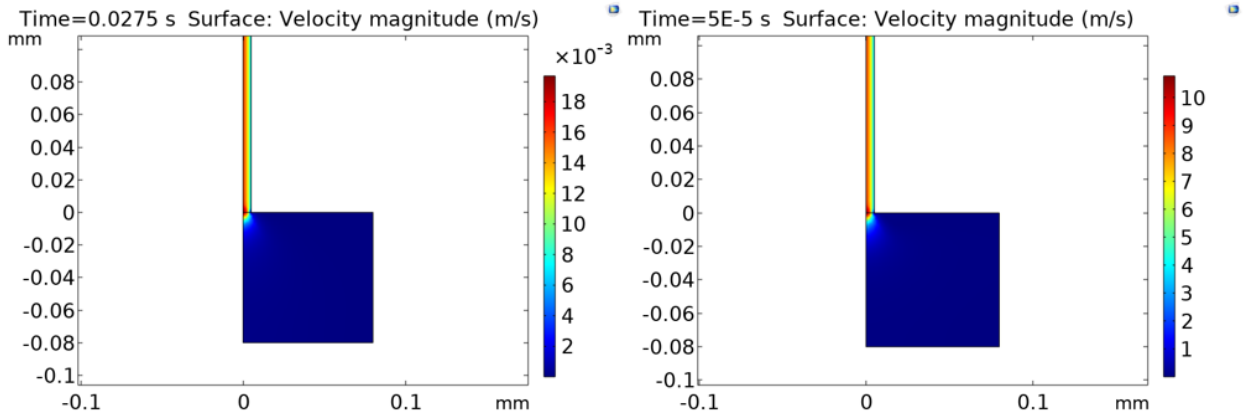

Figure 2.7. Velocity distribution for a liquid viscosity of 0.55 Pa s (left) and 0.001 Pa s (right), ΔP*=50.

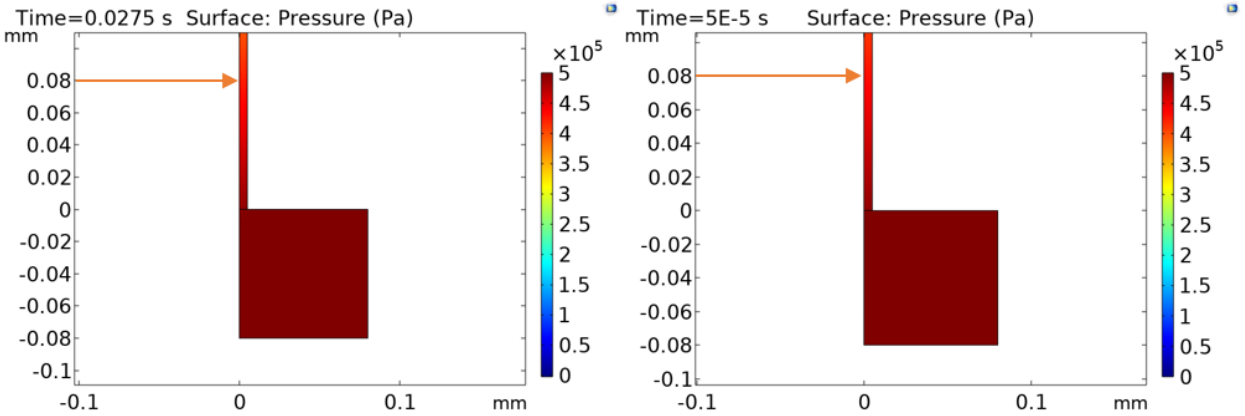

Figure 2.8. Pressure distribution for a liquid viscosity of 0.55 Pa s (left) and 0.001 Pa s (right), ΔP*=50.

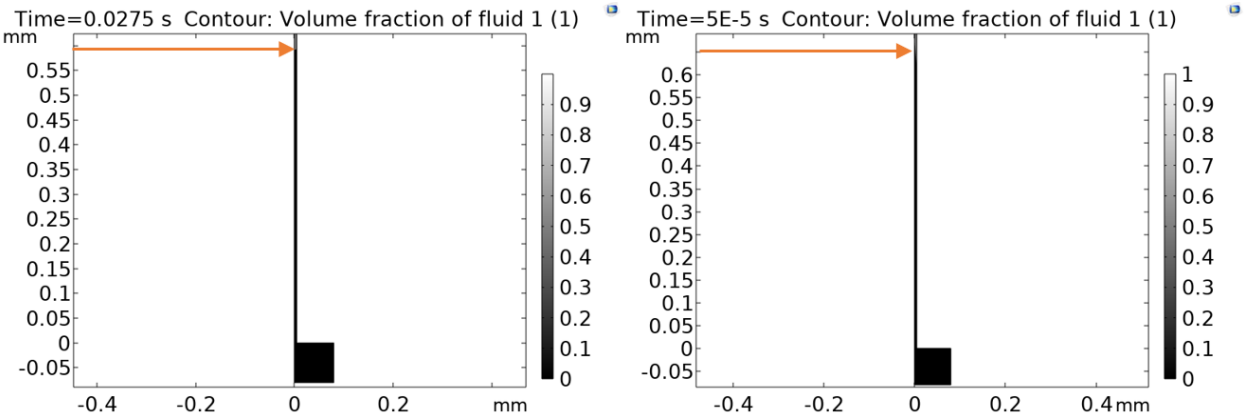

Figure 2.9. The advancement of the meniscus into the capillary for a viscosity of 0.55 Pa s (left) and 0.001 Pa s (right), ΔP*=50.

2.5 Concluding Remarks

A pore level model is developed to describe penetration during isothermal situations that take into account a constant viscosity of the fluid as it enters a pore. The model indicates that the fluid viscosity has an impact on the penetration depth. The model also confirms that more adhesive can be drawn into the pore as the inlet pressure increases or as the fluid viscosity decreases. For the full range of parameters, the normal mesh, and the slip length factor ($f = 1$) are the best to match the theoretical results. For cases that do not depend on temperature, where the viscosity is fixed, the model can give a good comparison to the Lucas-Washburn equation.

CHAPTER 3: MODELING THE PENETRATION OF POLYMER INTO PAPER DURING EXTRUSION COATING

3.1 Abstract

During the extrusion coating of paper or paperboard, a molten film of polymer is pressed against a paper surface to generate water-proof packaging materials. Hot melt glues also are applied to various porous materials and paperboard to generate packaging. In both cases, the penetration of the polymer into the pore space influences the product performance and the ability of the product to be recycled at the end of life. While there is much experimental work discussing various parameters in these operations, little theoretical work has been reported. Here, a simple model based on Darcy's law is proposed to predict the penetration of polyethylene (PE) into paper and paper that has been coated with cellulose nanofibers (CNF). Another model, based on the flow of a polymer into a pore that includes dynamic heat transfer is developed, where the viscosity is a function of temperature. Experiments were conducted where a PE film is pressed against samples and the amount of fiber recovery is characterized. The model predictions are compared to experimental results. Good agreement for different paper types, pressing times, and temperatures are obtained after a calibration factor is used.

3.2 Introduction

Polyethylene and other polymers are often extrusion coated onto paperboard to give a waterproof material for a number of common applications such as coffee cups, aseptic packaging, and juice cartons. This process has been common for over 40 years and is the subject of various patents (Avni et al. 1990). While this process is done on a large scale and in an economical manner, concerns around the ability of the coated paper to be recycled and the fate of these

products in the environment have become a concern. Recently, Starbucks put up a “cup” challenge with the goal of modifying the paper cup system to be more recyclable.

Other sustainable polymers have been applied to paperboard systems to generate an improved environmental footprint. Some groups are looking at the extrusion coating of polylactic acid (PLA) or other sustainable polymers onto paper (Cheng et al. 2015; Kuusipalo et al. 1997; Kuusipalo 2000I, 2000II; and Rhim et al. 2007). Often, the use of these biopolymers can lead to other issues such as adhesion with the paper substrate. The goal is to produce a coated substrate that can easily be recycled with the paper stream but also will degrade into benign materials if littered in the environment.

The adhesion of a polymer layer to a porous substrate has received limited attention in the literature (Ventresca et al. 2019; Ninness et al. 2011, and Putkisto et al. 2004). The influence of the polymer chemistry, the surface chemistry and porosity of the paper, and the processing conditions are known in general. The penetration of the polymer into the substrate is the most common mechanism that results in good adhesive strength for hot melt adhesives (Ninness et al. 2011). However, the interaction of pore size porosity, polymer rheology and processing conditions are not clear in relationship to the degree of polymer penetration. Good penetration also likely relates to poor recycling because the fibers are intermixed with the polymer. While there have been some fundamental models developed for the penetration of glues into wood, little has been reported in the area of molten polymers into paper.

Recently, the interest in cellulose nanofibers (CNF) in food packaging systems has grown because layers of CNF have excellent oxygen and oil barrier properties; oxygen barrier properties are around 100x better than common polymers (Wang et al. 2018; Lavoine et al. 2012; Spence et al. 2011; and Tayeb et al. 2020a, 2020b). These CNF layers can be applied with high speed

methods such as blade or slot dye coating, or as a top layer in the wet end of a paper machine (Kumar et al. 2016, 2017; Mousavi et al. 2018; and Johnson et al. 2019). However, these layers do not have good water vapor barrier properties and when they are exposed to moisture, the oxygen barrier properties are lost. Therefore, in a food packaging system, likely layers are needed to block water vapor from diffusion into the product and to protect the CNF layer. Limited results are published looking at the use of a biopolymers with CNF layers, but some have reported excellent results (Koppolu et al. 2019).

One other aspect of a CNF layer that could have a big impact on food packaging is the potential for the CNF layer to be a release layer for a polymeric film like PE. Upon exposure to water, as in a slushing operation in a paper recycling system, CNF loses its mechanical properties. Therefore, if the PE layer is on the CNF layer, it may have a clean separation from the regular pulp fibers. This concept has not been explored in the literature, but it could lead to PE coated paper products that are easy to recycle.

In this work, two models are developed to describe the penetration of a polymer into a porous material. One model is based on Darcy's law and links the viscosity of the polymer, nip pressure, and time with the degree of penetration. A second model is based on the flow into a single capillary using a finite element method; this method takes into account the change of viscosity of the polymer as it interacts and cools in contact with the porous web. Experiments are run that press a PE film at various temperatures against paper that has a CNF layer for two pressing times. The degree of fiber recovery in a recycling system is used to estimate the penetration degree of the polymer.

3.3 Theoretical Models and Methods

The flow in a porous media is known to be described by Darcy's law. When combined with a mass balance of an advancing liquid front into a porous media, an expression can be developed as

$$L = \sqrt{\frac{2\,\Delta P\,K\,t\,C}{\mu\,\varepsilon}} \qquad (3.1)$$

L is the penetration depth, ΔP is the pressure driving force, K is the Darcy permeability coefficient, t is time, C is a calibration constant, μ is viscosity and ε is the void fraction of the porous media. For the case of interest here, the air permeability of the samples is known and can be used to obtain K. Also, the void fraction, pressing time, and applied pressure are known values. The polymer viscosity as a function of temperature is standard to measure in the laboratory, but it is not clear what shear rate value to use in various situations. The calibration constant is to help correct for a number of assumptions such as the permeability under pressure of the molten polymer into the paper, the viscosity value used, and other issues.

The three papers used here are uncoated 80 g/m^2 wood free paper, and the same base paper with 2 and 4 g/m^2 coating of CNF. The CNF addition changes the air permeability as measured with the Gurley porosity test, that records the time for 100 cm^3 of air to flow through 645 mm^2 area of the paper with a pressure of 1.2 kPa. Using the viscosity of air and a sample thickness of 100 μm, the Gurely times of 20, 65, and 2000 s convert to permeabilities of 1x10^{-14}, 3x10^{-15} and 1x10^{-16} m^2, for uncoated, 2 and 4 g/m^2 samples, respectively. The void fraction of the paper is around 0.34 obtained from silicone oil tests.

Low-Density Polyethylene (LDPE) films from (McMaster-Carr, Item #1257T1), with a thickness of 51 μm, were cut into 127x127 mm squares. The LDPE could have been characterized in a rheometer for viscosity as a function of temperature, but concerns arose regarding sample preparation, oxidation, and other experimental artifacts. Therefore, literature values for LDPE were used for the physical properties as an estimation for the models with the realization that these properties may be quite different than this material. Aluminum foil and the paper sample were also cut to these dimensions. The foil keeps the sample from sticking to the heated block in the hot press (Carver, model: C 41000-003). The foil and PE film were first placed on the lower block for 1 min to allow the sample to obtain the set temperature of the block. The paper sample at room temperature, with the CNF layer down toward the PE film, is placed on top of the PE film. The hot press is already at the desired temperature. The press is activated to press for the desired time, here either 10 or 30 s. After accounting for the cross-sectional area of the cylinder and the sample, the pressure applied to the samples should be 0.24 MPa. After releasing, the sample is removed and cooled at room temperature. The foil becomes part of the sample but is peeled away. While these stages are quite different from the extrusion coating of paperboard, it should simulate the basic process on a laboratory scale. Figure 3.1 depicts the method.

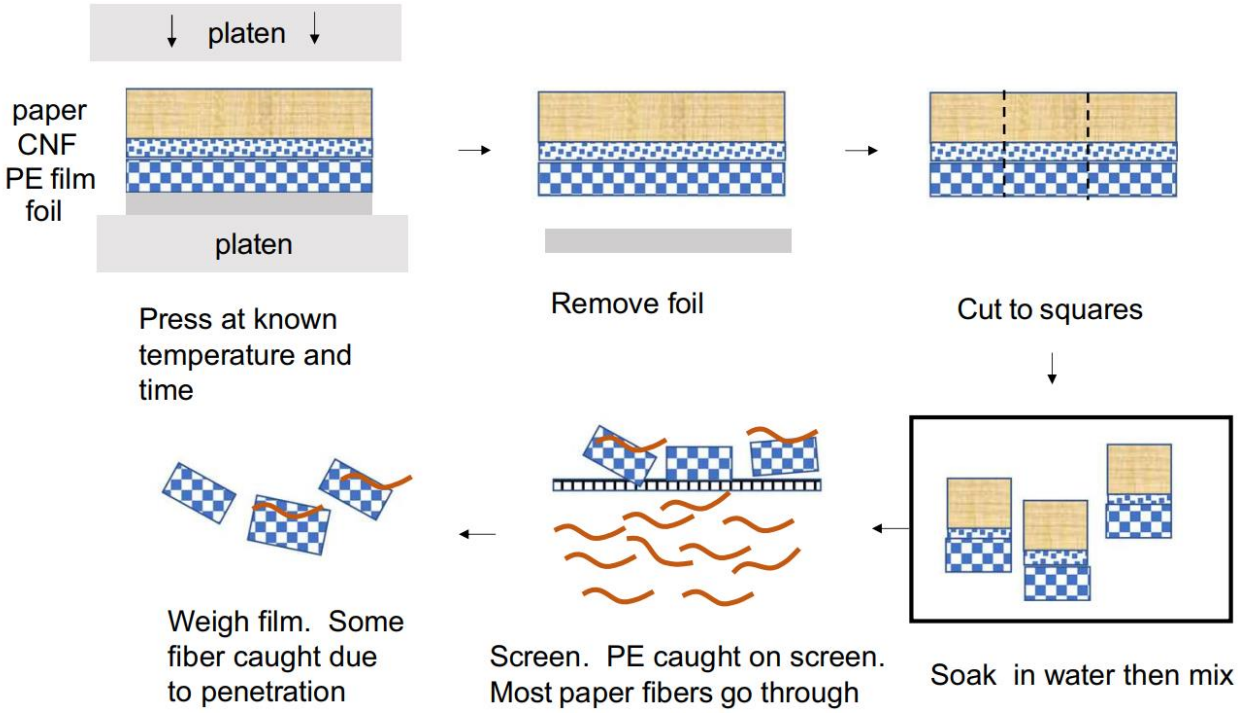

Figure 3.1. Experimental method. PE film is pressed against paper that has a CNF layer for a known time and temperature. The sample is cut and soaked to redisperse the paper fibers. After screening, the PE film is weighed to record amount of fibers caught up by the film.

After the samples are cooled, they are cut and placed into a container to stir and soaked in water for a day. The paper loses its strength and disperse in the water phase with some stirring. This process simulations the slushing process in the recycling of paper. The PE film is screened from the suspension, dried, and weighed. Any increase in weight of the PE film comes from fibers that have been incorporated into the PE film due to penetration of PE into the paper sample. The penetration depth is therefore estimated from the weight of fibers lost per area. The paper samples were around 100 μm thick. Therefore, for example, if 25% of the fibers are lost because they are incorporated into the polymer film, then the penetration depth of the polymer would be 25% of 100 μm or 25 μm.

For the CNF coated paper, the permeability is likely not uniform throughout the sample in the thickness direction. The dense top layer of CNF causes a pore layer that is quite dense, as some

SEM images have shown in the literature (Kumar et al. 2017; Mousavi et al. 2018). Therefore, the permeability measured with air is controlled by this dense layer. Since the PE is laminated to this dense layer, the permeability that controls the penetration is the measured values above. If the PE was laminated to the other side of the paper, it is expected that the penetration would be similar to the uncoated paper.

The flow of polymer or adhesive into a pore is also modeled with a commercial finite element code (COMSOL Multiphysics 5.5). Figure 3.2 shows the basics of the model set up. The inlet fluid at a set temperature is in the lower box surrounded by boundaries 1, 2, 7, and 8. The pore is the long region above this box. The problem is axi-symmetric around boundaries 1 and 3. The problem is time dependent, two phase flow using the level set method to keep track of phases, with air in the pore at the initial time. In addition, the physics "heat transfer in fluid" is used. The red line at location 4 is the initial interface between air and the adhesive. No-slip conditions are imposed at boundaries 6 and 7. Surface tension forces are imposed at the interface that can simulate capillary rise for an imposed contact angle. In addition, an inlet pressure boundary condition can be applied at boundaries 2 and 8 to simulate a pressure nip. The wetted wall and the movement of the interface along the boundary are controlled in the program under "wetted wall" applied to surface 6. Also, the temperature of the solid is imposed at this boundary. While various slip lengths were explored, the minimum element length factor f=1 gave good results.

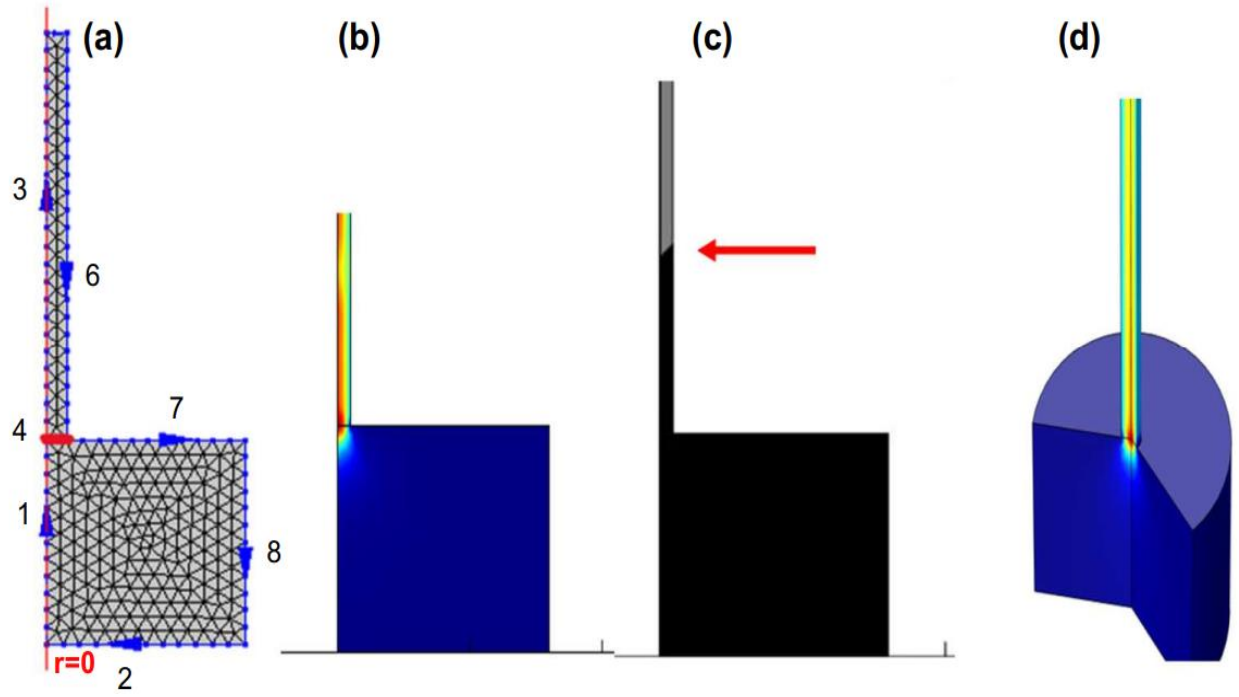

Figure 3.2. Single pore geometry in axisymmetric coordinate system a) mesh with boundary labels where position 4 is the initial meniscus between the polymer and air b) typical velocity field where blue is low viscosity and red is high, c) the advancement of the fluid into the pore with red arrow showing the meniscus, and d) a 3D rendering of the velocity magnitude.

The novel aspect of the model is that the inlet and initial temperature of the fluid can be different than the wall temperature of the pore (boundary 6). As fluid penetrates into the pore, it may cool to some extent and increase in viscosity. The viscosity of the fluid is a function of temperature. A simple expression is used as

$$\mu(T) = A\, exp\left(\frac{B}{T} - \frac{B}{T_o}\right) \qquad (3.2)$$

T_o is the initial temperature of the inlet fluid. The purpose of using this form of viscosity function is to make the viscosity increase as the temperature decreases, but at the initial temperature, the viscosity is the parameter A. If T is less than T_o, the viscosity increases to some high level depending on the value of B. The thermal conductivity of the fluid, density, and heat

capacity are the other parameters. The values of these are estimated from the literature, but a wide range of these parameters were studied.

Any model of this nature involves a number of assumptions compared to the real industrial situation. Some key assumptions here are that the pores are straight cylinders, that the polymer viscosity is not a function of shear rate but of just the temperature, and that the pores do not deform during the nip pressure pulse. We are also assuming that the pores do not interact and that the temperature of the surface of the pore does not change after contact with the hot polymer; this later assumption likely impacts the results and cause the model to over-estimate the role of the pore wall temperature. The model also neglects the influence of crystallinity and of crystal formation as the polymer may interact with the cellulose fibers. The molecular weight of the polymer, crystallinity, and the rate of cooling likely influence the results, but some of these effects should be taken into account through the viscosity-temperature relationship. The key goal of this work is to understand when heat transfer plays an important role in the penetration of polymer into the pore, and while the models are quite simple and the material parameters only estimated, the modeling work should give some guidance.

The results are compared to the Lucas-Washburn equation modified for an inlet pressure. Dimensionless quantities are used to reduce the number of parameters. The expression is

$$L^* = \sqrt{\frac{t^*}{2}\left(cos(\theta^*) + \frac{\Delta P^*}{2}\right) C} \qquad (3.3)$$

L*= L/R is the penetration depth normalized with pore radius, time is dimensionless with surface tension, viscosity and radius t* = t γ/A R, contact angle θ* = θ/θ$_r$ where r in contact angle expression is some reference angle, and ΔP* = ΔP R/γ. When ΔP* is on the order of one, surface

tension driven flow dominate the physics. When ΔP^* is larger than one, the external pressure drives the flow. C is a calibration constant used when comparing to the data.

Dimensionless groups related to heat transfer that are natural to this problem are straight forward to develop. The temperature can be scaled with T_o. Therefore, one dimensionless parameter is the magnitude of the wall temperature relative to the inlet temperature $T_w^* = T_w/T_o$. The dimensionless thermal conductivity that is natural to use is $k^* = k\, A\, T_o/\gamma^2$. The dimensionless heat capacity is $C_P^* = C_P\, A^2\, T_o/\gamma^2$. Density can be used to form a common dimensionless group called the Ohnesorge number $Oh = A/(\rho\, R\, \gamma)^{0.5}$; inertial factors are not important in the fluid mechanics because of the small pores and high viscosities involved. However, the product of the heat capacity and density appears in the energy conservation equation. Therefore, when comparing with experiments, the dimensionless group $C^* = \rho\, C_p\, R\, T_o/\gamma$ is important. The parameter B in the viscosity expression is scaled also with the initial temperature $B^* = B/T_o$.

To link the results of a single straight cylindrical pore to results with paper, an idealize situation is suggested. The void fraction, paper thickness and permeability of the paper are known. Therefore, the number of pores per unit area depends on the void fraction and pore radius. From the Hagen-Poiseuille flow in a tube, the permeability is obtained based on the number of pores per area. This picture of flow has commonly been used in the past and called parallel tube model. Combining these expressions gives the expression $K=\varepsilon\, R^2/8$. Therefore, knowing the permeability and the void fraction gives the effective radius of the pores. For the permeability of the three papers reported above, this expression gives pore sizes of 500, 270 and 50 nm, for the uncoated, 2 and 4 g/m^2 CNF coated papers, respectively. The real paper is a complex network of pores of various shapes, but this should give us an order of magnitude for the radius to use in the simulations.

3.4 Results and Discussion

Figure 3.3 shows the depth of penetration as obtained from the fiber loss data in recycling as a function of temperature of the PE film at the compression stage for three different papers that have different levels of CNF coated onto the surface. For the uncoated paper (0 g/m^2 CNF), as the PE temperature increases, the penetration increases from 11 to 35 μm. This behavior is expected because the high temperature PE film has a low viscosity: this low viscosity allows the polymer to intrude into the paper a large extent for a given applied pressure and time. The fibers that get surrounded by PE are incorporated into the PE film and are not dispersed back into the water phase during the recycling experiment. For samples with the CNF coating, the PE penetration is reduced to some extent for the 2 g/m^2 sample, and almost completely for the 4 g/m^2. These samples also had low permeability coefficients as determined by air. The viscosity of PE is a strong function of temperature; an expression is given by (Zatloukal 2016).

$$Ln(\mu) = \frac{6280}{T} - 5.7 \qquad (3.4)$$

T is in ^{o}K and viscosity is in Pa s. While this equation is not expected to be quantitative for the PE films used in the experiments, it should pick up the general temperature dependence of the PE. Other parameters needed in the model are estimated from typical values of PE given in the literature (Hansen et al. 1972; and Gaur et al. 1981).

Equation (3.1) can predict the penetration depth for various temperature and press times. Without a calibration factor, Equation (3.1) predicts quite low penetration. This could be caused by several factors such as the viscosity of the PE used does not follow Equation (3.4), the permeability of the paper is modified by polymer contact, or other assumptions in the model.

However, if the calibration factor is set to 150, the model results are obtained as shown in Figure 3.3. The results are better than expected for this simple expression considering the assumptions. The results of 30 s pressing for the 2 g/m^2 CNF layer are over predicted, but the data does not follow the expected trends either in that longer pressing time gives less penetration. While the comparison with this simple expression was better than expected, the change in the polymer temperature as it penetrates into a pore is not taken into account in this expression.

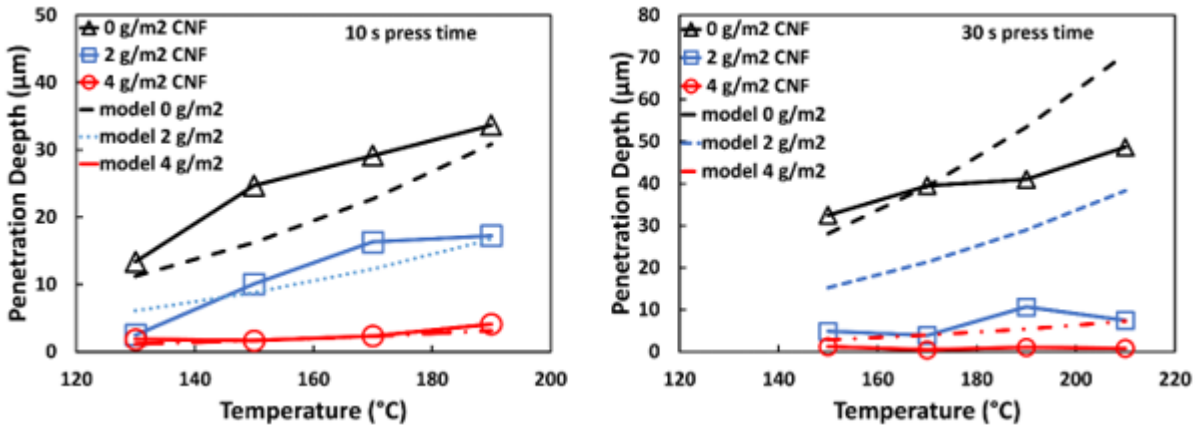

Figure 3.3. Penetration depth as a function of PE temperature for paper coated with CNF layer for 10 seconds pressing time (left) and 30 seconds pressing time (right). Model results are from Equation (3.1) using the viscosity as a function of temperature given above, and with a calibration factor of 150.

A number of issues can cause the calibration factor to be in this magnitude. First, the viscosity of the polymer was taken from literature and may not represent the viscosity of the films of PE used in the experiments. The pore space may be compressed in the experiments leading to a change in the permeability of the samples under experimental conditions. The permeability may also change as the pore space is in contact with a molten polymer. In any case, the expression after calibration does a good job at predicting the trends for different pressing times, temperatures and paper samples.

The prediction of the single capillary model using the finite element model, for isothermal conditions, is compared to Equation (3.3) in Figure 3.4 for various meshes when $\Delta P^*=50$. Various dimensional quantities such as pore radius, surface tension, pressure, and viscosity give quite similar results when compared in terms of dimensionless quantities. At short dimensionless times, there is a difference from Equation (3.3) caused by the free surface re-arrangement but at dimensionless time of 50, the normal mesh gives good results. However, as time increases, the normal mesh case tends to over predicts the penetration; finer meshes are needed to match with Equation (3.3) for long time predictions. Also, the slip factor for the three-phase contact line needs to be set to the default value of one in the code. In general, for the full range of parameters, the behavior of Equation (3.3) is captured by the model when using the normal mesh at small times and the slip factor in the code of f=1. Figure 3.2 shows a typical velocity profile and the advancement of the meniscus into the capillary.

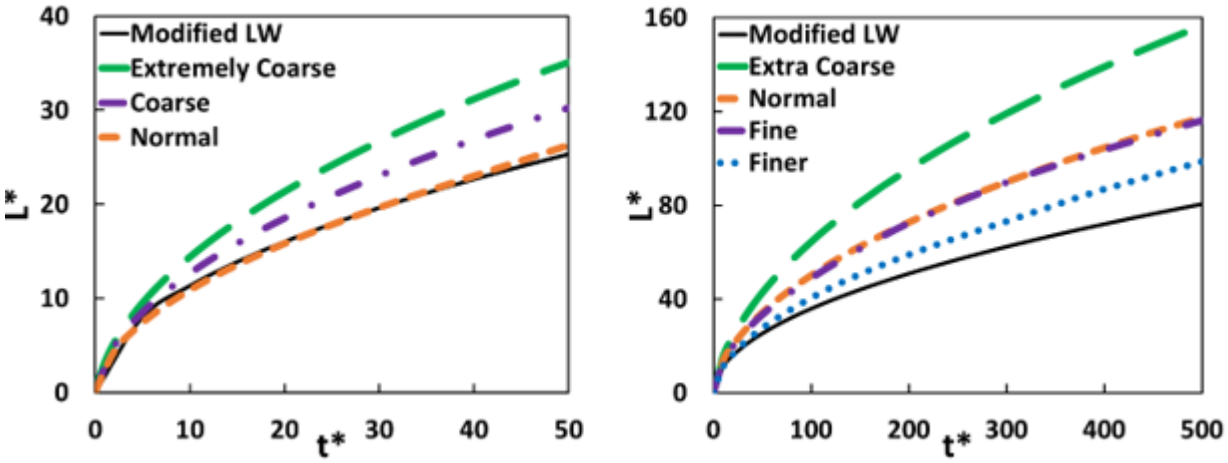

Figure 3.4. Influence of mesh on penetration prediction and comparison with Equation (3.3) for $\Delta P^*=50$. short time (left) and long time (right). These results are for isothermal conditions.

When the temperature of the capillary wall is cold compared to the fluid, the viscosity of the fluid can increase due to heat transfer as it enters the pore. Figure 3.5 shows the results for

capillary-driven flow $\Delta P^*=0$ and for pressure-driven flow $\Delta P^*=50$, with a range of wall temperatures. Other dimensionless groups are based on estimates of thermal properties of PE. When $T_w^* = 1$, the wall temperature is the same as the inlet and the behavior of Equation (3.3) is recovered. However, as T_w^* decreases, the temperature of the fluid inside of the pore decreases that leads to an increase in the viscosity of this fluid. This increase in viscosity leads to a decrease in the penetration depth of the fluid for a given time.

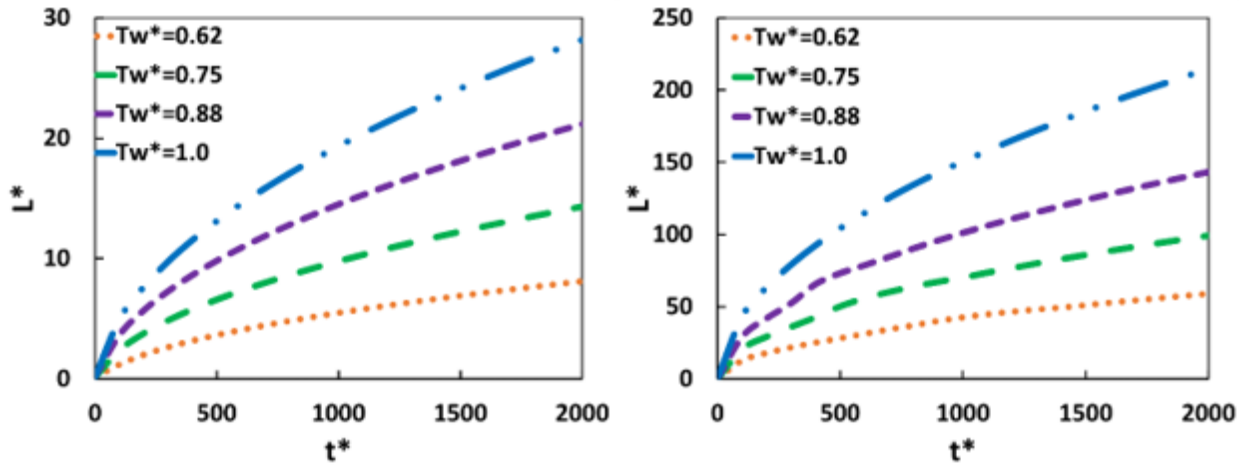

Figure 3.5. Effect of Tw* changes on the penetration depth for k*=4000, C_P^*=22,000, and B*=4 for $\Delta P^*=0$ (Left) and $\Delta P^*=50$ (Right). Equation (3.2) is used to represent the temperature dependence of viscosity.

The potential magnitude of the decrease in penetration is controlled by the parameters B* and T_w^*. The greater the temperature difference and the influence of temperature upon viscosity, the larger the potential decrease in penetration.

The conditions that lead to rapid enough heat transfer to decrease the temperature is determined by other parameters such as heat capacity, thermal conductivity, and density of the fluid; if the rate of flow into the pore is rapid compare to the rate of heat transfer, little cooling would be expected. The role of the thermal conductivity is to control the rate of cooling of the fluid inside of the pore. As k* decreases, the rate of cooling decreases, leading to the fluid in the pore

remaining at a high temperature or low viscosity. As C_p* decreases, the opposite is seen because low C_p* allows the fluid to cool rapidly in the pore and increase the viscosity. Figure 3.6 compares the behavior of the model for various values of k* and C_p* holding other parameters constant. The highest curve is for the case where the fluid mostly does not cool at all inside the pore and the lowest curves represent the cases when the fluid mostly is the pore wall temperature or a high viscosity.

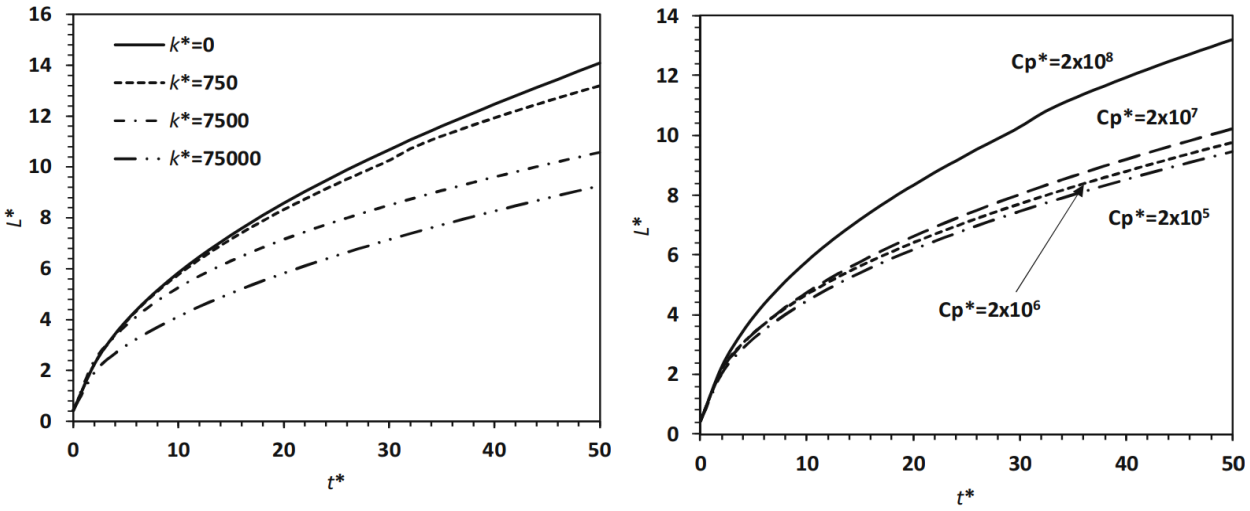

Figure 3.6. Non-isothermal flow of hot fluid into cold capillary for ΔP*=50, B*=10, Tw*=0.78 and for C_p* = 2x10^8 for various values of k*(left) and for k*=750 and with various values of C_p* (right).

When the thermal transport is small, the temperature of the fluid only cools near the surface of the capillary. The viscosity increases only a small amount. However, as the thermal transport increases, the fluid inside the pore reaches the temperature of the pore at a small distance inside the pore. The viscosity of the fluid becomes large everywhere inside the pore. Figure 3.7 shows the temperature and viscosity fields for various values of k*. It is interesting to notice when k* is small, the viscosity only increases along the layer near the pore boundary, but as k* increases, the viscosity is high throughout the pore region.

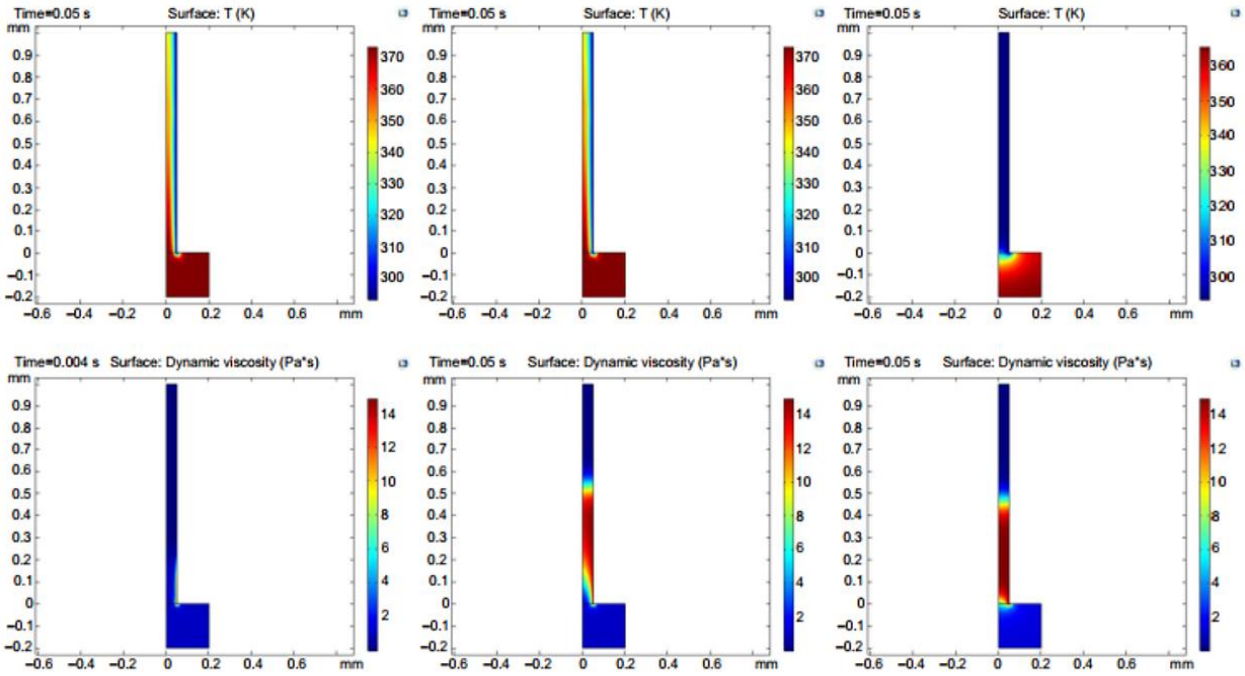

Figure 3.7. Temperature (top row) and viscosity (bottom row) distribution in the pore region for $\Delta P^*=50$, $B^*=10$, $T_w^*=0.78$, $C_p^*=2x10^8$ for values of k* of 750, 7,500 and 75,000 from left to right respectively. Blue is a low value and red is a high value.

It should be noted that even when k*=0, the code still predicts a decrease in penetration compared to the case when the wall temperature is set to the inlet temperature. This result may be due to the size of the mesh that is needed to represent the temperature distribution within the pore. Very fine meshes improve the predictions, but the computer time to run a case increases to values that are difficult. However, the penetration distance in the pore can just be predicted by Equation (3.3) for this situation, using the viscosity of the low temperature to make the dimensionless groups.

The parameters that control the importance of cooling in the pore can be combined into a single dimensionless group. If the pressure pulse is more important than capillary pressures, the dimensionless pressure has an influence; as is expected in most industrial cases, the capillary

pressure will be small compared to the pressure pulse. A combination of groups to form a new group gives

$$D^* = \frac{c^* \Delta P^*}{k^*} = \frac{\rho \, C_p \, R^2 \Delta P}{k \, A} \qquad (3.5)$$

When D* > 1000, little cooling occurs in the pore. When this group is less than 1000, the fluid cools inside the pore and the viscosity increases. This new dimensionless group is interesting in that it combines the fluid flow and heat transfer parameters into a single group; the group is similar to Prandtl number multiplied by a Reynold's number, but instead of velocity, the pressure terms are present. Small values of viscosity or thermal conductivity link to high flow rates into the pore or low heat transfer leading to less cooling in the pore. Small pore sizes generate slow flow into the pore and small heat transfer distances required to cool the fluid. Large values of pressure increase the flow and decrease the chance for cooling. This group can be useful in a practical situation in that if this combination of parameters is less than 1000, it can be assumed that the polymer cools upon entering the pore and the penetration will be reduced from what may be expected. For most reasonable estimates for material parameters for polymer, this group is often small. For example, for a pore radius of 50 μm, density of 1000 kg/m^3, heat capacity of 1200 J/kg ^{o}K, pressure pulse of 500 kPa, and a viscosity of 100 Pa s, and for a thermal conductivity of 0.5 J/m s ^{o}K, the group D* = 30. If the pore size is 5 μm, the value drops to 0.3. For these parameters, the fluid cools in the pore and the viscosity increases everywhere in the pore as represented by the right side of Figure 3.7. Even if the material parameters are changed by a factor of 10, the dimensionless group will be less than the critical value. Therefore, the temperature of the substrate is important to increase if more penetration is desired for good adhesion. For low values of

viscosity or thermal conductivity or for large pore sizes, the fluid cools only along the side of the pore, as in the left side of Figure 3.7.

For a wide range of viscosity parameters, thermal conductivity and other parameters estimated for the case of hot melt adhesives or PE films, the fluid rapidly cools as it enters the pore. This has important implications to real world operations: the temperature of the substrate is important in the process space. If penetration is too small, leading to poor adhesion performance, then one solution would be to heat up the web to allow more penetration.

One assumption in the finite element model is that the pore surface is at a set temperature and it does not change. Actually, the paper fibers would increase in temperature as it is in contact with the hot polymer. This effect can be included in future models of this system, but the goal of this work was to get an indication of the influence of substrate temperature. One assumption that can simplify the analysis is that the paper fiber surface temperature is the average of its initial temperature and the temperature of the penetrating fluid. If D* is small, we can assume that the viscosity of the fluid is the value at the average temperature and simple predictions can be obtained.

To compare the finite element model predictions to the data, parameters were taken from the experiments and from estimations of properties given in the literature. For a given temperature of the polymer, the viscosity function given above gives a value of viscosity. Knowing the predicted value of viscosity at room temperature, the value of B is obtained as 6200 ^{o}K. The pressing time was 10 and 30 s. The pressure applied to the sample from the press is around 250,000 Pa. The heat capacity and thermal conductivity of the polymer were estimated to be 0.2 J/m s ^{o}K and 1200 J/kg ^{o}K, respectively, from typical values reported in the literature. The density of the polymer was assumed to be around 1000 kg/m^3. For these parameters, the polymer is predicted to rapidly cool to the paper temperature as in the right side of Figure 3.7. Again, this assumes that

the pore surface does not heat up when in contact with the polymer. In the actual situation, the wall temperature will increase as it is in contact with the polymer. Without accounting for this issue, the model would predict that the polymer temperature would have no influence on the amount of penetration because the pore surface temperature determines the viscosity of the fluid in the pore.

Figure 3.8 compares the predictions of Equation (3.3) for the uncoated paper samples, using the viscosity that is the average between the viscosity at the applied polymer temperature and the viscosity at the paper temperature, to obtain a viscosity, with $\Delta P^*=2.5$, a pore size of 500 nm, and a correction factor of 200. This factor is even larger than the one used for the Darcy model and is a direct result of using the average temperature between the polymer and the paper, where the Darcy model just used the polymer temperature. The correct trends in the data are captured by the model and helpful projections seem possible. If careful measurements of the polymer viscosity as a function of temperature, and the permeability of the paper with a high viscosity fluid under pressure gradients were completed, the issues around a correction factor should be reduced.

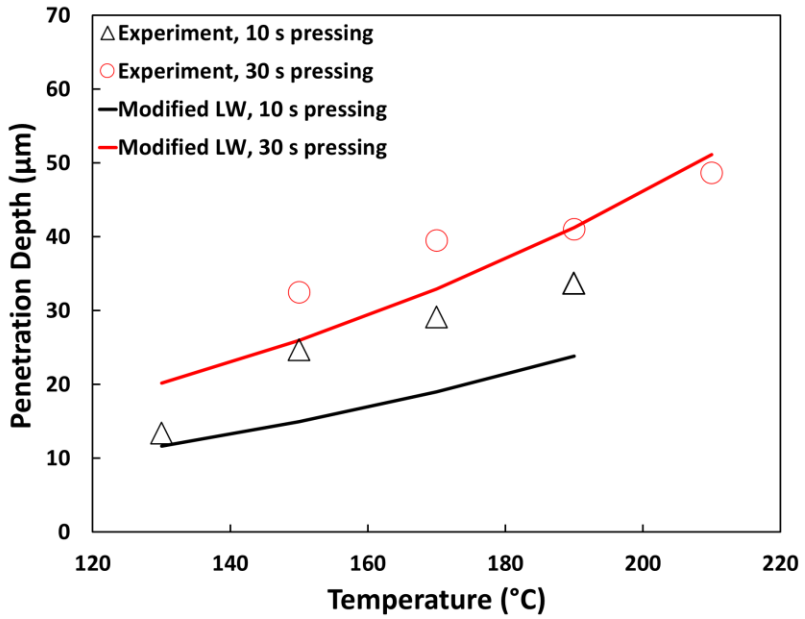

Figure 3.8. Predictions of Equation (3.3) with $\Delta P^*=2.5$, using the average of the applied and paper temperatures to obtain a viscosity, with pore size of 500 nm and two pressing times with a correction factor of 200.

3.5 Concluding Remarks

A simple expression for the penetration of a molten polymer into paper was developed based on Darcy's law. This expression predicts the behavior of PE penetration for different papers, pressing temperature, and pressing times after using a calibration factor. A pore level model was developed to describe penetration during non-isothermal situations that takes into account the change of viscosity of the fluid as it enters a pore. The model indicates that the substrate temperature is a critical parameter in the penetration of fluid because the viscosity of the fluid can increase a large amount due to cooling in the pore.

The dimensionless groups B* and T_w* determine the magnitude of the viscosity increase that links to the decrease in penetration. A new dimensionless group D* is proposed that can help predict if cooling in the pore is important or not: if D* > 1000, cooling is not expected to occur. However, for expected parameters associated with hot melt adhesives or extrusion coating of paper, this group is small and the paper temperature is expected to influence penetration. The pore level model predicts the penetration amount to some degree by using an average temperature between the paper and the polymer to estimate the viscosity.

CHAPTER 4: COMPARISON OF METHODS TO CHARACTERIZE THE PENETRATION OF HOT MELT ADHESIVE INTO PAPER

4.1 Abstract

In the use of hot melt adhesives in the production of paper-based packaging, the controlled penetration of the adhesive is important to obtain rapid setting rates, good bond strength, and the efficient use of adhesive. Measuring adhesive penetration depth has been limited to cross-sectional images, but quantifying the depth of penetration is difficult from these images. No quantitative method is well established in the literature. Four different techniques are compared to quantitatively measure adhesive penetration depth. Two methods involve separating the paperboard from the adhesive layer. Two other methods use of silicone oil penetration and mercury porosimetry to measure the decrease of pore volume after the adhesive is applied. These methods are compared with samples generated for various parameters. Experiments were conducted using a typical hot melt glue on uncoated and coated paperboard sample. Cross-sectional images from Scanning Electron Microscopy (SEM) confirm the penetration of some samples. The accuracy and repeatability of these methods were compared. Because of some issues with trying to repeatably remove the paper layer for the weight and thickness methods, and the time and cost of the mercury porosimeter method, the silicone oil method is a nice method to characterize the adhesive penetration depth.

Nomenclature

K	Permeability
μ_{air}	Air viscosity
δ_p	Paper thickness before adhesion test
V_{air}	Air volume
ΔP	Pressure driving force
a	Sample area
t_g	Gurely time
γ_{Hg}	Mercury surface tension
θ_{Hg}	Mercury contact angle
R	Pore radius
ε_s	Sample void fraction after adhesion test
W_2	Sample weight after oil soaking
W_1	Sample weight before oil soaking
ρ_{So}	Silicone oil density (0.967 g/ml)
L	Adhesive penetration depth
ε_p	Paper void fraction before adhesion test
W_B	Paper basis weight before adhesion test
V_p	Paper cumulative pore volume filled by mercury before adhesion test
V_s	Sample cumulative pore volume filled by mercury after adhesion test
δ_{rl}	Remaining layer thickness (adhesive layer plus any fibers)
δ_a	Adhesive thickness only
W_a	Adhesive weight only
ρ	Adhesive density (1 g/ml)
W_{rl}	Remaining layer weight (adhesive layer plus any fibers)
W_p	Paper weight before adhesion test
SEM	Scanning Electron Microscopy

4.2 Introduction

The penetration of liquids into a porous media is of interest to a number of industrial processes and situations. Penetration of coating and inks into paper are important in the coating and printing processes. Coating penetration and dewatering can influence the coating process (Jäder et al. 2003). (Xiang et al. 2003) discuss the influence of ink absorption into paper and the influence of this absorption on ink setting. Absorption of ink-jet inks into the paper surface is important for the quality of ink jet printing (Kettle et al. 2010). While much work has been reported for coating and inks, little attention has been given to adhesives.

Hot melt adhesives are often used to form boxes and other structures used in packaging. The adhesive is applied at a certain temperature allowing the material to flow and conforming to the paper surfaces as well as to penetrate into the pores. Water-based adhesives are also common and set by dewatering of the solution and drying. In both cases, some penetration of the material is desired to obtain good bond strength. The quality of the bond is often characterized by pulling the bond apart and looking for "fiber tear". If fibers are visible in the tear zone, the bond was stronger than the paper and is assumed to reach the best situation.

The penetration of adhesives into wood has been of interest for a number of years. Some have used imaging techniques to measure adhesive penetration depths into wood. (Paris et al. 2015) adopted the micro X-ray computed tomography (XCT) in which 3D wood–adhesive bond lines were analyzed. (Hass et al. 2012) used the synchrotron radiation X-ray tomographic microscopy (SRXTM) to measure adhesive penetration depth into the wood structure. In a review collected by (Kamke et al. 2007), the techniques used in measuring adhesive penetration into the wood are each transmitted and reflected light microscopy, fluorescence microscopy, scanning electron microscopy (SEM), transmission electron microscopy (TEM), optical microscopy, UV-

absorbance spectra captured with a UV photometer microscopy, neutron activation analysis, micro X-ray tomography (XT), and X-ray Spectromicroscopy. (Bachtiar et al. 2017) used the Scanning Electron Microscope (SEM) to measure penetration depths for the Melamine urea-formaldehyde (MUF) and animal glues (Fish and Bone glues) in a beech wood.

Little has been published around the topic of adhesive penetration into paper. Most of the previously published literature were focused on “fiber tear” after a bond is formed (Farwaha et al. 2012; Ventresca et al. 2019). Fiber tear method shows when the adhesive has penetrated enough to incorporate the first layer of fibers. Scanning electron microscopy and confocal laser scanning microscopy have been used by (Ninness et al. 2011): various tracers such as the monodisperse metallic oxide nanoparticles and Rhodamine-B dye were mixed with the glue to monitor the liquid adhesive penetration into the porous network of the coating structure after application, however, they did not try to quantify images. They also concluded the confocal laser scanning microscopy (CLSM) is the best compared to the scanning electron microscopy (SEM) and the optical microscopy in determining quantitively the extent of penetration into coating layers. These methods are good but require specialized equipment and image analysis to obtain a quantitative measurement of the penetration depth.

Paper and paperboard coatings are commonly used to increase the printing properties of paper and improve the appearance. The basic relationship of materials is reviewed by (Lepoutre 1989). The porosity of the coating layer is likely important in the setting and adhesive properties. (Dahlstrom et al. 2012) and others have reported on the various parameters that control the pore size and porosity of a coating layer. (Daub et al. 1990) also studied paper properties influencing penetration and adhesion processes. The substrate pore size is expected to play a major role in penetration and bond strength. (Dadvar et al. 2015) studied the impact of molten wax droplets on

porous Polyethylene and Teflon surfaces. This was not on paper but on polymers surfaces in which they measured droplets adhesion strengths considering substrate pore size and impact velocity.

Here, samples are generated by applying a hot melt adhesive on coated and uncoated paperboard in a hot press. Four methods to quantify the penetration of the adhesive are developed and compared. Two methods involve the removal of the paper layer from the adhesive layer after soaking in water; by weighing the final layer or by measuring its thickness, a penetration depth is determined. One method uses silicone oil to soak the sample; by looking at the decrease in the pore volume, the penetration depth can be quantified. In a similar manner, using mercury porosimetry, the loss of pore volume after the adhesive is applied can be quantified.

4.3 Materials and Methods

4.3.1 Characterization of Coated and Uncoated Paper

Uncoated 336 g/m^2 bleached wood free paper (supplied by SAPPI NA) was used in all experiments. Paper was conditioned in an environment of 23 ^{o}C and 50% relative humidity for 24 hours prior to use.

Simple paper coatings were prepared using a styrene acrylate latex (Acronal S 504 na, BASF) and a kaolin pigment (Premier, IMERYS). The coating suspension was prepared by mixing the latex with the dry pigment and adding water to obtain 60% solids. A single paperboard (432 mm × 305 mm) was coated on one side. The coating process used a rod draw down coater. Immediately after coating, the paperboard was dried in an oven maintained at 100 ^{o}C for 5 minutes.

The coated and uncoated samples were characterized in terms of porosity, surface roughness, and other basic parameters such as thickness and coat weight. The thickness of the sample was measured with a digital micrometer (Marathon) with a resolution of 1 μm while the

weight of the sample was measured with a Mettler Toledo Analytical Balance (AL204) with a resolution of 0.1 mg. The coat thickness was calculated by dividing the coat weight by the estimated density of the dry coating. The coat weight for samples was about 16 g/m^2 while the coat thickness was about 16 µm with a standard deviation of about 2 for both.

Air permeability was measured with the Gurley porosity test applying the TAPPI standard. This entailed recording the time for 100 cm^3 of air to flow through 645 mm^2 paper area with a 1.2 kPa pressure drop. The Gurley time was used to calculate the permeability of the samples as

$$K = \frac{\mu_{air}\ \delta_p\ V_{air}}{\Delta P\ a\ t_g} \qquad (4.1)$$

Where μ_{air} is air viscosity, δ_p is paper thickness, V_{air} is air volume, ΔP is pressure driving force, a is area, and t_g is Gurley time. The mercury porosimeter (Poresizer 9320, Micromeritics) was used to characterize the porosity and pore size distribution of paper. The pressure is increased as the amount of mercury that penetrates into the sample is recorded. This pressure is converted to a pore diameter using an assumed contact angle of 130^o and surface tension of 485 dyne/cm as shown in Young-Laplace equation which assumes cylindrical pores as

$$\Delta P = \frac{-2\ \gamma_{Hg}\ cos(\theta_{Hg})}{R} \qquad (4.2)$$

Where ΔP is pressure, R is radius of cylindrical pore being intruded, γ_{Hg} is mercury surface tension, and θ_{Hg} is contact angle between the mercury and the pore wall.

4.3.2 Glued Paper Preparation

Glued samples were prepared for one coated and uncoated paper sheet using a typical hot melt adhesive (TECHNOMELT® SUPRA 126, supplied by Henkel). A portable adhesive dispensing system (Mini Squirt, Nordson) was used to melt adhesive pellets at a known temperature of 175 ºC. A melted glue spot (about 10 mm in size) was applied on a paper sample equilibrated to temperature on a heated press (Model C, Carver USA). Another paper, also heated in the press, was placed on top of the spot and the press is activated to a known pressure of 0.5 or 1 MPa and time of 10 seconds. These two pressures were used after accounting for the cross-sectional area of the cylinder and the sample. After release, the sample was removed and cooled at controlled room temperature of 23 ºC and relative humidity of 50% for 24 hours. Both paper sheets were either heated to 175 ºC or kept at 25 ºC prior to pressing.

The initial masses of paper strips were recorded before the adhesion test begins. After pressing and cooling in a controlled environment, the samples were weighed to determine the amounts of adhesive used. A cut region is taken from the center of the samples with dimensions of 30 mm × 20 mm. This center region should be free of any edge effects. The weights of the cut samples were recorded. The thicknesses of the cut samples were also measured.

A workflow is summarized in Figure 4.1 showing how all the samples were generated beginning with a sheet of paper. The methods used to measure the adhesive penetration depth are described in detail in the following section.

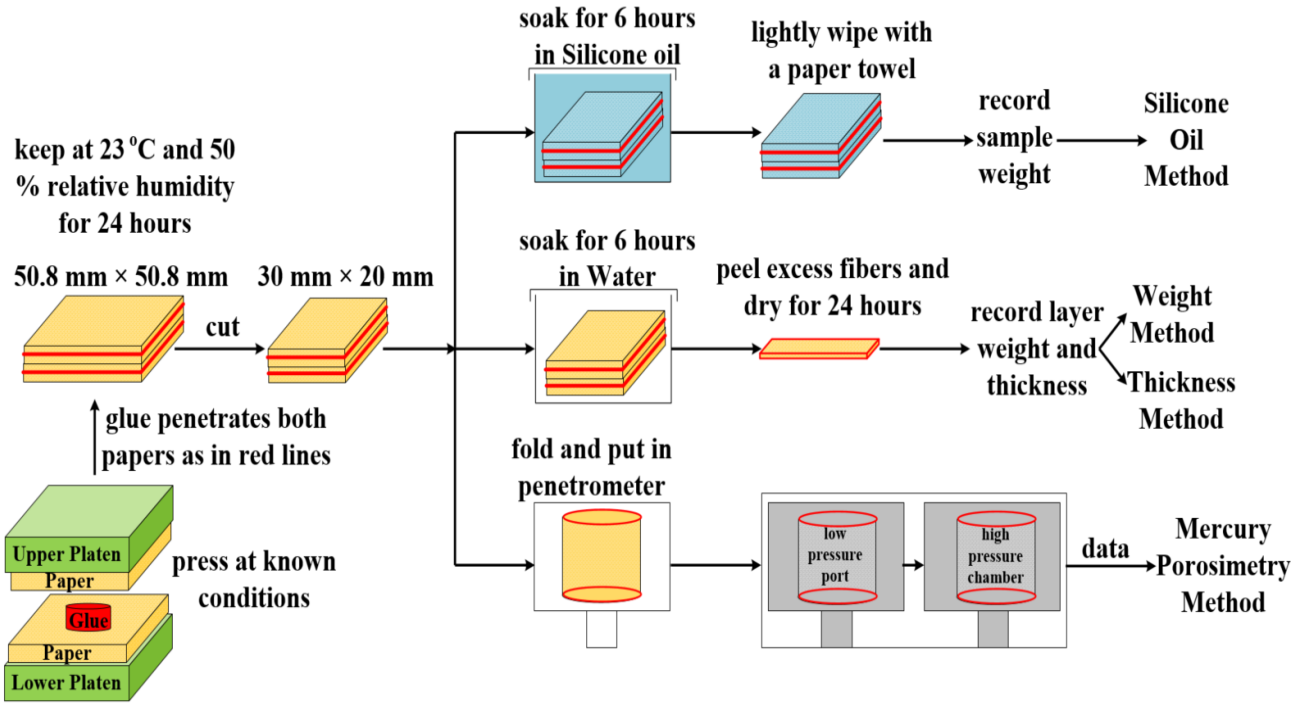

Figure 4.1. Experimental methods. Adhesive film is pressed against paper (uncoated or coated) for a known time, pressing pressure and paper temperature. The sample is cut and soaked in silicone oil test or soaked in water to re-disperse the paper fibers. Also, some cut samples are placed in penetrometer for mercury porosimetry test.

4.3.3 Adhesive Penetration Measurement Techniques

4.3.3.1 Silicone Oil Method

For the silicone oil method, we assume the oil penetrates all pores without adhesive present. Any decrease in pore volume is caused by adhesive filling up pores. Glued samples were soaked in 45 ml of silicone oil (Sigma-Aldrich, 0.1 Pa s) for 6 hours. The 6 hours soaking time was selected after trying various soaking times where 6 hours was the time required to fully saturate the paper. The soaked samples were removed and lightly wiped with a paper towel to remove any surface oil. The saturated samples were weighed to determine the mass of oil in the pores. This mass, together with the oil density, sample area, and sample thickness, should represent the percentage of the void fraction not filled by the adhesive and left in the sample, ε_s. From knowing the sample

void fraction before the adhesion test starting, ε_p, the penetration depth of adhesive into the sample is calculated from the change in void fraction as in Equation (4.4).

$$\varepsilon = \frac{W_2 - W_1}{a \ \delta_p \ \rho_{So}} \qquad (4.3)$$

$$L = \frac{\varepsilon_p - \varepsilon_s}{\varepsilon_p} \ \delta_p \qquad (4.4)$$

Where L is adhesive penetration depth, W_2 is sample weight after oil soaking, W_1 is initial sample weight, a is sample area, δ_p is paper thickness before adhesion test, ρ_{so} is silicone oil density which is 0.967 g/ml, ε_p is paper void fraction before adhesion test, and ε_s is sample void fraction after adhesion test. The subscripts p, s, and so refer to paper, sample, and silicone oil, respectively.

4.3.3.2 Mercury Porosimetry Method

The mercury porosimeter (Poresizer 9320, Micromeritics) is used to characterize the porosity and pore size distribution of paper. The instrument increases the pressure from 0 up to 30,000 psia (207 MPa) with an accuracy of ±1% psia of full scale. This range of pressure covers a pore diameter ranging from 0.006 to 360 μm. The device has two built-in low-pressure ports and one high-pressure chamber. The size and volume of the pores are related to the pressure causing the intrusion and the volume of mercury forced into the pores, respectively. The final data provided by the instrument are the pressure psia, pore diameter μm, mean diameter μm, cumulative pore area ml/g, log differential intrusion ml/g, and incremental pore area ml/g.

The mercury porosimetry method is similar to the silicone oil method. Mercury intrusion into pores without adhesive occurs at high pressure. Glued samples were mounted in the

penetrometer (a cylinder of a maximum of 25 mm in diameter and 25 mm long) that uses a wire coil to avoid contact with the walls. The sample chamber was evacuated and filled with mercury. The pressure was increased and the amount of mercury penetration into the sample was recorded. The total intruded volume was recorded for the base paper and the paper-adhesive combination. Any differences in the volumes should represent the volume of pores taken up by the adhesive. The equation to measure the adhesive penetration depth for this method is shown below:

$$L = W_B\ (V_p - V_s) \qquad (4.5)$$

Where L is adhesive penetration depth, W_B is paper basis weight before adhesion test, V_p is paper cumulative pore volume per sample weight filled by mercury before adhesion test, and V_s is sample cumulative pore volume per sample weight filled by mercury after adhesion test. The subscripts p, and s represent paper, and sample, respectively. The cumulative pore volume of pores 0.01-285 μm in diameter are used with this method. The intrusion volumes are not corrected for compression effects as others have done because the volumes are subtracted from each other in Equation (4.5).

4.3.3.3 Thickness and Weight Methods

For these methods, paper without adhesive penetration was removed from the glued samples by soaking in water. Glued samples were placed into containers of 100 ml of water at room temperature for 6 hours. After water soaking, the paper loses its strength and can be removed from the adhesive layer with embedded fibers. In some cases, a sharp knife was needed to separate the adhesive layer from the paper.

The thickness of the dry adhesive layer plus the embedded fibers of the water-soaked samples was used to quantify the adhesive penetration depth. The thickness of the sample was measured using a micrometer. The initial adhesive layer thickness can be obtained from the weight of the adhesive using the density of the adhesive and the area of the sample. Therefore, the penetration depth is the difference between the measured thickness of adhesive layer plus fibers and the initial adhesive layer thickness. This gives the thickness of fibers embedded, which represents the adhesive penetration depth. The set of the equations for this method is shown below:

$$L = \delta_{rl} - \delta_a \qquad (4.6)$$

$$\delta_a = \frac{W_a}{\rho\, a} \qquad (4.7)$$

Where L is adhesive penetration depth, δ_{rl} is thickness of adhesive and fibers embedded in, δ_a is adhesive thickness only, W_a is adhesive weight only, ρ is adhesive density which is around 1 g/ml, and a is sample area.

The weight method involves measuring the mass of the adhesive layer plus the embedded fibers after water soaking. The dry mass of this layer was measured. Knowing the paper basis weight and area, the adhesive weight is known. Then, the adhesive penetration depth is calculated as

$$L = \frac{W_{rl} - W_a}{W_p}\ \delta_p \qquad (4.8)$$

Where L is adhesive penetration depth, W_{rl} is weight of adhesive and fibers embedded in the adhesive layer, W_a is adhesive weight only, W_p is paper weight before adhesion test, and δ_p is paper thickness before adhesion test. The weight of the adhesive layer was determined by the weight increase per unit area of the sample.

All of the methods have various draw backs or assumptions. The silicone oil method depends on removing the surface oil after taking the sample from the soaking stage without removing oil inside the sample. The mercury porosimetry method may have artifacts related to mercury access to all pores, sample mounting and preparation. The weight and thickness method depends on separating the paper fibers away from the adhesive layer without removal of the adhesive. The depth of penetration of the hot melt adhesive is compared using all methods described above.

4.3.3.4 Scanning Electron Microscopy (SEM)

The glue penetration depth into uncoated and coated paper samples was characterized by Scanning Electron Microscopy (Amray 1820) of sample cross-sections. Glued samples were cut into 0.5 cm × 1 cm with a razor blade and mounted on an SEM stub (flat and on edge) with carbon adhesive pads. Sample edges were painted with colloidal silver liquid (Electron Microscope Sciences) and dried. The samples were then coated with 6 nm of Au/Pd using a Creesington 108 auto sputtercoater with a Cressington 20 mtm thickness controller. The stubs were then imaged using an Amray 1820 SEM at a working distance of 10 mm and an operating voltage of 5 kV. Penetration depth was estimated as the distance from the surface to the deepest adhesive indication.

4.4 Results and Discussion

The paperboard properties of the uncoated and coated papers are shown in Table 4.1. All properties are within the normal expected ranges. The void fraction is obtained from Equation (4.3) and the average pore diameter is from the mercury porosimetry results of the base sheet.

Table 4.1. Uncoated and coated paperboard properties.

	Thickness (μm)	Basis Weight (g/m^2)	Air Permeability (m^2)	Void Fraction	Pore Diameter (μm)
Uncoated	430	336	3.0×10^{-14}	0.50	6.57
Coated	446	352	1.3×10^{-15}	0.48	0.05

Figure 4.2 shows initial mercury porosimetry results for a sample glued at 175 °C paper temperature and 0.5 MPa pressing pressure with a control sample (no glue). The data indicate higher pore volume in the glued sample which is hard to explain. This result was repeatable and was seen in other cases. Either the high-pressure mercury can separate the glued paper and create additional pores within the glue/fiber interface, or water vapor is formed when the hot adhesive contacts the paper and gets trapped in the sample generating extra pores. Paper clips were used to prevent the paper from separating under mercury pressure and to remove pores which may occur from extra pores generated by water vapor during pressing. The exact mechanism causing more pores to be generated is not clear at present. The results after securing the glued sample with paper clips are also shown in Figure 4.2. Because the paper clips generate results in line with expected trends, paper clips were used on all of the mercury porosimetry data to quantify adhesive penetration.

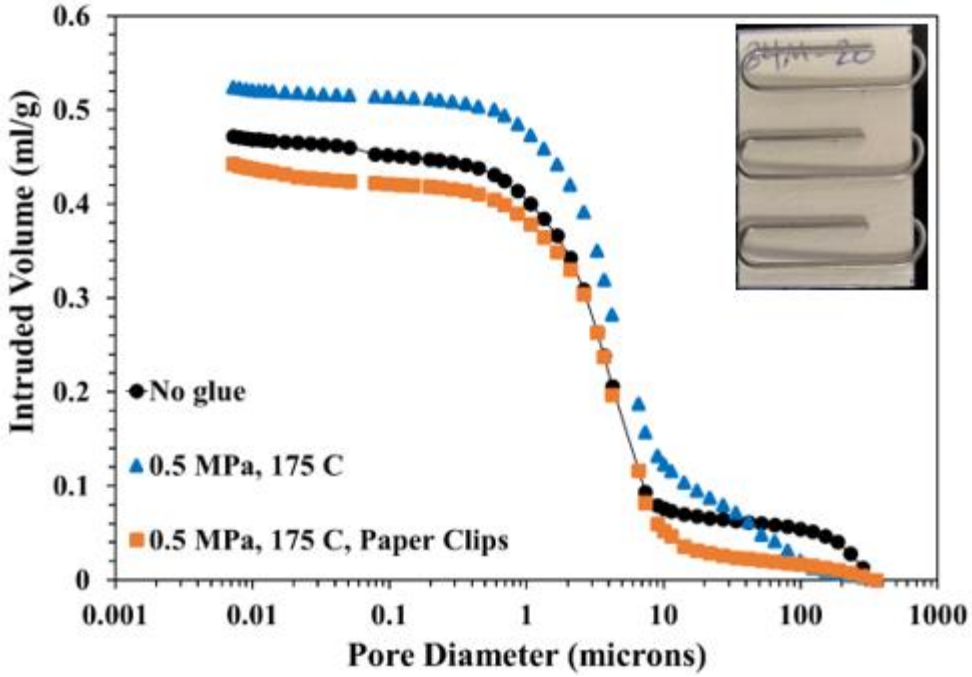

Figure 4.2. The effect of paper clips on the mercury porosimetry results (orange curve). Image of the sample with paper clips is in the upper right corner.

Average adhesive penetration depths and their 95% confidence intervals for uncoated paper are shown in Table 4.2. Measurements were made in triplicate for all methods except mercury porosimetry. Overall, the different methods roughly measure the same average penetration depths. Moreover, they all follow the expected trend with changes in adhesion conditions. High paper temperature should promote penetration because the adhesive does not cool upon contact with the paper.

For the lower paper temperature and pressing pressure (25 ºC and 0.5 MPa), the silicone oil method resulted in slightly high average penetration depth followed by the thickness method then the weight method. However, within a confidence interval of each other, they are all giving a similar result. The average penetration depth was between 18−46 µm for all methods at 25 ºC paper temperature and 0.5 MPa pressing pressure. Increasing pressing pressure to 1 MPa at the same paper temperature of 25 ºC resulted in lower average penetration, but still within the

confidence interval. Increasing paper temperature to 175 ºC at the same 0.5 MPa pressing pressure did increase in the average penetration depths to between 88−130 μm for all methods. This trend is expected. Based on modeling results, the adhesive does not cool increasing viscosity as it penetrates into the pore space. Increasing pressing pressure further to 1 MPa at 175 ºC did not influence penetration depths for both paper temperatures. At 25 ºC paper temperature, both silicone oil and mercury porosimetry methods were close in penetration depths for both pressing pressures. At 175 ºC paper temperature, the silicone oil and weight methods were in good agreement for both pressing pressures.

The maximum confidence interval calculated was ±29 μm for all pressing pressures and paper temperatures. This value seems reasonable, especially if we are comparing four methods that are different in their calculations, experimental preparations, and uncertainties. In a conclusion for the glued uncoated samples, the agreement is good for the average adhesive penetration depths with reasonable confidence intervals for all methods regardless of paper temperatures and pressing pressures.

Table 4.2. Average penetration depths and their 95% confidence intervals for glued uncoated paper (μm) for different paper temperatures and press pressures.

T (ºC)	ΔP (MPa)	Silicone Oil Method	Thickness Method	Weight Method	Mercury Porosimetry Method
25	0.5	42±17	32±11	18±17	46
175	0.5	130±16	88±29	111±27	107
25	1	40±17	22±15	10±8	52
175	1	135±8	101±27	121±19	110

Penetration depths are for one direction of samples.

For the coated paper samples, average adhesive penetration depths and their 95% confidence intervals are shown in Table 4.3. Similar to the uncoated results, measurements were made in triplicate for all methods except mercury porosimetry. For samples prepared under identical conditions, there was good agreement across all measurements, within confidence intervals. All methods follow the expected trend with changes in conditions. Penetration depths were lower than the uncoated samples, as expected because of reduced porosity of the surface.

The other important finding in these results is the adhesive penetration depths were not much influenced by the pressing pressures. Modest increases were observed from 38 to 66 μm for the silicone oil method, 32 to 43 μm for the thickness method, and 20 to 46 μm for the weight method as pressing pressures increased from 0.5 to 1 MPa. The average penetration depths were in good agreement between thickness and mercury porosimetry methods for all conditions. Overall, the average penetration depths were in good agreement between all methods compared to the average penetration depths measured for the glued uncoated samples regardless of paper temperatures and pressing pressures.

Table 4.3. Average penetration depths and their 95% confidence intervals for glued coated paper (μm) for different paper temperatures and press pressures.

T (°C)	ΔP (MPa)	Silicone Oil Method	Thickness Method	Weight Method	Mercury Porosimetry Method
25	0.5	38±32	32±11	20±4	35
175	0.5	46±11	36±20	43±4	38
25	1	49±15	29±12	20±19	24
175	1	66±30	43±7	46±10	32

Penetration depths are for one direction of samples.

The cross-sectional image obtained from the SEM analysis for the glued uncoated samples is shown in Figure 4.3. It is difficult to tell what is adhesive and what is fiber when interpreting SEM images. The cracks in the paper on both sides is an indication of adhesive penetration depth. The penetration depth is indicated and marked with arrows inside the image. From this image, one can conclude the glue penetrates deeper inside the paper than the case with the glued coated sample and it was within a 106 µm distance inside the paper. This value was obtained from the average penetration depths in six different locations in the image. On the other hand, the average penetration depths for uncoated samples (Table 4.2) which were glued at 175 °C and 1 MPa ranged from 101 to 135 µm for the silicone oil, thickness, weight, and mercury porosimetry methods. The agreement is reasonable between the four methods and the SEM data.

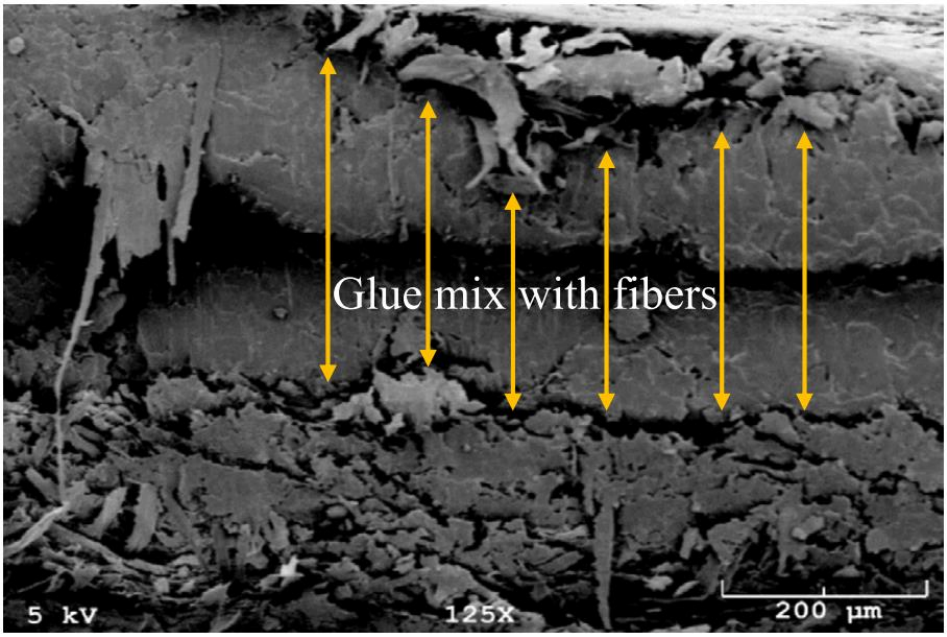

Figure 4.3. SEM cross sectional images for glued uncoated paper sample. The sample was glued at 175 °C paper temperature, 1 MPa pressing pressure, and 10 seconds pressing time.

Figure 4.4 shows the SEM images for the coated sample. The glue penetrates through the coating layer into the fiber matrix; this is evident in the red rectangle in the right-hand side image. For the left-hand side image, arrows were drawn to indicate the penetration depths. From the red rectangle and arrows, the penetration depth was around 52 µm distance inside the paper. This measurement was obtained from the average penetration depths in six different locations in the image. The average penetration depths for coated samples glued at 175 ºC and 1 MPa were listed in Table 4.3 and ranged from 32 to 66 µm for the silicone oil, thickness, weight, and mercury porosimetry methods. The agreement is good between all methods and SEM data.

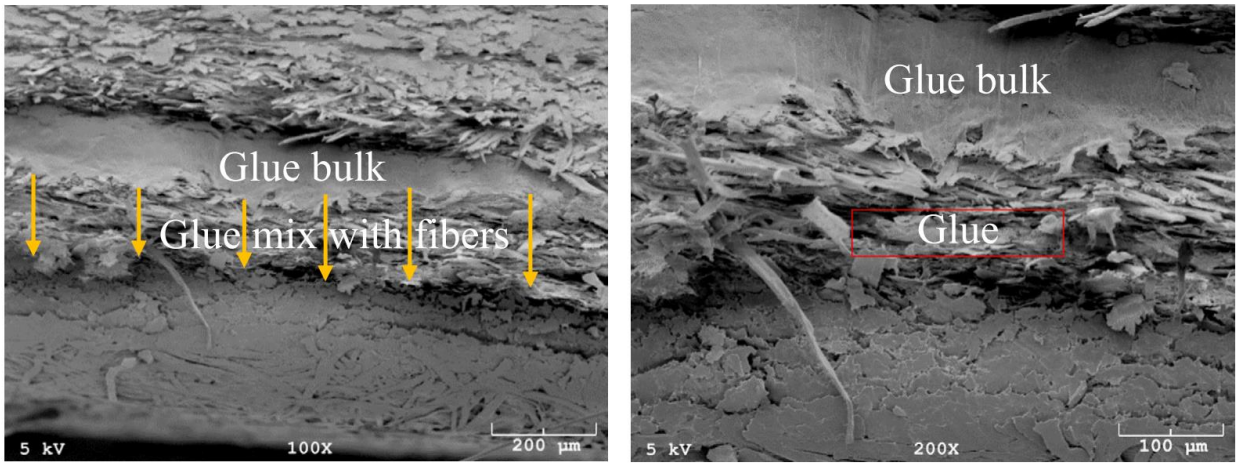

Figure 4.4. SEM cross sectional images for glued coated paper sample. The sample was glued at 175 ºC paper temperature, 1 MPa pressing pressure, and 10 seconds pressing time. Left image is at 100x and right image is at 200x showing the region of adhesive mixed with fibers.

4.5 Comparison of Methods

Table 4.4 summarizes the strengths and weaknesses of the different adhesive penetration measurement methods. The silicone oil method does not require the peeling of samples and is quite simple, but the thickness and area of the samples are needed as well as the weight before and after soaking. There is some skill in removing the silicone oil that is not in pores but on the outside of the sample. The mercury porosimetry method also does not require peeling and is calculated easily from output of the device, but the measurement requires special equipment, and some questions remain about the need for paper clips on the samples. The weight and thickness methods both require the removal of the paper from the adhesive layer. Therefore, both of these are listed as moderate difficulty because of the uncertainty about this removal and its influence on the weight or thickness of the adhesive layer.

Table 4.4. Strengths and weaknesses of all methods.

Methods	Peeling samples after soaking	Numbers of variables in calculations	Uncertainty	Assumptions	Relative complexity	Results repeatability based on 95 % confidence intervals
Silicone Oil Method	No	5	Moderate	Oil is removed from the surface of the sample only after taking the sample from the soaking stage	Low	±17 to ±32
Mercury Porosimetry Method	No	3	Low	Samples generate extra pores that was needed to use paper clips to compress them	High	–
Thickness Method	Yes	4	Low	Separating the paper fibers away from the adhesive layer is done without removal of the adhesive	Moderate	±7 to ±29
Weight Method	Yes	6	High	Separating the paper fibers away from the adhesive layer is done without removal of the adhesive	Moderate	±4 to ±27
Scanning Electron Microscopy	No	1	High	Penetration depth is measured as an average of approximate depths in different locations in the image	High	–

4.6 Concluding Remarks

Four novel experimental techniques were developed to measure adhesive penetration depths into coated and uncoated paper. The four techniques were internally consistent. Three of the techniques require minimal laboratory equipment and expertise while providing good quantification of adhesion penetration depth. The mercury porosimetry method picked up extra pores which seem to be generated by the high-pressure mercury intrusion into the samples. Securing the sample with paper clips eliminated this problem and the method gave similar results to the other three methods.

The accuracy, complexity, repeatability, and assumptions of all methods were compared. Interpreting SEM images to quantitively measure adhesive penetration depths are difficult especially when the fibers are encapsulated with the glue. However, the cross-sectional images from the SEM confirmed the adhesive penetration depth of some samples and agreed well with the four developed techniques. All methods agreed with what was expected: more penetration when the paper is hot and less penetration when there is a coating layer. The silicone oil method seems to be a good balance between ease of use, accuracy, and costs.

CHAPTER 5: PREDICTION OF NON-ISOTHERMAL POLYMER PENETRATION INTO TWO POROUS LAYERS

5.1 Abstract

Understanding the dynamic fluid flow in a porous media considering temperature changes is of general interest over a wide range of applications such as flow in porous catalytic reactors, flow in packed distillation columns, and hot melt adhesive flow into paper and wood. The penetration of a hot melt adhesive into paper substrate is important to quantify in order to make good use of the adhesive and to obtain good adhesion, but the literature is lacking in this area. A model, based on Darcy's law, is developed that accounts for temperature differences between the adhesive and the paper; an energy balance is used to determine the temperature and viscosity of the adhesive in the pore space. The model also accounts for different layers of pore space and for the limited supply of adhesive. Experiments were conducted to quantify penetration depth and final bond strength of a hot melt adhesive that is pressed into well-characterized paperboard and coated paperboard under different conditions of temperature and pressure. The model agreed well with experimental results for different papers, press pressures, and paper temperatures. The permeability of the coating layer was found to be a key parameter in controlling the penetration degree. For uncoated samples, the paper temperature was a key parameter that influenced penetration depth.

5.2 Introduction

The general problem of predicting viscous fluid penetration into a porous substrate is important in a wide range of industries and applications. Examples include polymer glue-based adhesion of porous materials, reactant penetration into porous catalysts, polymer penetration into textiles, and coating penetration into wood. With the move to replace plastic packaging with sustainable options, gluing operations are needed to form cellulose-based packaging such as boxes or other structures. When hot-melt adhesives are used, the penetration of the adhesive into the pore structure of the paper is important to characterize. A quantitative understanding of the penetration of hot melt adhesives is needed to optimize the use of these adhesives and to obtain good quality products.

The flow in a porous material has been studied for decades. In some cases, the flow is steady-state, such as in a catalyst bed or an absorption column. In other situations, the flow is dynamic such as the penetration of a fluid into a capillary or porous structure. The penetration of liquids into capillaries and porous membranes has been recently summarized: for the viscous liquids, the liquid front follows the square root of time or the Lucas-Washburn equation, while for the low viscous liquids, they found that the liquid penetrated with a constant velocity that was different from the Bosanquet value (Kornev et al. 2001). Others have introduced a three-dimensional multiphase lattice Boltzmann model to solve two-phase fluids penetration in complex porous media (Shi et al. 2019). They summarized how porosity, contact angle, density ratio, hydrophobic-hydrophilic surfaces, interfacial tension, and viscosity ratio affect the penetration process. Lubrication theory was used to model a droplet spreading on rough permeable substrates that included absorption and contact line motion (Espín et al. 2015). Others used a finite element method to describe the flow into complex geometry obtained from X-ray tomography images from

a soil sample (Cooper et al. 2017). One- and two-phase flows in highly permeable porous media was recently reviewed for isothermal flows (Davit et al. 2019): Darcy's law was modified to capture inertial effects and extended for the two-phase flows to couple the two phases via cross terms. The droplet flow on the surface of a textile was modeled and confirmed that the penetration was driven by inertia at the initial stages and viscous forces at later stages; the later stages were controlled by threshold pore size, liquid characteristics, and droplet diameter (Zhang et al. 2018).

Heat or mass transfer may be important in these processes as the fluid interacts with the porous media, especially if the porous media and the fluid are at different temperatures. An experimental study on a steady fluid flow with heat and mass transfer in a porous packed bed shows how heat transfer can influence the fluid flow (Sheridan et al. 1992). The numerical investigation on a steady and incompressible laminar flow with heat and mass transfer in a porous cylindrical duct also shows how non-isothermal effects influence the flow (Bousri et al. 2017). A method to solve the steady multi-dimensional fluid flow with heat or mass transfer in porous media using mass and energy conservation laws and Darcy's law has been presented; the solution requires the coupling of the viscosity terms with the temperature (Younes 2003). A pore-scale numerical study on steady flow and heat transfer in fibrous porous media has been proposed: both permeability and thermal conductivity coefficients were studied as functions of solid volume fraction and temperature, respectively (Hosseinalipour et al. 2019). Scanning electron microscope images were used to obtain medium characteristics such as fibers diameter, orientation, and contact areas. A strong relationship was observed between the fiber diameter and the medium permeability but the effect of viscosity as a function of temperature was not included. A review of the most common models for nanofluid flow and heat transfer in porous media has been given (Kasaeian et al. 2017).

Adhesives are used in a variety of applications and industries. Examples of adhesives are polyurethane, epoxies, starch, and hot melt adhesives. Hot melt glues are a common type of system that requires applying a molten polymer to the surface that sets as it cools. A wide range of polymers has been used for hot melt adhesives such as ethylene-vinyl acetate (EVA) copolymer, polyethylene (PE), alkyl acrylate ethylene copolymer, ethylene butyl acrylate (EBA), polyamide polymers as well as amorphous poly alpha olefins (Lee et al. 2000; Godfrey et al. 1994). In the setting of hot melt glues in paper systems, the polymer often needs to penetrate a small distance into the paper to generate mechanical interactions and bonding. Adhesion is not usually obtained by the formation of covalent bonds but by the mechanical interlocking between the polymer when cooled and the paper. It is known that coatings on paper influence the ability for the adhesive to work properly but little is reported on this in the literature.

Isothermal fluid penetration into paper has been examined for decades because of the importance of the application of surface treatments to paper. Some previous literature focused on the penetration that occurs during the paper coating process and during the setting of inks on a porous coating layers: expressions were based on Darcy's law but also included the effect of filtercake formation in the ink layer (Xiang et al. 2004). The penetration depth of fluid into paper during slot die coating has been reported: fluid viscosity was not the key parameter affecting the penetration depth while coating speed, flow rate, permeability, and porosity were important in the process (Ding et al. 2013). A pore network model for the imbibition of a coating fluid in a paper during coating has been proposed: both the paper pore space and the coating fluid's viscosity were found to influence the penetration in a time-dependent flow (Ghassemzadeh et al. 2001; Ghassemzadeh et al. 2004). A review of the penetration during slot die coating on porous media

has been given (Ding et al. 2017). These models and studies were not concerned with the viscosity change of the fluid that may occur as it interacts with the porous layer of a different temperature.

To account for the influence of temperature on the viscosity of the fluid, the unsteady-state heat transfer problem must be solved along with the momentum equation. Our group modeled the penetration of polyethylene into paperboard coated with cellulose nanofibers: the flow into a single capillary was modeled and the change of temperature and its influence on viscosity was included (Khlewee et al. 2021). Dimensionless groups were developed to characterize when the change of viscosity influenced the flow in the capillary. For typical condition of paper and hot melt adhesives, the adhesive is expected to cool a significant amount as it penetrates into the paper pores. While this model gave insights into non-isothermal penetration, it is limited to understanding of a single pore and requires finite element methods.

The final bond strength is usually a function of the ability of the polymer to penetrate to some extent into the substrate. When an adhesive penetrates a porous medium, bonds will be formed based on both intermolecular forces and mechanical interlocking (Dadvar et al. 2015). The influence of latex type and content in a coating layer on the adhesion of coated paper has been reported but the penetration of the hot melt adhesive into the coating layer was not characterized.

In this work, we describe a model for viscous fluid penetration into a porous media in conjunction with experimental measurements of penetration depth. The model accounts for heat transfer between the hot melt glue and the coated paper, and subsequent viscosity changes in the glue during penetration. Experimentally, the paperboard was coated with a typical paper coating composed of latex and pigments. The amount of latex and the pigment type was varied to generate different porosities in the coating layer. A typical hot melt adhesive is applied at a known temperature onto paper samples that are held at a known pressure and temperature. The degree of

penetration is characterized by a silicone oil absorption method that characterizes the decrease in pore volume after the adhesive is applied.

5.3 Materials and Methods

Uncoated 336 g/m^2 bleached kraft paper (supplied by SAPPI NA) was used in all experiments. Paper was conditioned in an environment of 23 ^{o}C and 50% relative humidity for 24 hours prior to use.

Simple paper coatings were prepared using a styrene acrylate latex (Acronal S 504 na, BASF) and kaolin pigments that are medium, fine, and coarse (Premier, Astra-glaze, Astra-plate, IMERYS), respectively. The amount of latex was varied at 10, 20, 30 and 40 pph (parts per hundred parts pigment). The coating suspension was prepared by mixing the latex with the dry pigments and adding water to obtain 60% solids. A single paperboard (432 mm × 305 mm) was coated on one side with a rod draw down coater. Immediately after coating, the paperboard was dried in an oven maintained at 100 ^{o}C for 5 minutes.

The coated and uncoated samples were characterized in terms of porosity, surface roughness, and other basic parameters such as thickness and coat weight. The thickness of the sample was measured with a digital micrometer (Marathon) with a resolution of 1 μm while the weight of the sample was measured with a Mettler Toledo Analytical Balance (AL204) with a resolution of 0.1 mg. The coat thickness was estimated by dividing the coat weight by a typical density of the dry coating. The coat weight for samples was about 15-17 g/m^2. The dry coat thickness was estimated to be about 16 μm.

The mercury porosimeter (Poresizer 9320, Micromeritics) was used to characterize the porosity and pore size distribution of paper. The pressure is increased as the amount of mercury that penetrates into the sample is recorded. This pressure is converted to a pore diameter using an

assumed contact angle of 130º and surface tension of 485 dyne/cm from the Young-Laplace equation.

Glued samples were prepared for paper coated with 10, 20, 30, and 40 pph (parts per hundred parts pigment) styrene acrylate, SA, and medium pigment size, 10 pph styrene acrylate and fine pigment size, and 10 pph styrene acrylate and coarse pigment size. Glued samples were also generated using uncoated paper sheets. A typical hot melt adhesive (TECHNOMELT® SUPRA 126, supplied by Henkel) was used for all experiments. A portable adhesive dispensing system (Mini Squirt, Nordson) was used to melt adhesive pellets at a known temperature of 175 ºC. A melted glue spot (about 10 mm in size) was applied on a paper sample equilibrated to temperature on a heated press (Model C, Carver USA). Another paper, also heated in the press, was placed on top of the spot and the press is activated to a known pressure of 0.5 or 1 MPa and time of 10 seconds. These two pressures were used after accounting for the cross-sectional area of the cylinder and the sample. After release, the sample was removed and cooled at controlled room temperature of 23 ºC and relative humidity of 50% for 24 hours. Both paper sheets were either heated to 175 ºC or kept at 25 ºC prior to pressing.

The initial masses of paper strips were recorded before the adhesion test begins. After pressing and cooling in a controlled environment, the samples were weighed to determine the amounts of adhesive in the region of interest; some adhesive is squeezed out radially from the region of interest. After that, a cut region from the center of the samples is taken with dimensions of 30 mm × 20 mm. This center region should be free of any edge effects. The weights of the cut samples were recorded. The thicknesses of the cut samples were also measured.

A workflow is summarized in Figure 5.1 that shows how all the samples were generated beginning with a sheet of paper. The method used to measure the adhesive penetration depth is by looking at the decrease in pore volume after the adhesive is applied.

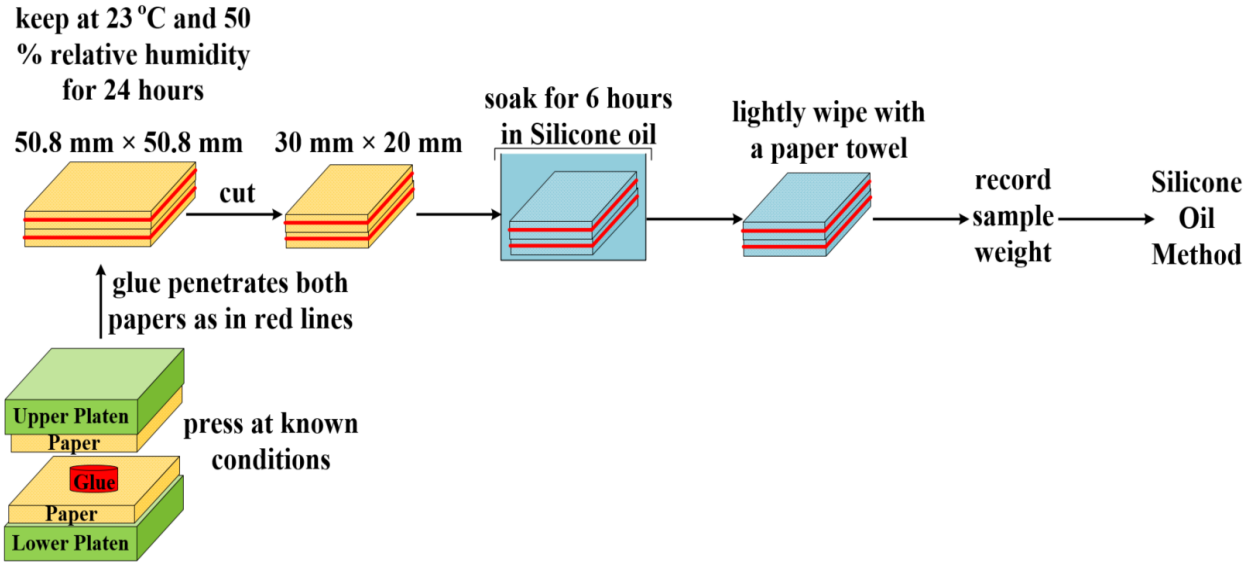

Figure 5.1. Experimental method. Adhesive film is pressed against paper that is uncoated or coated for a known time, press pressure and paper temperature. The sample is cut and soaked in silicone oil. The change in void fraction is linked to penetration depth.

Some of the glued samples at 50.8 mm wide and 50.8 mm long were peeled using a mechanical tester (model 5564, INSTRON, Norwood, MA, USA). Unbounded regions of 1 cm are clamped into a grip of the mechanical tester on one side and into a peel wheel with tape on the other side. Figure 5.2 shows an image of a sample being installed on a peel wheel and ready for peeling test. The peeling occurs at 90° as the paper-glue region is peeled from the paper at a rate of 50.8 mm/min. The force and displacement are recorded.

Figure 5.2. Peel wheel test separating two glued samples.

Adhesive penetration depths were measured using a silicone oil absorption method. This method was compared with three other methods to quantify adhesive penetration and was found to be repeatable and convenient (Khlewee et al. 2022). The loss of pore volume should correlate to the volume of pores filled with adhesive. Glued samples were soaked in 45 ml of silicone oil (Sigma-Aldrich, 0.1 Pa s) for six hours to fully fill pores in the sample. The soaked samples were removed and lightly wiped with a paper towel to remove any surface oil. The saturated samples were weighed to determine the mass of oil in the pores that allows the calculation of void fraction of the sample as:

$$\varepsilon = \frac{W_2 - W_1}{a \ \delta_p \ \rho_{So}} \qquad (5.1)$$

The void fraction, ε, can be calculated for the paper that does not have glue and for the sample after the adhesion test as in Equation (5.2) below. W_2 is the sample weight after oil soaking, W_1 is the initial sample weight, a is the sample area, δ_p is the paper thickness before adhesion test, and ρ_{so} is the silicone oil density which is 0.97 g/ml. The void fraction that is not filled by the adhesive and left in the sample, ε_s, can be determined as well as the starting void fraction. From knowing the sample void fraction before the adhesion test starting, ε_p, the penetration depth of adhesive into the sample is calculated from the change in void fraction as:

$$L = \frac{\varepsilon_p - \varepsilon_s}{\varepsilon_p} \ \delta_p \qquad (5.2)$$

Here L is the adhesive penetration depth, ε_p is the paper void fraction before adhesion test, and ε_s is the sample void fraction after adhesion test.

Due to the limited amounts of adhesive applied, there is a penetration depth that uses up all of the adhesive available in the region of interest and is called the maximum penetration depth. This depth can be calculated from the weight and density of the adhesive transferred to the sample divided by the area and porosity of the sample. Knowing the paper basis weight and area, the adhesive weight is known from the sample weight. The maximum penetration depth can be then calculated as:

$$L_{max} = \frac{W_a}{\rho \ a \ \varepsilon_P} \qquad (5.3)$$

Where L_{max} is maximum penetration depth for the amount of adhesive applied, W_a is adhesive weight only, ρ is adhesive density which is around 1.0 g/ml, a is paper area, and ε_p is

paper void fraction before adhesion test. The L_{max} was divided by two because experiments have the adhesive flowing in two directions.

Air permeability was measured with the Gurley porosity test applying the TAPPI standard. This test entailed recording the time for 100 cm^3 of air to flow through 645 mm^2 paper area with a 1.2 kPa pressure drop. For a single uniform layer, the permeability of the paper is calculated from Darcy's law as:

$$K = \frac{\mu_{air}\ \delta_p\ V_{air}}{\Delta P\ a\ t_g} \qquad (5.4)$$

Where K is permeability, μ_{air} is viscosity of air, δ_p is thickness of paper, V_{air} is volume of air, ΔP is pressure drop, a is area for flow, and t_g is Gurley time.

When there are two layers, the paper and the coating, the pressure drop over each layer must sum to the total pressure drop but each layer has a different permeability and thickness. The expression is:

$$\Delta P = \Delta P_1 + \Delta P_2 = \frac{L_1\ \mu_{air}}{K_1\ t_g}\left(\frac{V_{air}}{a}\right) + \frac{L_2\ \mu_{air}}{K_2\ t_g}\left(\frac{V_{air}}{a}\right) \qquad (5.5)$$

Solving for the coating layer permeability in terms of other quantities gives:

$$K_2 = \frac{L_2}{\frac{\Delta P\ t_g\ a}{\mu_{air} V_{air}} - \frac{L_1}{K_1}} \qquad (5.6)$$

Where L_1 is paper thickness, K_1 is paper permeability, L_2 is coating layer thickness, and K_2 is coating layer permeability. The thicknesses are known and K_1 is obtained from measuring the

paper only. Equation (5.6) therefore allows a good estimate of the permeability of the coating layer on paper.

5.4 Model of Penetration into Two Layers Accounting for Cooling

As a hot adhesive enters a pore, the adhesive will cool, increasing its viscosity. This change in viscosity in turn should change the rate of its flow into the pore. Earlier work showed that for most situations, the heat transfer inside the pore will be rapid, equilibrating the paper and the adhesive temperature (Khlewee et al. 2021). Therefore, one simple and practical approach is to assume that the viscosity of the adhesive inside the pore is that of the conditions from the energy balance. The energy increase of the paper must equal the energy loss of the adhesive. For example, if the adhesive temperature is T_o and the porous media is at T_p, then the equilibrated temperature of the adhesive T would be given by an enthalpy balance as:

$$\rho\ Cp\ \varepsilon_p(T_o - T) = \rho_p Cp_p\ (1 - \varepsilon_p)(T - T_p) \qquad (5.7)$$

Where ρ is density of adhesive, Cp is heat capacity of adhesive, T_o is inlet temperature of adhesive, T is adhesive equilibrated temperature given by an enthalpy balance, ρ_p is density of paper, Cp_p is heat capacity of paper, ε_p is void fraction of paper before adhesion test, and T_p is temperature of paper. Solving for the equilibrated temperature gives:

$$T = \frac{\rho\ Cp\ \varepsilon_p\ T_o + \rho_p Cp_p\ (1 - \varepsilon_p)\ T_p}{\rho\ Cp\ \varepsilon_p + \rho_p Cp_p\ (1 - \varepsilon_p)} \qquad (5.8)$$

The adhesive viscosity is adjusted to the equilibrated temperature. For most reasonable estimates for material parameters for adhesive and paper, the temperature obtained from the energy balance is close to the simple average of the paper and adhesive temperature. Now Darcy's law

can be used with the viscosity of the adhesive adjusted to the appropriate temperature. The viscosity is assumed to be a function of temperature as:

$$\mu(T) = A\, exp\left(\frac{B}{T} - \frac{B}{T_o}\right) \qquad (5.9)$$

Where T is temperature calculated from Equation (5.8), T_o is adhesive application temperature, and A and B are constants that are known from viscosity-temperature behavior of the adhesive. The values that best match the data provided by the adhesive supplier are A = 0.92 Pa s and B = 4427 ºK. If T is less than T_o, the viscosity increases to some high level depending on the value of B. For the adhesive used here, the viscosity is 6.7 Pa s at 100 ºC and 0.92 Pa s at 175 ºC.

Darcy's Law is used to model the flow and calculate the penetration depth of adhesive into porous paper. If the adhesive viscosity is constant during the press, the adhesive penetration depth for pressure-driven flow into a porous media can be predicted by integrating Darcy's law combined with a mass balance V=L a ε, where V is the volume penetrated and a is area, gives:

$$\frac{dL}{dt} = \frac{K\,\Delta P}{\mu\,\varepsilon\,L} \qquad (5.10)$$

Where K is permeability coefficient, ΔP is pressure driving force, μ is viscosity, ε is void fraction of the porous space and L is penetration depth. This expression has been reported by others to predict the penetration of inks into porous coatings (Xiang et al. 2004). Figure 5.3 shows a schematic of the adhesive, the paper coating layer, and the paper layer. If the adhesive penetrates the coating layer only, then a single-layer model is adequate.

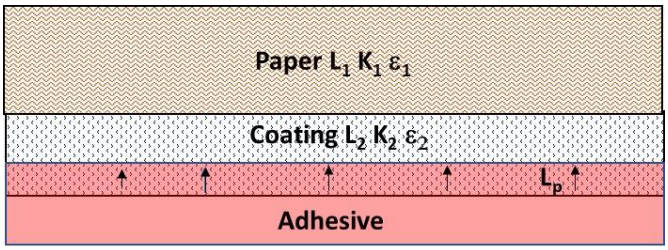

Figure 5.3. Two-layer system penetration.

When there is a limited amount of adhesive, we can modify the expression with a term that causes the rate of penetration to go to zero as the depth of penetration reaches the maximum L_{max}. A possible expression for the penetration depth, L_p for a single layer is:

$$\frac{dL_P}{dt} = \frac{K_2\, \Delta P\, (1 - \frac{L_P}{L_{max}})}{\mu\, \varepsilon_2\, L_P} \qquad (5.11)$$

Equation (5.11) is a modification of Darcy's law to account for a limited amounts of adhesive. As L_P increases to L_{max}, the rate goes to zero. L_p is the instantaneous penetration depth of the adhesive into the porous paper, t is time, μ is viscosity, ΔP is pressure driving force, K_2 is coating layer permeability, ε_2 is coating layer porosity, and L_{max} is maximum penetration depth. If we are using uncoated sheets without coating layers, then Equation (5.11) is still being used but with K_1 and ε_1 instead of K_2 and ε_2, respectively.

If the adhesive goes past the coating layer, then it is called L_{P1} and can be calculated based on the resistance to flow through the coating layer plus the increasing resistance to flow in the paper. The two-layer model becomes:

$$\frac{dL_{P1}}{dt} = \frac{\Delta P\ (1 - \frac{L_{P1}}{L_{max}})}{\frac{L_{P1}\,\mu\,\varepsilon_1}{K_1} + \frac{L_2\,\mu\,\varepsilon_2}{K_2}} \qquad (5.12)$$

Equation (5.12) can be integrated where L_{P1} is adhesive penetration depth into the paper layer in addition to the coating layer thickness. The viscosity used in the models is the value at the temperature obtained in Equation (5.8) inserted into Equation (5.9).

In summary, the basic concept of viscous flow in a porous media is modified to include the multi-layer system with finite adhesive quantity, using the viscosity of the adhesive that corresponds to the expected temperature of the adhesive obtained from an energy balance.

5.5 Results and Discussion

The paperboard properties of the uncoated and coated papers are shown in Table 5.1. All properties are within normal ranges. The permeabilities in Table 5.1 are calculated assuming that the paper and its coating are one uniform material, applying Equation (5.4). As latex content increases in the coating layer, the pore size and permeability decrease. The pigment size had a small influence on the pore size and permeability compared to the latex content. Knowing the permeability of the paper only, and using Equation (5.6), the permeability of the coating layer can be obtained and reported in Table 5.1. The permeabilities of the coating layers are three orders of magnitude smaller than that of the paper. The average pore diameter of the coating layers is less than 100 nm. The pore size reported is the peak obtained in the log-differential volume plots of the mercury porosity data in the low range of the data of Figure 5.4.

Table 5.1. Uncoated and coated paperboard properties.

	Thickness (μm)	Basis Weight (g/m^2)	Void Fraction	Pore Diameter (μm)	Paper and coating layer Permeability (m^2)	Coating layer Permeability (m^2)
Uncoated	430	336	0.50	6.6	3.0×10^{-14}	–
10 pph SA+Medium Pigment	446	352	0.48	0.05	1.3×10^{-15}	4.8×10^{-17}
20 pph SA+ Medium Pigment	446	352	0.47	0.03	8.0×10^{-16}	3.0×10^{-17}
30 pph SA+ Medium Pigment	446	352	0.44	0.02	5.5×10^{-16}	2.0×10^{-17}
40 pph SA+ Medium Pigment	446	352	0.44	0.02	3.8×10^{-16}	1.4×10^{-17}
10 pph SA+Fine Pigment	446	352	0.47	0.04	1.1×10^{-15}	4.1×10^{-17}
10 pph SA+Coarse Pigment	446	352	0.48	0.05	7.4×10^{-16}	2.7×10^{-17}

All is an average of a minimum of five repeats except the pore diameter.

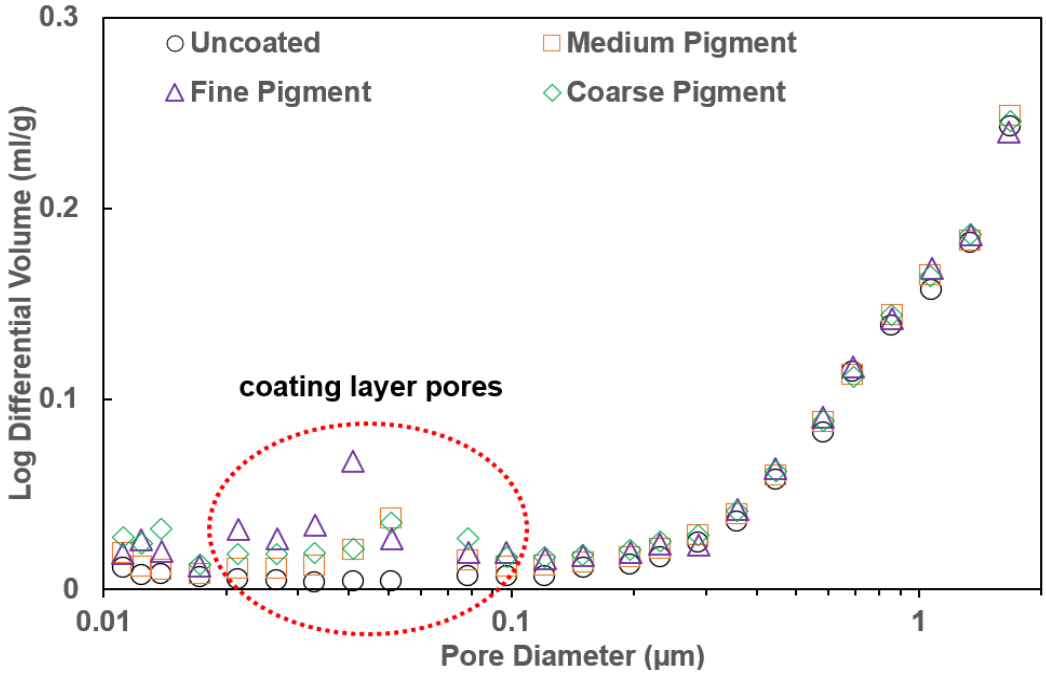

Figure 5.4. Log differential volume results of mercury porosimetry for non-glued coated and uncoated paper for paper coated with 10 pph latex and fine, medium, and coarse pigment sizes in the fine pore region. The coating layer generates pores in the range of 20-100 nm.

For all samples and process conditions, the normal one-layer model, Equation (5.10), overpredicted the experiments by a large amount. For example, Equation (5.10) overpredicted the uncoated results of 680 μm for conditions of 175 °C paper temperature and 0.5 MPa press pressure. This value is more than the thickness of the paper. This result likely is due to the limited amount

of adhesive in the experiment, where Equation (5.10) assumes an unlimited supply. This result clarifies the need to have a limit on the penetration depth.

Table 5.2 shows the experimental adhesive penetration depths compared to the model predictions for uncoated samples glued at different paper temperatures and press pressures. The experimental and model results were not influenced to a large degree by the increased press pressures but the paper temperature did influence the experimental results. The 175 ^{o}C paper temperature increased the penetration depth to about three times that of the 25 ^{o}C at the same press pressures, respectively. The model overpredicted the experiments by a significant amount at the low paper temperature but at the high paper temperature, the agreement is good. This overprediction may be due to the viscosity value used in Equation (5.11). The viscosity values of the adhesive were in the range of 163 – 191 ^{o}C. While the viscosity-temperature function Equation (5.9) fits the values well in this range, it is not clear that the adhesive viscosity at 100 ^{o}C is predicted by the viscosity function.

Table 5.2. Average penetration depths and their 95% confidence intervals for uncoated paper and the one-layer limited adhesive model (μm) for different paper temperatures and press pressures.

T (°C)	ΔP (MPa)	Experiment	One-layer model
25	0.5	42±17	165
175	0.5	130±16	157
25	1	40±17	193
175	1	135±8	152

For coated paper samples, to calculate the adhesive penetration depth from the model, we first use Equation (5.11) to see if the adhesive penetrates the coating layer only. If the number calculated is greater than the coating layer thickness (16 μm), Equation (5.12) is used to account for second layer.

Two forms of the model were used for all figures below: the triangle is calculated from Equation (5.11) and shows the one-layer limited adhesive model. The circle is calculated from Equation (5.12) and shows the two-layer limited adhesive model. Experimentally, a total of six different coating layers with different porosities and pore size were used to generate the glued samples. The penetration depths in all figures are for one direction of samples. Measurements were made in triplicate for all experimental results.

Figure 5.5 shows the experimental adhesive penetration depths compared to the model predictions for samples glued at 25 ^{o}C paper temperature and 0.5 MPa press pressure using four latex levels for the medium pigment size. It is clear that as the latex level increases, the adhesive penetration depth decreases, in line with the permeability. The penetration depth decreased from 38 to 8 μm as the latex level in the coating increases from 10 pph to 40 pph. This trend likely is caused by the reduced permeabilities of the samples that were coated with high latex levels. The difference in penetration depth between coated and uncoated is dramatic and also correlates with the difference in permeability. Equation (5.11) underpredicted the penetration for the 10 and 20 pph. This result may be caused by the weak coating layer that could get incorporated into the adhesive layer instead of remaining as a layer that resists flow. Using Equation (5.8) to predict the glue temperature inside the pore and substituting this value in the viscosity function, Equation (5.9), significantly improved the agreement between the model and experiment.

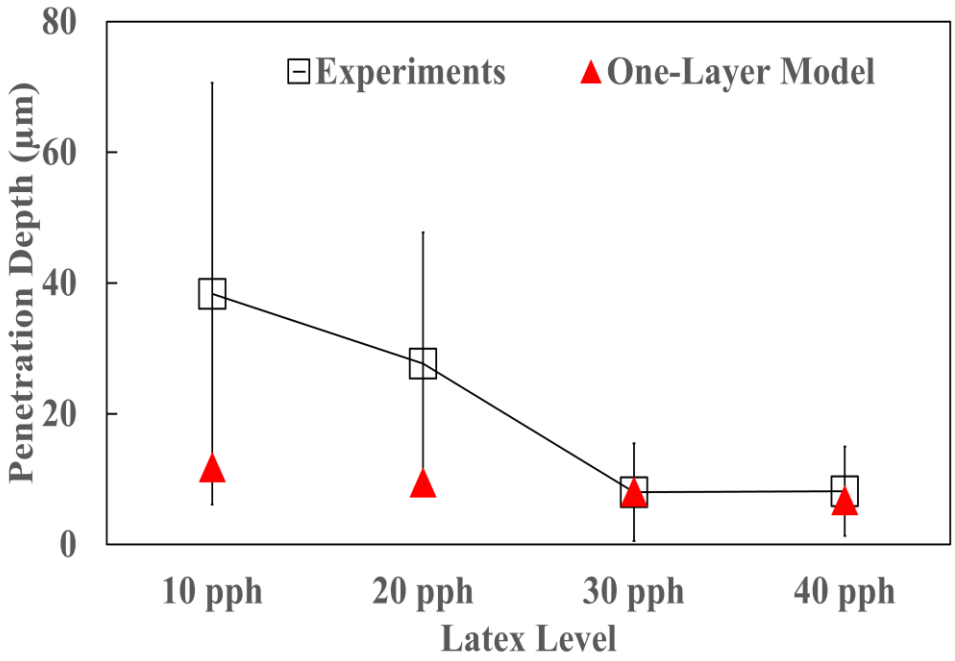

Figure 5.5. Penetration depth results for 0.5 MPa press pressure and 25 ºC paper temperature, for the medium size pigment.

Figure 5.6 shows the penetration depth results for samples glued at 175 ºC paper temperature and 0.5 MPa press pressure. Here, the paper temperature was increased to the same value as the adhesive which should result in little cooling as the adhesive flows into the pores. The temperature increase did not influence the results for the coated glued samples at the same press pressure. To compare the theory to the experiment data, the modification of Darcy's to have two-layer and limited adhesive, Equation (5.12), resulted in excellent agreement with the experimental results for all coated samples. It is worth mentioning that when the paper temperature increased to 175 ºC, the results of the model agreed well with the 10 and 20 pph compared to the 25 ºC case above.

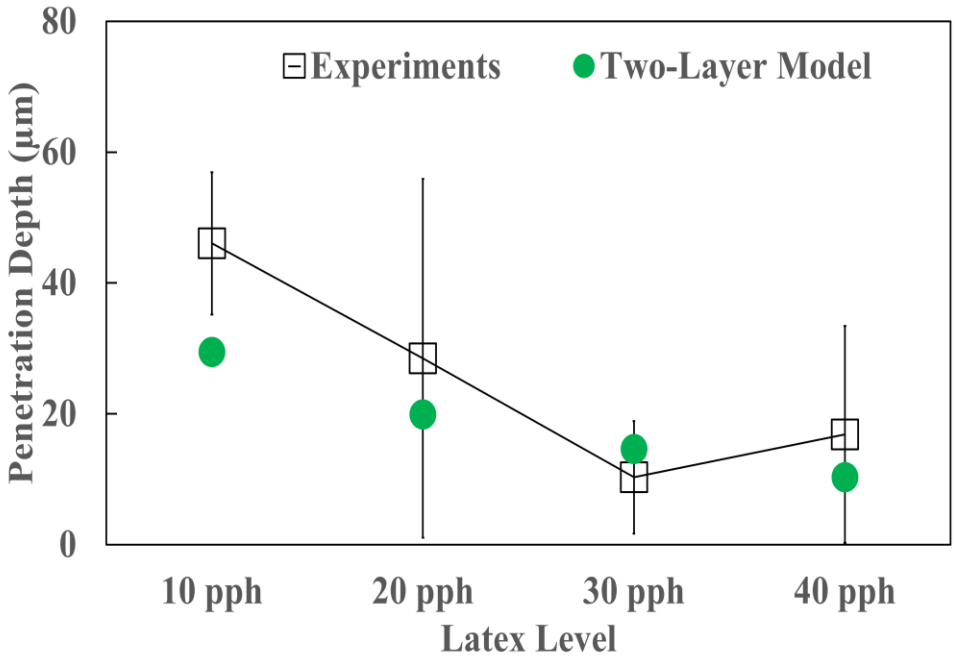

Figure 5.6. Penetration depth results for 0.5 MPa press pressure and 175 ^{o}C paper temperature, for the medium size pigment.

Increasing the press pressure further to 1 MPa did not significantly influence the experimental and model data for both 25 ^{o}C and 175 ^{o}C paper temperatures. Figure 5.7 shows the experimental results and model predictions for samples glued at 25 ^{o}C paper temperature and 1 MPa press pressure. As the press pressure increased to 1 MPa at the same 25 ^{o}C paper temperature, the predicted penetration depths increased around 3-5 µm. Similarly, the experimental penetration depths increased to about 5-11 µm for coated samples. In general, Equation (5.11) gives a reasonable prediction for the coated paperboard samples.

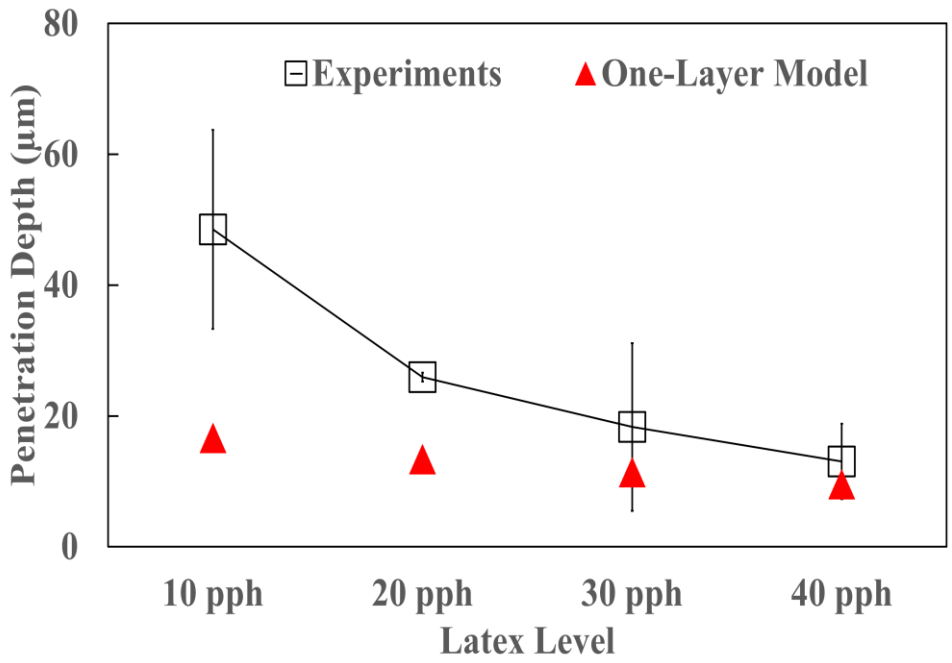

Figure 5.7. Penetration depth results for 1 MPa press pressure and 25 °C paper temperature, for the medium size pigment.

Figure 5.8 shows the comparison of experiments with the model for samples glued at a paper temperature of 175 °C and press pressure of 1 MPa. Similar to Figure 5.6, the agreement was within reason between the experiments and the model for the coated samples. Fixing the pressure at 1 MPa and increasing the paper temperature to 175 °C resulted in more penetration into the pores structure. For example, the penetration depths obtained from the model were increased by about 24 µm for the 10 pph glued samples. For the experimental results, the increase in depths was about 20 µm for the 10 pph glued samples.

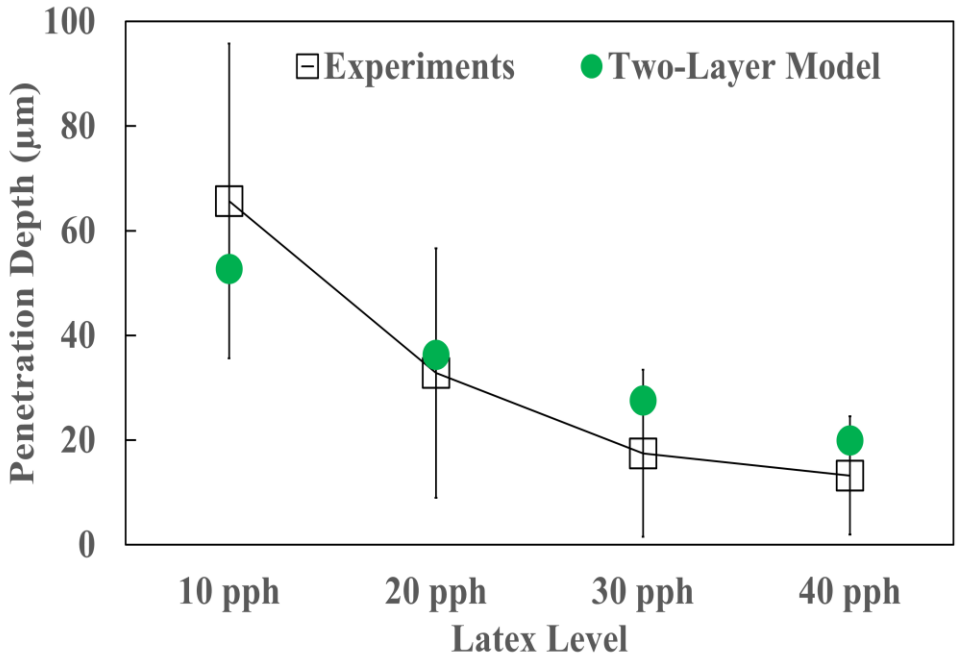

Figure 5.8. Penetration depth results for 1 MPa press pressure and 175 °C paper temperature, for the medium size pigment.

Changing the pigment size at the same latex level did not influence the results to a large extent. This correlates to the change in permeability of the coating layers. Table 5.3 shows the penetration depth results at 0.5 MPa press pressure and 25 °C paper temperature for samples coated with 10 pph latex level and fine, medium, and coarse pigment sizes. In comparison to the model results, the results for the one-layer limited adhesive model underpredicted the experimental results by around 20 µm for this case. This underprediction is hard to explain but may link to the viscosity used at the calculated average temperature that is out of the range of the correlation.

Table 5.3. Average penetration depths and their 95% confidence intervals for experimental glued 10 pph coated paper and the one-layer limited adhesive model (µm) for 0.5 MPa press pressure and 25 °C paper temperature, for the fine, medium, and coarse pigment sizes.

	Fine	Medium	Coarse
Experiments	30±23	38±32	33±4
One-layer model	11	12	9

Some tensile test analyses were performed on samples glued at the same adhesion conditions reported above. Figure 5.9 shows adhesive strength (load) versus penetration depth for various samples glued at two press pressures and two paper temperatures. In Figure 5.9, a and b are the results for adhesions at the low press pressure while c and d are the results for adhesions at the high press pressure. When the penetration depth is high due to the high paper temperature (low adhesive viscosity), the load needed to peel the sample apart is high as well, especially for the uncoated samples. The loads were close for the samples glued at 25 ^{o}C paper temperature.

When the press pressure increased to 1 MPa as in Figure 5.9 (c, d), the loads increased in some places and remained constant in other places for both paper temperatures. As the paper temperature increased from 25 to 175 ^{o}C, the adhesive penetration depth increased from 42 to 130 µm and the load needed to peel the sample apart increased from 11 to 40 N for the 0.5 MPa press pressure. On the other hand, the 1 MPa press pressure resulted in penetration depth increased from 40 to 135 µm and the load from 13 to 46 N as the paper temperature increased from 25 to 175 ^{o}C, respectively.

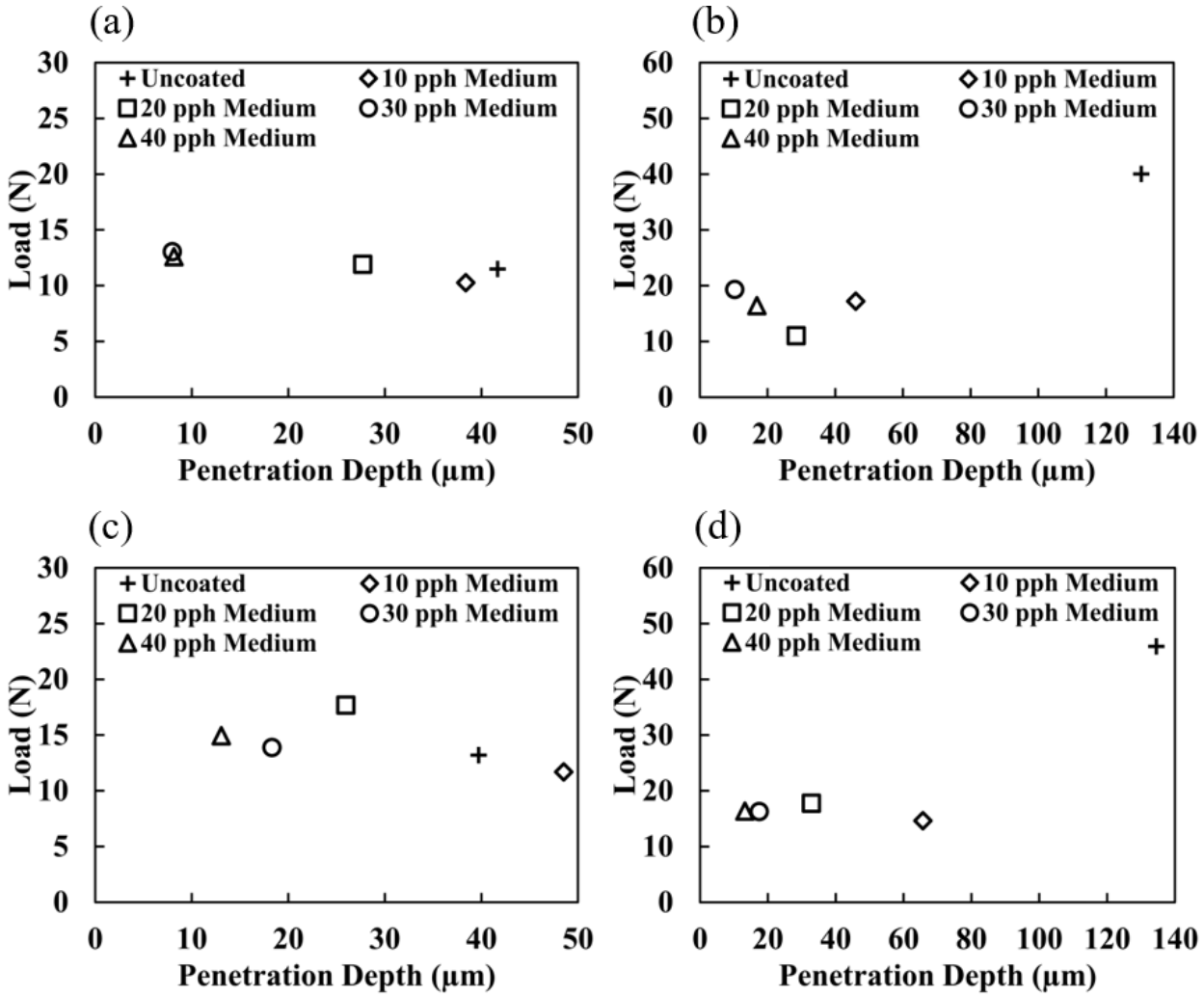

Figure 5.9. Peeling test results for a) 0.5 MPa and 25 ^{o}C, b) 0.5 MPa and 175 ^{o}C, c) 1 MPa and 25 ^{o}C, d) 1 MPa and 175 ^{o}C, for the medium size pigment as well as for the uncoated case as a function of the penetration depth.

The pigment size had a small influence on the load needed to peel the sample apart compared to the latex content and that could be explained by the similar penetration depths all pigments had as in Table 5.4.

Table 5.4. Average penetration depths and their 95% confidence intervals for experimental glued 10 pph coated paper and the load for 0.5 MPa press pressure and 25 ^{o}C paper temperature, for the fine, medium, and coarse pigment sizes.

	Fine	Medium	Coarse
Experiments (µm)	30±23	38±32	33±4
Load (N)	11	10	11

5.6 Concluding Remarks

A Darcy's law based model was developed to describe penetration of a hot melt adhesive during non-isothermal situations that take into account the change of viscosity of the fluid as it enters the pore, a limited amount of adhesive, and the two layer situation of a coating and the paper. The model was compared to results for uncoated paperboard, and coated paperboard, where the coatings had different latex levels and pigment sizes. The initial temperature of the paper and the press pressure were also changed in the experiments.

The penetration depth decreased when the paperboard was coated and further decreased as the latex level increased. The pigment size had minor influence for the range of pigments used here. The initial temperature of the paper had a big influence on penetration depth, especially for the uncoated samples. The model agreed within reasonable range with the experiments for all cases. Mechanical testing confirmed that more penetration leads to stronger bond strength.

CHAPTER 6: PREDICTION OF WATER-BASED POLYMER PENETRATION INTO TWO POROUS LAYERS

6.1 Abstract

Understanding the flow of water-based polymers in porous mediums is important in many industrial processes especially if water particles diffuse through pore walls. This situation can cause the first set of polymer particles to accumulate and pack blocking other particles to flow into the pore space. This situation can also cause the viscosity of polymer to increase due to concentration increases because of dewatering and lead eventually to stopping penetration at some point. In the setting of water-based adhesive in the paper, the penetration depth is important to obtain good green and final bond strengths so it is important to understand this mechanism by studying various parameters in various systems. Adhesion experiments were conducted to quantify penetration depth using the carver press and roll press testers in which a water-base adhesive was pressed against coated and uncoated paperboards at different press times, pressures, and adhesive solid contents. The strength of the bond at various setting conditions is also measured with the mechanical tester. The depth of penetration of the polymer was estimated from the silicone oil method. Several models were used to track penetration depth into paper. A model was developed based on Darcy's law to describe the dynamic penetration of water-based polymer into paper and paper that has been coated with various coating formulations. The model results are compared to experimental ones and good agreement for uncoated paper is obtained. In addition, a second model based on the finite element (COMSOL MULTIPHYSICS 5.5) is used to predict the penetration of a polymer into a single capillary that includes dynamic diffusion through the capillary wall. The viscosity of adhesive was a function of concentration for both models. Finally, the filtercake equation was utilized to estimate the filtercake resistance at different conditions.

6.2 Introduction

Adhesives are important to produce a number of products such as corrugated boards, paper cartons, and stationery applications. However, their set requires controlled conditions and environment. For example, water-based adhesives are set by water absorbed by fibers depositing the polymer in the joint. This process increases adhesive viscosity as time progresses and forms a solid material as water evaporates. The setting of aqueous adhesives in the paper is unique since it may involve the fluid to change properties as it penetrates the porous structure interacting with the walls of the pores or fibers.

The penetration depth of an adhesive is usually measured with cross-sectional images from microscopic techniques. (Ninness et al. 2011) showed how the aqueous adhesives setting is influenced by the coating layer and measured penetration of this adhesive in various microscopic ways. (Rapp et al. 1999) used electron energy loss spectroscopy in combination with transmission electron microscopy to monitor synthetic resin penetration in wood cell walls. Others have also confirmed that the coating layer affects the results. Therefore, various binders (Farwaha et al. 2012) and different binders and levels (Ventresca et al. 2019) have been used in the coating layer to see how that could impact the percentage of fiber tear in the glued samples.

(Tirumkudulu et al. 2003a; 2003b) were concerned with the flow of waterborne adhesives (colloidal dispersion containing soft polymer spheres dispersed in water) between the probe and the substrate and used the lubrication equations to generate a force, but correct the gap for the deformation of the load cell. They were not concerned much about the "wicking" of water away from the latex phase into the paper or the rate of that. They also were not concerned about the depth of penetration of the latex into the paper surface.

(Parker 2004) considered gluing coated paperboard substrates using aqueous adhesives. Glued joints were undergone a fiber tear test to determine bond strength. This article concluded that in order to get a good fiber tear percentage, water should diffuse into the fiber matrix to weaken the fibers and cause fracture inside the fibers leaving the polymer particles trapped in the pores of the substrate forming the bond. The success of this process depends on the ability of moisture to penetrate either side of the coated substrate which depends on the pore structure. It has also been highlighted that the starch concentration in the coating layer increases the adhesion force and makes it hard to achieve the fiber tear.

The setting of dispersion adhesives on paperboard was also studied by (Mika Vähä-Nissi 2009). Different adhesives with various viscosities were applied to a board while it connects to a tensile tester that measures force as time progresses. It concluded that the rheological properties of the adhesive and the structure of the board surface are the key parameters that influence the setting process of dispersion adhesives.

Adhesively bonded joints have been the focus for decades. Most past works have concentrated on understanding the parameters that affect the setting of different adhesives in various systems. (Budhe et al. 2017) put on a review collecting studies published from 2009 to 2016 regarding parameters affecting adhesively bonded joints in composite materials using various adhesives including water-based adhesives. The swelling of fibers upon receiving water could be an important factor in adhesive setting systems. The swelling and shrinking between wood and adhesive could initiate bond failure due to wood-adhesive interface stresses (Frihart 2009).

Various modeling techniques were performed to understand fluid flow accompanying mass transfer in porous mediums. (Yao et al. 2019) applied multi-scale pore network to simulate the mass transfer of fluid in nano-micro porous media and to estimate the properties of the fluid. The

flow of highly concentrated non-Newtonian emulsions was modeled in a porous media taking into account the influence of various parameters (Błaszczyk et al. 2020). (Routh et al. 2004) examined the effect of solvent evaporation from films containing particles on the distribution of particles. The dependency of concentration on liquid diffusion coefficients were studied in various systems by (Fujita et al. 1960; Gainer 1970; Tyn et al. 1975; Han et al. 1981; Muralidharan et al. 1998).

If the fluid changes concentration as it enters the pore, a complex interaction may occur. In the case of a water-based adhesive, the cellulose fibers may absorb water into amorphous regions or the fine pits concentrating the polymer particles in the pore space. Therefore, the polymer particles will accumulate as they enter the pore space. This accumulation will lead to a filter cake formation and an increase in the concentration of the polymer which will lead eventually to an increase in the viscosity of the polymer, especially the polymer that is in contact with the solid. This change in viscosity, in turn, changes the rate of flow into the capillary affecting the setting rate and the strength of the final bond. This situation has not been described in the previous literature to our knowledge. While much is reported on the penetration of coatings and ink into paper, adhesives are unique in that a concentration change may occur during penetration. Therefore, to better understand this situation, the parameters that control the setting rate of adhesives and the bond strength need to be addressed well. When better control of all key parameters happens, the outcome would be good bond strength.

In this work, a model based on Darcy's law is proposed accounting for concentration changes because of the dewatering of adhesive as it penetrates the substrates. In addition, the filtercake resistance was calculated using the filtercake equation to account for the filtercake formation during penetration. Experimentally, the paperboard was coated with two latex levels and one pigment size to generate different porosities and pore structures in the coating layer. The

water-based adhesive was applied to the various substances in the press using two methods namely the carver press tester and the roll press tester at four press times, two press pressures, and two adhesive solids contents. The silicone oil method was used to characterize adhesive penetration depth while the mechanical tester was used for bond strength determination.

6.3 Materials and Methods

This section includes (1) standard preparation and characterization methods for uncoated and coated paper; (2) preparation of glued paper samples for analysis; and (3) characterization methods for adhesive penetration depth and bond strength determinations.

6.3.1 Characterization of Coated and Uncoated Paper

Different analytical tests were performed to determine the characteristics of the uncoated and coated paperboard substrates such as the pore size distribution, porosity, thickness, coat weight, and permeability. Uncoated 336 g/m^2 bleached wood free paper (supplied by SAPPI NA) was used in all experiments. Paper coatings were prepared using styrene acrylate latex (Acronal S 504 na, BASF) and a medium size particle kaolin pigment (Premier, IMERYS) at 60% solids. A single paperboard (432 mm × 305 mm) was coated on one side with latex amounts of 10 and 40 pph (parts per hundred parts pigment) using a rod draw down coater, followed by drying immediately in an oven maintained at 100 ºC for 5 minutes. The coat weight for samples was about 15-17 g/m^2.

The paperboard was characterized by the Bristow wheel absorption tester that is used to determine the wettability and dynamic liquid absorption properties in given short time periods. In this test, 10 µl of water containing a dye-based ink was held within the trough. The rotating wheel runs at different speeds of 0.5-10 cm/s which gives contact times ranging from 0.01 to 2 seconds.

The contact time is calculated by dividing the width of the opening of the liquid container by the speed of rotation. The amount of liquid volume transferred into the paper per the area of the track length on the substrate at a certain contact time is called Total Liquid Volume (TLV, cm^3/m^2). For all contact times used, the TLV was between 4-5 cm^3/m^2.

The Digital Sartorius MA35 Moisture Analyzer was used to determine the percentage of water in the samples. The mercury porosimeter (Poresizer 9320, Micromeritics) is an excellent method to characterize the properties of paper and coating layers where it can provide useful information like porosity, pore size distribution, and density (skeletal and bulk). This tester was used to characterize the porosity and pore size distribution of paper by applying Young-Laplace equation described earlier in Equation (4.2). The thickness of the sample was measured with a digital micrometer (Marathon) with a resolution of 1 μm while the weight of the sample was measured with a Mettler Toledo Analytical Balance (AL204) with a resolution of 0.1 mg. Air permeability was measured with the Gurley porosity test applying the TAPPI standard as described in Equation (5.6). The silicone oil test was used to measure paper void fraction as in Equation (5.1).

The contact angle and surface tension were measured using the Double Sessile Drop measurement method by the mobile surface analyzer (Model MSA, KRÜSS USA, ADVANCE 1.6.2.0). The contact angle and surface tension were measured using Young's Equation as

$$\gamma_{sg} = \gamma_{sL} + \gamma_{Lg}\, cos(\theta_{young}) \qquad (6.1)$$

Where γ_{sg} is the surface tension at the solid and gas interface, γ_{sL} is the surface tension at the solid and liquid interface, γ_{Lg} is the surface tension at the liquid and gas interface, and θ_{young} is the young contact angle at which the liquid-gas interface meets the solid-liquid interface.

The water retention value was measured using the metal crucible method. The equation used to calculate the water retention value is shown below where the letter W represents the weight of both pulp paper and crucible, the subscript ac refers to "after centrifugal", ad refers to "after drying", and Wc is the crucible weight as

$$WRV = \frac{W_{ac} - W_{ad}}{W_{ad} - W_c} \qquad (6.2)$$

6.3.2 Characterization of Adhesive

The water-based adhesive (PRODUCER® 32-0214, supplied by Henkel) was used at the standard solids but also lower solids to slow down the set rates and to test the models. The solid level of the adhesives was modified by diluting them with known volumes of water. The viscosity of adhesive as a function of solids was characterized using Brookfield (model RVDVI+ serial number AE27483, Stoughton MA USA). This test was held at ambient temperature with a constant spinning of 30 seconds for all diluted adhesives. For the 55% solids adhesive, the spindle used was number 7 at rpm of 100. For the 45% solids adhesive, the spindle used was number 4 at rpm of 100 as well. The average value of viscosity taken from five runs was fitted into an equation to use when compared to the model as shown in Figure 6.1. The density of the adhesive was also measured at these different solid contents as shown in Figure 6.2. The adhesive was "tagged" with Rhodamine B to help it contrast with the latex and pigments.

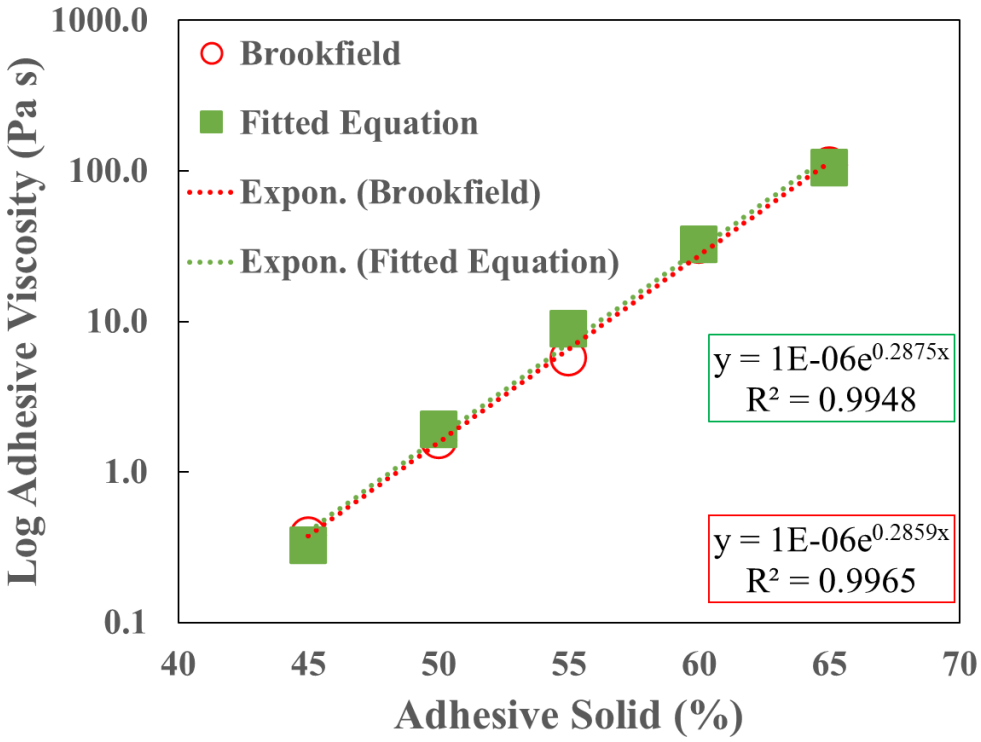

Figure 6.1. Fitting of Brookfield data to an equation for various adhesives solids.

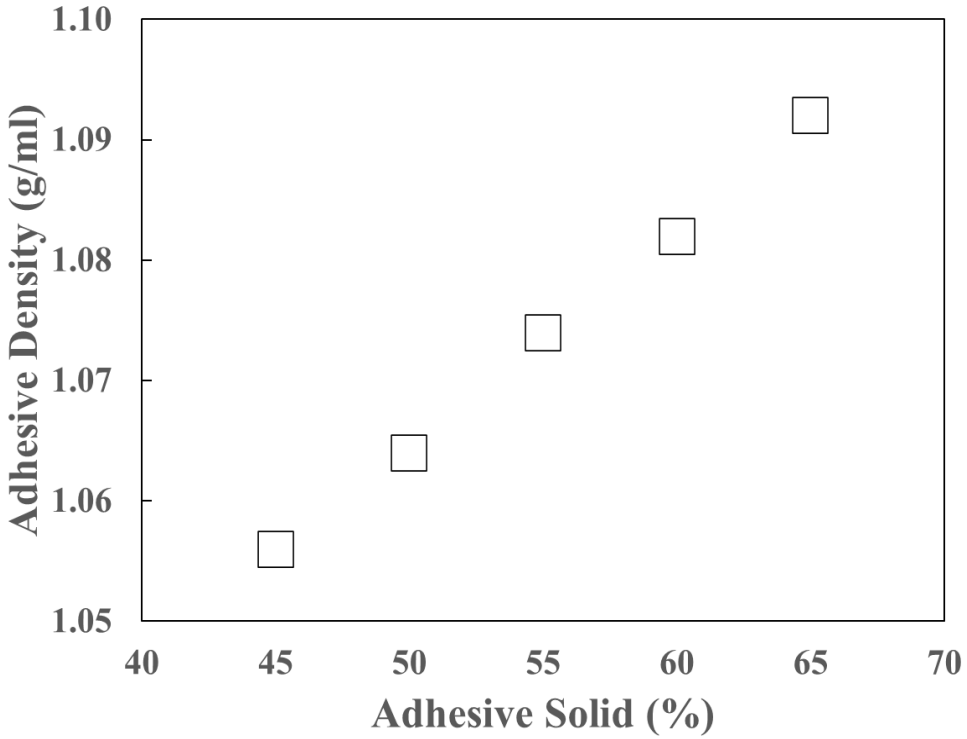

Figure 6.2. Density of water-based adhesive as a function of various solids.

6.3.3 Carver Press Tester

The carver press tester (Model C, Carver USA) was used to set the water-based adhesive. In this test, a syringe was used to apply a glue spot (about 0.4 ml) on the bottom porous sample at ambient temperature. Another paper was placed on top of the spot and the press is activated to a known pressure of 0.15 or 1 MPa and times of 1, 10, 30, and 60 seconds. These two pressures were used after accounting for the cross-sectional area of the cylinder and the sample. After release, the sample was removed and cooled at a controlled room temperature of 23 °C and relative humidity of 50% for 24 hours. After that, a cut region from the center of the samples is taken with dimensions of 30 mm × 20 mm. This central region should be free of any edge effects. These cut regions were then soaked in silicone oil to measure adhesive penetration depths. The process of bonding two substrates is summarized in Figure 6.3 beginning with a sheet of paper.

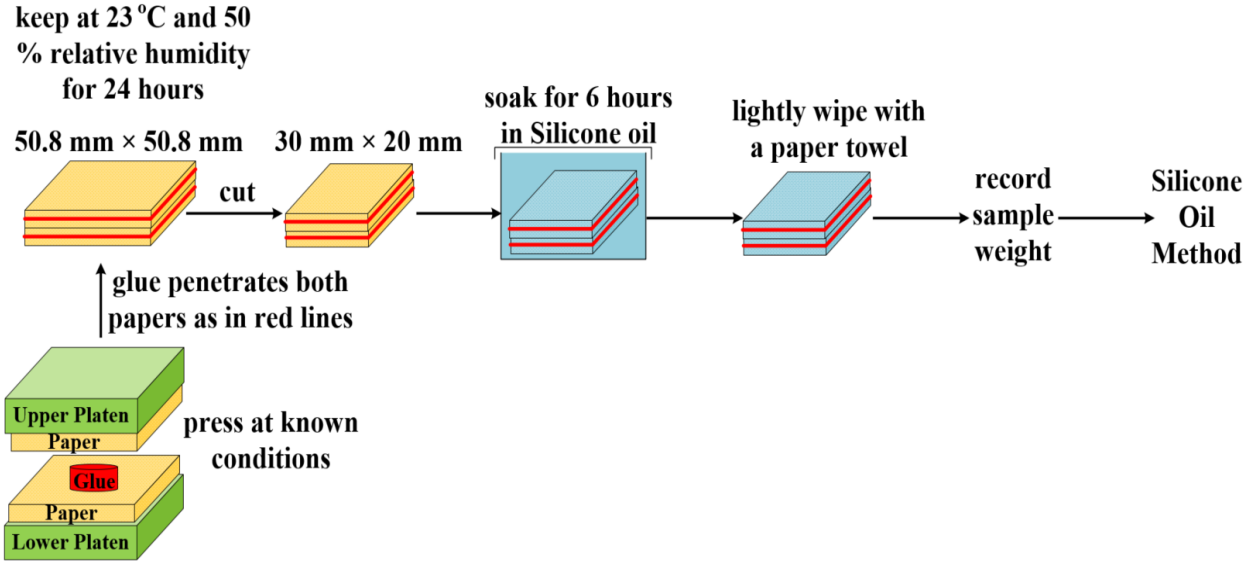

Figure 6.3. Adhesive film is pressed against paper that is uncoated or coated for a known time and press pressure. The sample is cut and soaked in silicone oil for penetration depth determination.

The carver press tester was also used to bond samples at 50.8 mm wide and 101.6 mm long. All of these generated samples that were bonded at different adhesion conditions were taken to a mechanical tester (model 5564, INSTRON, Norwood, MA, USA) for a peeling test to measure the force needed to peel the glued sample apart. Unbounded regions of 2.54 cm are clamped into the grip of the mechanical tester on one side and a peel wheel with tape on the other side. This tester is used to detect the bond strength by stretching the length of the strip, and the glued samples, at the desired angle and direction. The peeling occurs at an approximate angle of 90° as the paper-glue region is peeled from the paper at a rate of 50.8 mm/min. The actual angle of peeling is lower because of the stiffness of the paperboard. A bonded sample generated from the carver press tester during peeling is shown in Figure 6.4.

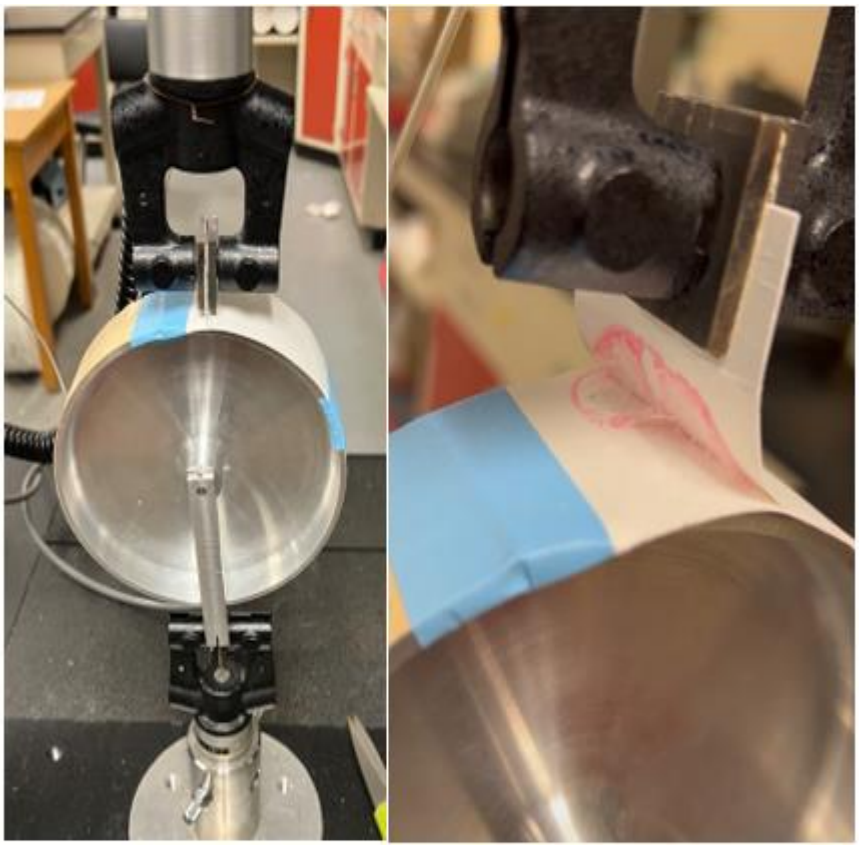

Figure 6.4. Instron test separating two uncoated substrates glued with the water-based adhesive.

6.3.4 Roll Press Tester

A 0.3 ml of the water-based adhesive was applied to the first substrate using a hand held "block" coater (QTG-a wet film coater) shown in Figure 6.5 at a groove depth of 100 µm. The end of the tester is close to the INSTRON mechanical tester (model 5564, INSTRON, Norwood, MA, USA) in the lab. The adhesive is metered onto the strip of paper (25.4 mm wide and 330.2 mm long) while it is flat on the table. A second strip of paper is placed on top of the wet adhesive layer. A roll is used to laminate both surfaces to form the bond with approximate pressure of 1 MPa and a time of 1 second. The pressure was used after accounting for the contact area of the roll and the sample. The sample is then attached to the double sided tape on a peel wheel and the other surface is clamped in the Instron. The peeling test is started then to measure the green and final bond strength. The peeling occurs close to 90° as the paper-glue region is peeled from the paper at a rate of 50.8 mm/min. The force and displacement are recorded. The whole process is captured in Figure 6.6.

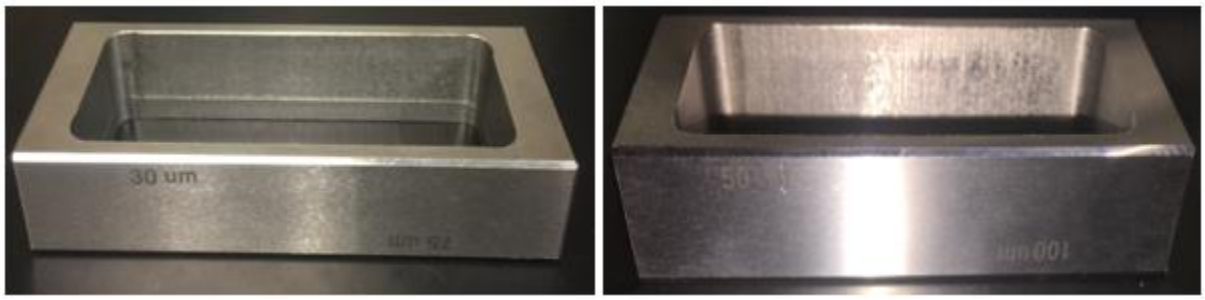

Figure 6.5. Hand held "block" coater.

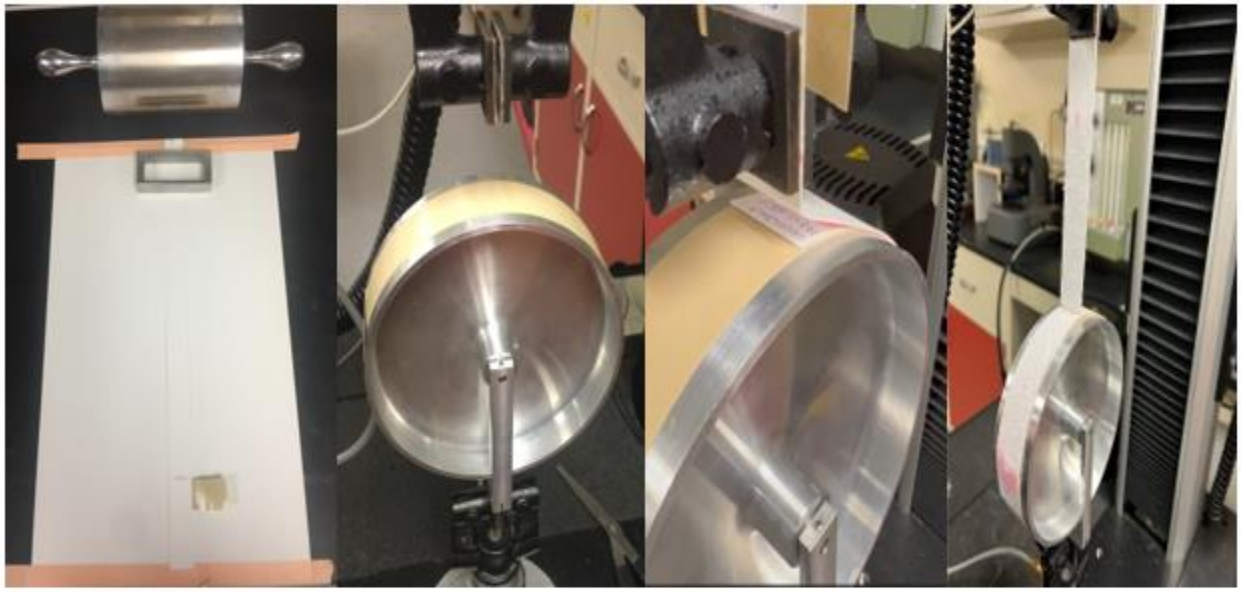

Figure 6.6. From left to right respectively: spreading adhesive onto one strip of paper flat on the table using block coater and pressing using a roll; double side tape fixed to the peel wheel clamped in the Instron; glued sample fixed to the peel wheel; and sample being peeled few minutes after starting peeling test.

A dynamic peeling result may be seen as the setting should increase the peel force as the test progresses. The advantage of this method is that the time between peel testing and the application of the glue is likely the shortest of the suggested ideas. The disadvantage is that the amount of glue applied is approximate based on the machining of the notch. This amount of glue that is applied can be measured by the weight gain of a dried. The repeatability of obtaining a certain glue amount can be obtained from repeat experiments. Depending on the peeling speed, we may see the force change from the start of the test to the end. The final bond strength is measured as well by letting the sample fully dry before being inserted in the mechanical tester. If the bond results in mostly fiber tear, the force generated is related to the internal bond strength of the paperboard. If the coating layer is the weak layer, this should be possible to see in the failed samples.

To measure the adhesive penetration depth using this technique, the sample was bonded as mentioned above but was put at a controlled room temperature of 23 ^{o}C and relative humidity of 50% for 24 hours and not peeled. After that, the sample was cut from the center with dimensions of 30 mm × 20 mm, and this center region should be free of any edge effects. These cut regions were soaked in silicone oil to determine the degree of penetration depth.

6.3.5 Characterization Method for Adhesion Penetration Depth Determination

The degree of penetration and the penetration depth was measured with the silicone oil method. The porous samples were weighed before the pressing process begins. After pressing, the samples were weighed again to determine the amount of adhesive in the sample and were cut and subjected to oil soaking in 45 ml of silicone oil (Sigma-Aldrich, 0.1 Pa s) for six hours. The six hours of soaking time was selected after trying various soaking times where six hours was the time required to fully saturate the paper as shown in Figure 6.7. After soaking, the sample was lightly wiped with a paper towel to remove any excess oil on the surface. By calculating the paper void fraction before and after adhesion, the loss of pore volume should correlate to the volume of pores filled with adhesive. The change in the void fraction is linked to penetration depth as in Equations (5.1) and (5.2) described earlier. Penetration depths are measured for one direction of samples and measurements were made in triplicate for all experimental results.

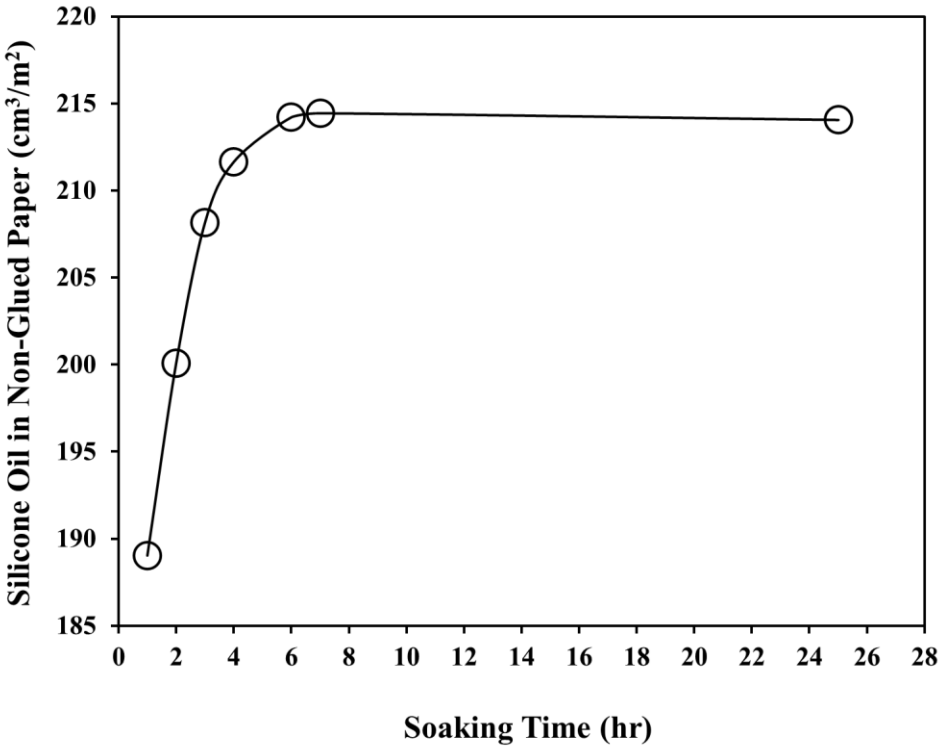

Figure 6.7. Various soaking times to determine the time for full saturation of paper.

6.4 Model of Penetration into Two Layers

To compare the model predictions to the experimental results, we need to estimate the viscosity of adhesive inside the fibers. In this regard, a set of equations was generated first to track water diffusion inside the fibers by applying mass balance around water as

Mass of water in the adhesive (initially):

$$\frac{L\ a\ \varepsilon_P\ \rho\ (1 - S_o)}{2} \qquad (6.3)$$

Mass of water in fibers:

$$\frac{L\ a\ (1 - \varepsilon_P)\ \rho_f\ SWU}{2} \qquad (6.4)$$

Mass of water in void fraction:

$$\frac{L\ a\ \varepsilon_P\ \rho\ (1 - S_{new})}{2} \qquad (6.5)$$

Where L is the final penetration depth of adhesive, a is the area of the sample, ε_p is the void fraction of paper before the adhesion test, ρ is the wet density of adhesive which is around 1 g/ml, ρ_f is the density of fibers which is around 1.5 g/ml, SWU is the short time water uptake, S_o is the initial solid content of adhesive, and S_{new} is the new solid content of adhesive. Factor 2 in the equations is for one paper direction. As the water with polymers penetrate, water will diffuse into the cellulose increasing the viscosity. If we just assume that this is fast compared to the slow flow of penetration, the viscosity of the fluid in the porous media would be from a mass balance (mass of water in fibers + mass of water in void fraction = mass of water in the adhesive (initially)). The new solid content of the adhesive is now calculated based on the new mass of water within the adhesive as

$$S_{new} = S_o + \frac{(1 - \varepsilon_P)\ \rho_f\ SWU}{\varepsilon_P\ \rho} \qquad (6.6)$$

If we want to check if this equation is valid, then we simply apply SWU = 0 which means that the water does not diffuse into the fibers and stays within the adhesive itself. In this case, S_{new} should be equal to S_o. It is important to point out that we tried to adjust the viscosity using the water retention value calculated from Equation (6.2) but it caused the solids to go over 100%, So, it is an unrealistic adjustment because it is showing too much water absorption and therefore not useful in this modeling. Therefore, the short time water uptake (SWU) value that is calculated from the Cobb sizing tester is used instead of the water retention value to measure the quantity of water

that is absorbed by the paper in a short contact time under standardized conditions (23 ºC and 50% RH) as

$$SWU = \frac{V_w \, \rho_w \, (1 - \varepsilon_P)}{W_B} \qquad (6.7)$$

Where V_w is the volume of water absorbed, ρ_w is the density of water, and W_B is the basis weight of paper. The viscosity is set as a function of concentration as

$$\mu(C) = A \, exp\left(\frac{E}{C_{AO}} - \frac{E}{C_A}\right) \qquad (6.8)$$

Where C_A is the concentration distribution inside the pores, and C_{Ao} is the initial concentration of polymer in the water phase that is penetrating the pores. The parameters A and E are constants and determined by measuring the viscosity of the adhesive at different polymer concentrations. Parameter A has units of viscosity while parameter E has units of concentration. By fitting Brookfield data to the results of Equation (6.8), the viscosity of adhesive as a function of the solid content of adhesive can be written now in Pa s units as

$$\mu(S_{new}) = 9.7359 \times 10^{-7} \; exp\,(0.28747 \times S_{new}) \qquad (6.9)$$

The basic concept of viscous flow in a porous media using Darcy's law is modified to include the multi-layer system, Equations (5.11) and (5.12), with finite adhesive quantity, Equation (5.3), using the viscosity of the adhesive, Equation (6.9), that corresponds to the solid content of the adhesive obtained from the water diffusion measurements above. For example, the solid content of the adhesive increases during penetration to around 9% which corresponds to a viscosity of 5.37 Pa s for the 54% solids (45+9%) and 95.18 Pa s for the 64% solids (55+9%). These

viscosities were used in the one-layer model for the uncoated glued samples. So, the model used the adjusted viscosity calculated from Equation (6.9) based on the solid content of the adhesive that was calculated from Equation (6.6).

If the fluid particles penetrating the sample are bigger than the pore size distribution of the sample, then the filtercake equation can be used to explain that by calculating the filtercake resistance. This equation assumes that when the fluid has particles, a filtercake will increase with time and particles will be captured on a membrane as shown in Figure 6.8. So, the fluid will penetrate the paper filling out some pores but then the particles clog and stop flowing due to filtercake forming. In this case, the flow rate of the fluid will be decreased depending on the particle size distribution. The factors that most impact penetration depth during the filtercake formation are the original pore size of the paper, the particle size of the fluid, and the drying rate.

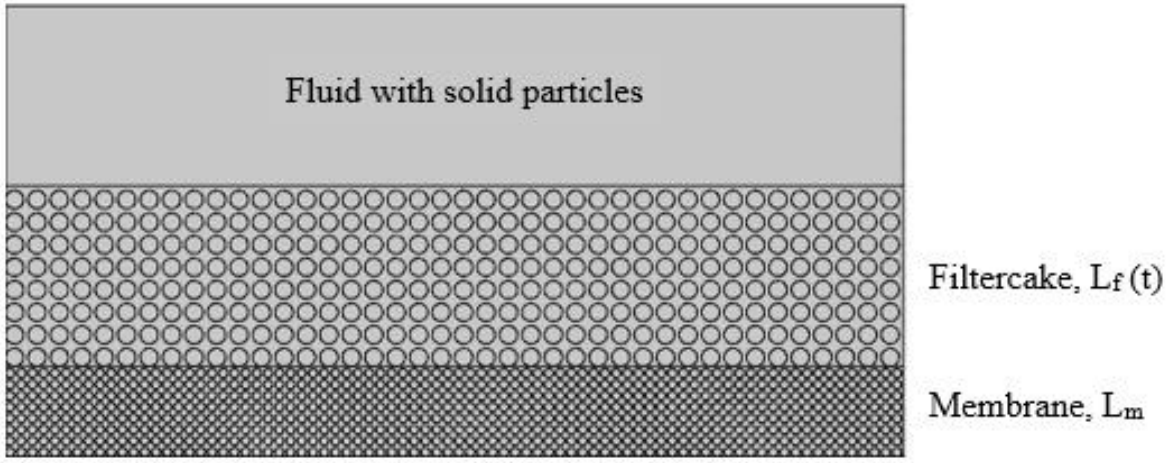

Figure 6.8. Depiction of filtration.

The filtercake equation is derived from Darcy's law that applies to flow through the membrane as well as the filtercake

$$\frac{d\left(\frac{V}{a}\right)}{dt} = \frac{K_f \, \Delta P_f}{\mu \, L_f} \qquad (6.10)$$

$$\frac{d\left(\frac{V}{a}\right)}{dt} = \frac{K_m \, \Delta P_m}{\mu \, L_m} \qquad (6.11)$$

Where V/a is the filtered volume of fluid per unit area, t is the press time, μ is the viscosity of water (0.001 Pa s), ΔP_f is the pressure drop over the filtercake, K_f is the permeability of filtercake, L_f is the thickness of filtercake, ΔP_m is the pressure drop over the membrane, K_m is the permeability of the membrane, and L_m is the thickness of the membrane. The total pressure difference is the sum of the pressure drop over the filtercake and the membrane as

$$\Delta P = \Delta P_f + \Delta P_m \qquad (6.12)$$

Applying the pressure drop equation, the new equation is

$$\frac{d\left(\frac{V}{a}\right)}{dt} = \frac{\Delta P}{\frac{\mu \, L_f}{K_f} + \frac{\mu \, L_m}{K_m}} \qquad (6.13)$$

When a mass balance is done on the particles, then the volume of particles in the filtercake has to equal the volume of particles in the fluid that has been filtered and the volume of the particles can be calculated as

$$L_f \, a \, (1 - \varepsilon) \, \rho = V \, C_S \qquad (6.14)$$

Where Cs is the solids concentration in the adhesive being filtered and it is calculated by multiplying the density of adhesive (1 g/ml) by its solid content, ε is the void fraction of filtercake, and ρ is the density of particles or fibers. Now if we replace L_f in Equation (6.13) with Equation (6.14), and integrate over time assuming constant time and pressure, then the filtercake equation is

$$t = \frac{\mu}{\Delta P}\left(\frac{\left(\frac{V}{a}\right)^2 C_s}{2\,K_f\,(1-\varepsilon)\,\rho} + \frac{L_m}{K_m}\left(\frac{V}{a}\right)\right) \qquad (6.15)$$

The filtercake resistance is defined as below in some literature where it increases as the filtercake is compressed.

$$\alpha = \frac{1}{K_f\,(1-\varepsilon)\,\rho} \qquad (6.16)$$

If V/a is replaced by the experiments penetration depth multiplied by the void fraction of paper before the adhesion test and substituting Equation (6.16) into Equation (6.15) and rearranged, the filtercake resistance then is

$$\alpha = \frac{\frac{t\,\Delta P}{\mu} - \frac{L_m}{K_m}\,L\,\varepsilon_P}{\frac{C_s\,L^2\,{\varepsilon_P}^2}{2}} \qquad (6.17)$$

Equation (6.17) is used to experimentally calculate the filtercake resistance at different press times, pressures, and adhesive solid contents. The filtercake resistance is a function of how particles are packed and on pore space generated by this packing.

6.5 Results and Discussions

Tables 6.1 and 6.2 show the properties of the paperboard that was held constant for all experiments. These properties were measured after conditioning in an environment of 23 ºC and 50% relative humidity (RH) for 24 hours. All values are based on an average of a minimum of five repeats except the pore diameter. The pore size reported is the peak obtained in the log-differential volume plots of the mercury porosity data in the low range of the data. Table 6.3 shows the permeability of the uncoated paperboard compared to other permeabilities from previous literature.

Table 6.1. Uncoated and coated paperboard properties.

	Thickness (µm)	Basis Weight (g/m^2)	Void Fraction	Pore Diameter (µm)	Permeability (m^2)	Surface Free Energy (mN/m)	Contact Angle (degree)	Cobb Test (µm)
Uncoated	430	336	0.50	6.60	3.0×10^{-14}	19.33	117.84	40.77
10 pph SA	446	352	0.48	0.05	4.8×10^{-17}	34.75	79.54	48.85
40 pph SA	446	352	0.44	0.02	1.4×10^{-17}	29.76	83.98	46.55

Table 6.2. Water uptake and moisture content for the uncoated paperboard.

	Bristow Wheel (10-200 ms) (µm)	Water Retention Value (g water/g dry pulp)	Moisture Content (%)
Uncoated	5	1.26	8

Table 6.3. The air permeability of this work compared to previous literature data.

	Thickness (µm)	Basis Weight (g/m^2)	Air Permeability (m^2)	Substrate
This work (Uncoated)	430.0	336.0	3.0×10^{-14}	bleached wood free paper
(Tutak et al. 2019)	16.7	350.0	5.0×10^{-15}	3-ply paperboard
(Shallhorn et al. 2009)	103.9	60.3	2.2×10^{-13}	paper sheet from softwood chemical pulp
(Pal et al. 2006)	321.0	70	1.4×10^{-14}	unbleached kraft paper
(Aaltosalmi et al. 2004)	120-200	300	3.0×10^{-13}	paper sheet from bleached softwood kraft pulp
(Rasi et al. 1999)	160.0	64	3.0×10^{-15}	paper sheet from mechanical groundwood pulp
(Nilsson et al. 1997)	1020.0	752	4.8×10^{-14}	paper sheet from hardwood

6.5.1 Results of Carver Press Tester

For all tables and figures below, all results are from the average of three values and penetration depth values are for one paper direction. Figure 6.9 shows the experimental adhesive penetration depths compared to the model predictions for uncoated samples glued at 55% solids, 0.15 MPa pressure, and four press times. The maximum penetration depths are also shown in all figures below as blue stars and were calculated from Equation (5.3). Surprisingly, the results are almost the same with no significant variations as time progresses where they were around 34 µm on average. For comparison, on the other hand, the model predictions increased with time. The maximum penetration depths stayed at 83 µm on average for all press times and were high compared to both experiments and the model; the maximum penetration depth is based on the available adhesive applied to the sample that did not get squeezed out during pressing.

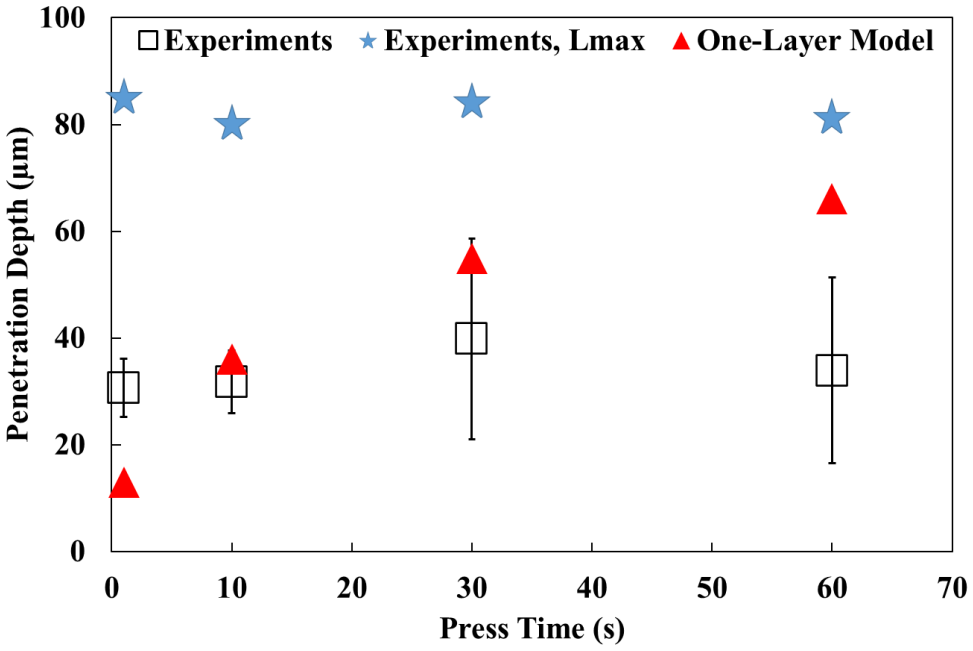

Figure 6.9. Penetration depth results and their 95% confidence intervals for 0.15 MPa press pressure and 55% adhesive solids, for the uncoated samples.

Figure 6.10 shows the experimental adhesive penetration depths compared to the model predictions for uncoated samples glued at 55% solids, 1 MPa pressure, and four press times. Similar to what has been seen for the low pressure results, increasing pressure seems to not influence the penetration depths which were around 39 µm on average after was 34 µm for the low press pressure. For modeling, however, the predictions followed the trend with little over prediction for 10, 30, and 60 seconds and little under prediction for the 1 s press time. In addition, the model reached the maximum penetration depths for all press times except for the 1 s press time. The maximum penetration is lower than the low press pressure results because more adhesive is squeezed out from the nip leaving less available for penetration. Again, the results are hard to understand in that high pressing times gives about the same penetration as the short pressing times.

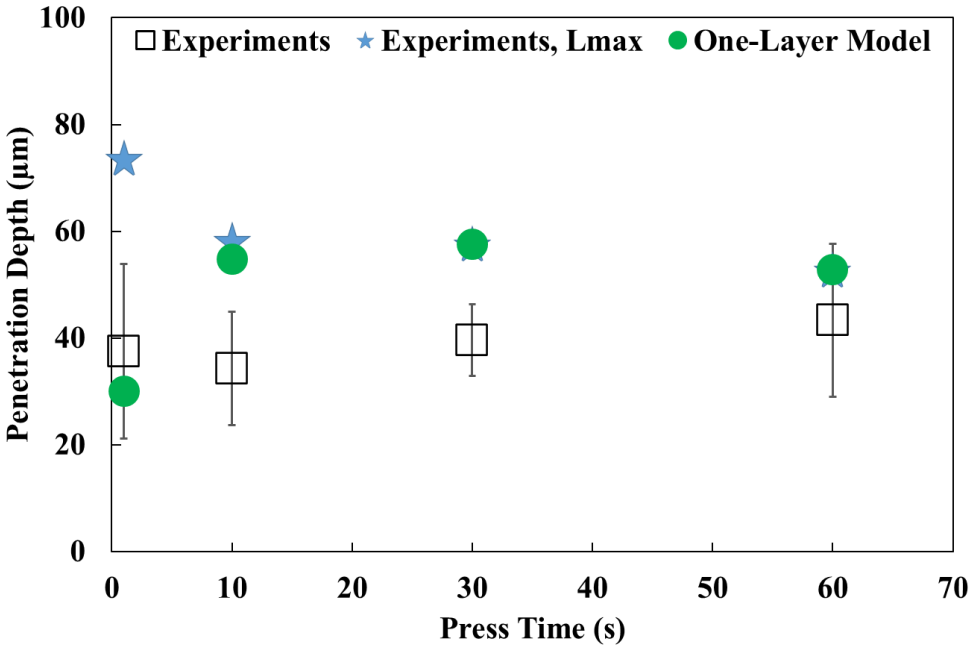

Figure 6.10. Penetration depth results and their 95% confidence intervals for 1 MPa press pressure and 55% adhesive solids, for the uncoated samples.

The adhesive was diluted to 45% solids to slow the setting rate and also to see the influence of low solids on the penetration depth and the final bond strength. This diluted adhesive was tested on paper using two press pressures and four press times. Figure 6.11 shows the experimental adhesive penetration depths compared to the model predictions for uncoated samples glued at 45% solids, 0.15 MPa pressure, and four press times. The experimental depths here showed different behavior where the depth was higher at 1 second press time then decreased as time increased. This may be due to the diluted adhesive that was easily squeezed out of the paper leaving less adhesive on the paper as a function of press time. The predictions of the model followed the experiment's trend and were at the maximum penetration depths for all times except for the 1 second press time.

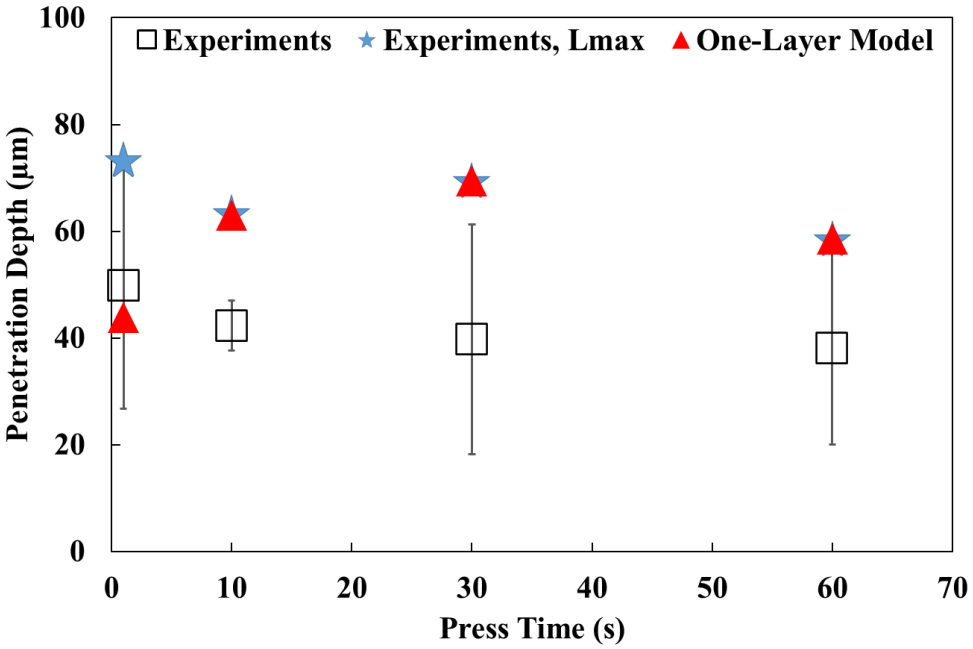

Figure 6.11. Penetration depth results and their 95% confidence intervals for 0.15 MPa press pressure and 45% adhesive solids, for the uncoated samples.

Figure 6.12 shows the experimental adhesive penetration depths compared to the model predictions for uncoated samples glued at 45% solids, 1 MPa pressure, and four press times. Similar to 55% solids results, the increased pressure did not change the experimental depths which

were almost the same at 47 µm on average for all times. However, the increased pressure caused the model to predict the maximum penetration depth, that is close to the results for the high times. Moreover, both experiments and the model reached the maximum penetration depths for all runs. For the high pressure, therefore, the penetration depth seems to be controlled by how much adhesive is left after the pressing event.

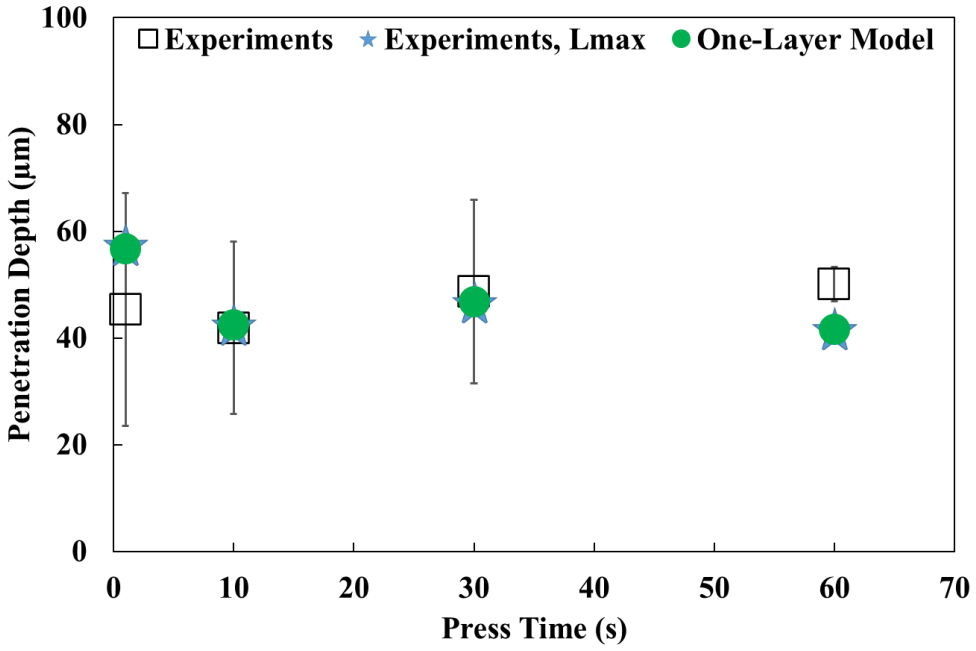

Figure 6.12. Penetration depth results and their 95% confidence intervals for 1 MPa press pressure and 45% adhesive solids, for the uncoated samples.

Besides the uncoated paper, coated surfaces were also tested for penetration depth determination and final bond strength using the 55% solids adhesive with two press pressures and four press times. Table 6.4 shows the experimental adhesive penetration depths compared to the model predictions for the 10 pph samples glued at 55% solids, 0.15 MPa pressure, and four press times. The maximum penetration depths are also shown in all tables below. This case was not so far from the uncoated one in which the results of the experiments were almost the same regardless of the press times and way far from the maximum penetration depths. The reason for getting high

penetration depths for the experiments may be due to the weak coating layer that could not hold out the adhesive during pressing: the adhesive pushes the coating pigments into the paper under the pressure. The model, on the other hand, showed low predictions which is due to the permeability of the coating layer that was used. However, if the viscosity of the adhesive does not change and remains constant during penetration then an improvement occurs in the model as shown in the last column of the table. If the coating layer breaks under pressure, this low permeability layer would not exist. The penetration obtained is quite similar to the uncoated paper.

Table 6.4. Average penetration depths and their 95% confidence intervals for the 10 pph coated paper and the one-layer limited adhesive model glued at 55% solids and 0.15 MPa pressure.

Time (sec)	Experiment (μm)	Lmax (μm)	One-Layer Model (μm)	One-Layer Model (μm), No change in viscosity ($S_{new}=S_o$)
1	29±10	96	0.4	2
10	32±19	94	1	7
30	35±11	93	2	12
60	31±13	92	3	9

Table 6.5 shows the experimental adhesive penetration depths compared to the model predictions for the 10 pph samples glued at 55% solids, 1 MPa pressure, and four press times. The experimental depths did not enhance with pressure increases and the difference was a few microns in both pressure cases. The model predictions enhanced a bit here but were still low. Here, if we set the adhesive viscosity to a fixed value in the model (last column in the table), then that brings the model close to the experiments in some places. The maximum penetration depths were low here due to the adhesive squeezed out of the paper at high pressure. The weak coating layers could be the reason here as well.

Table 6.5. Average penetration depths and their 95% confidence intervals for 10 pph coated paper and the one-layer limited adhesive model glued at 55% solids and 1 MPa pressure.

Time (sec)	Experiment (μm)	Lmax (μm)	One-Layer Model (μm)	One-Layer Model (μm), No change in viscosity ($S_{new}=S_o$)
1	30±4	83	1	6
10	34±10	70	3	10
30	43±10	69	6	26
60	32±16	69	8	42

Besides 10 pph coated papers, adhesion tests were performed on 40 pph coated substrates to look at the influence of the increased latex level on the penetration depth and final bond strength. Tests here used 55% solids adhesive with two press pressures and four press times as well. Table 6.6 shows the experimental adhesive penetration depths compared to the model predictions for the 40 pph samples glued at 55% solids, 0.15 MPa pressure, and four press times. This case showed a significant decrease in experimental depths due to the increased latex level that blocked the adhesive from penetrating through it into the fiber matrix. The data shown in the table proved that the adhesive penetrated the coating layer only. This could be contributed to the fact that the coated paper has a lower permeability and minimal penetration while the uncoated paper has a higher permeability and deeper penetration. The 40 pph coated surfaces differ from the 10 pph in that the 40 pph coating layer is stronger and did not break during adhesion events. Here, the model underpredicted the experiments by around 16 μm for the highest range but it did provide that the adhesive is in the coating layer only as well. So, if we assume that the coating layer itself would not have any ability to absorb water and the paper fibers can absorb the water, then the original viscosity in the model seems to make sense and helps the model to agree with the experiment as shown in the last column of the table.

Table 6.6. Average penetration depths and their 95% confidence intervals for 40 pph coated paper and the one-layer limited adhesive model glued at 55% solids and 0.15 MPa pressure.

Time (sec)	Experiment (μm)	Lmax (μm)	One-Layer Model (μm)	One-Layer Model (μm), No change in viscosity ($S_{new}=S_o$)
1	10±8	114	0.2	1
10	12±5	99	0.5	4
30	17±5	101	1	7
60	16±15	102	1	10

Table 6.7 shows the experimental adhesive penetration depths compared to the model predictions for the 40 pph samples glued at 55% solids, 1 MPa pressure, and four press times. Not many changes are seen for experiments and the model with pressure increases where the adhesive is still within the coating layer only for both cases. However, using the original viscosity in the model seems to give better results than the adjusting viscosity (last column in the table).

Table 6.7. Average penetration depths and their 95% confidence intervals for 40 pph coated paper and the one-layer limited adhesive model glued at 55% solids and 1 MPa pressure.

Time (sec)	Experiment (μm)	Lmax (μm)	One-Layer Model (μm)	One-Layer Model (μm), No change in viscosity ($S_{new}=S_o$)
1	10±6	82	0.4	3
10	13±6	64	1	10
30	14±12	68	2	10
60	18±7	68	3	18

Some tensile tests were performed on samples glued using the carver press tester at the same adhesion conditions reported above. Figure 6.13 shows adhesive strength (load) versus press time for uncoated samples glued at 0.15 and 1 MPa pressure and 55% solids while Figure 6.14 shows adhesive strength (load) versus press time for uncoated samples glued at 45% solids. The results here confirmed the same penetration depth seen across all adhesion tests. The figure clearly

shows that the loads were close across the different press times except for a few variations with around 15 N load on average for all conditions.

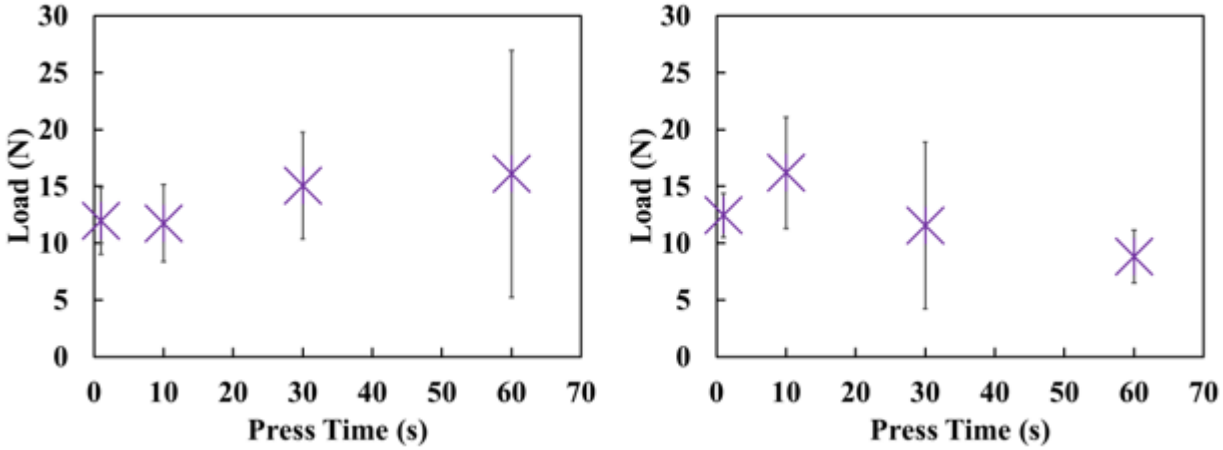

Figure 6.13. Peeling test results and their 95% confidence intervals for 55% adhesive solids and 0.15 MPa (left) and 1 MPa (right), for the uncoated samples.

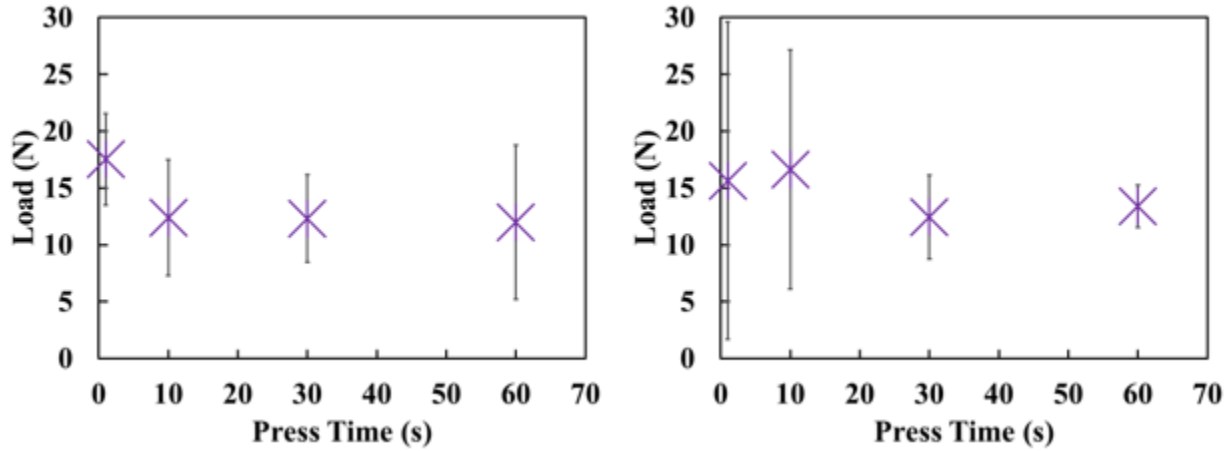

Figure 6.14. Peeling test results and their 95% confidence intervals for 45% adhesive solids and 0.15 MPa (left) and 1 MPa (right), for the uncoated sample.

Figure 6.15 shows adhesive strength (load) versus press time for the 10 pph coated samples glued at 0.15 and 1 MPa pressure and 55% solids. The results here confirmed the previous conclusion that the coating layer is the weakest part during adhesion. This is seen with the 5 N load across all times and pressures.

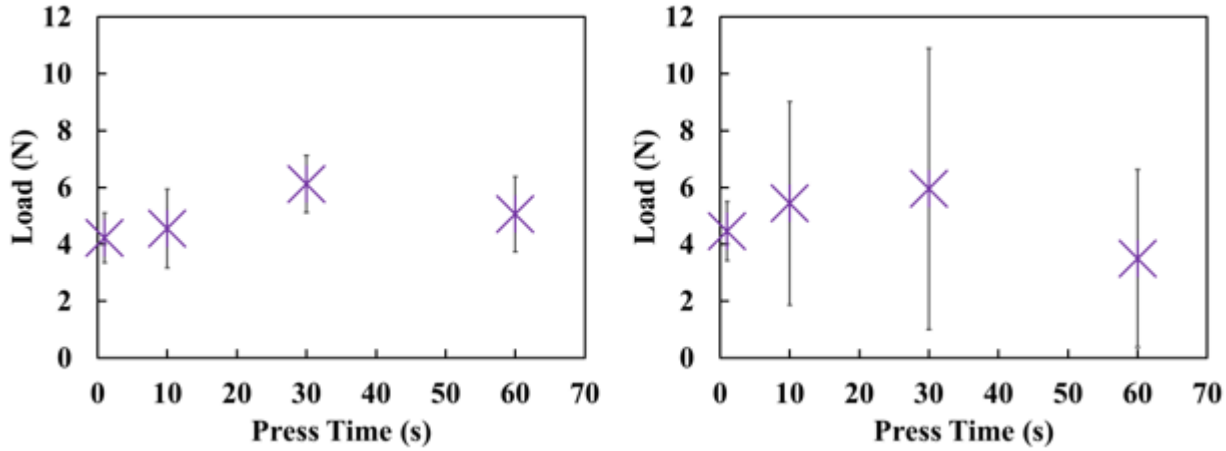

Figure 6.15. Peeling test results and their 95% confidence intervals for 55% adhesive solids and 0.15 MPa (left) and 1 MPa (right), for the 10 pph samples.

Despite the low penetration depths associated with the 40 pph samples, the loads were higher and close in values to the uncoated samples. Figure 6.16 shows adhesive strength (load) versus press time for the 40 pph coated samples glued at 0.15 and 1 MPa pressure and 55% solids. The higher loads here could be due to the strength of the coating layer that needs higher force to peel the samples apart. The loads were on an average of 15 N for all times and pressures.

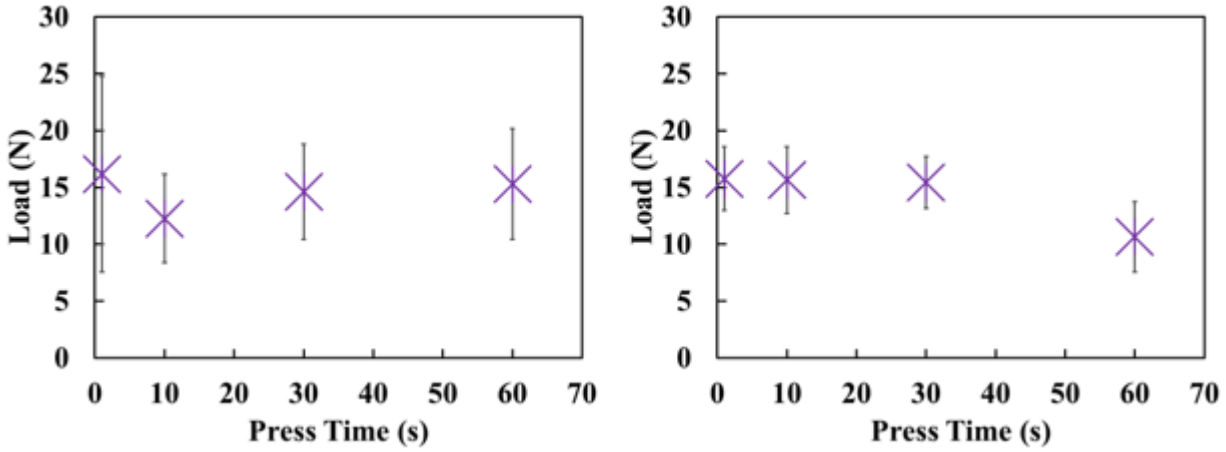

Figure 6.16. Peeling test results and their 95% confidence intervals for 55% adhesive solids and 0.15 MPa (left) and 1 MPa (right), for the 40 pph samples.

6.5.2 Results of Roll Press Tester

Similar to the carver press tester, the roll press tester was used to glue two substrates first and then the silicone oil method was used to determine the final penetration depth. Conversely, this method is limited to one press pressure and one press time, however, the adhesive solids are different. Table 6.8 shows the experimental adhesive penetration depths compared to the model predictions for the coated and uncoated samples glued at 1 MPa pressure and 1 second time using two adhesive solids. The results of the roll press tester agreed well with the results of the carver press tester in which the uncoated and 10 pph surfaces gave close results and penetration was in the coating layer only for the 40 pph surfaces. The model underpredicted the whole set of samples with a high underprediction for the 10 pph samples due to the weakness of the coating layer discussed earlier. Similar to the carver press tester, the underprediction of the model here can be improved when using the original viscosity in the model as shown in the last column of the table. Again, this can be explained by the coating layer that cannot absorb water and viscosity stays almost constant except for the 10 pph samples where the coating layer is weak and water is passing through to the fibers.

Table 6.8. Average penetration depths and their 95% confidence intervals for the coated and uncoated paper and the one-layer limited adhesive model glued at 1 MPa pressure and 1 second time.

Sample	Solids %	Experiment (μm)	Lmax (μm)	One-Layer Model (μm)	One-Layer Model (μm), No change in viscosity ($S_{new}=S_o$)
Uncoated	55	34±11	33	24	33
10 pph SA+Medium	55	33±13	42	1	6
40 pph SA+Medium	55	18±4	40	0.4	3
Uncoated	45	30±16	32	32	32
10 pph SA+Medium	45	35±20	56	4	14
40 pph SA+Medium	45	10±14	47	2	12

The tensile tests were also performed on samples glued using the roll press tester at the same adhesion conditions reported above. This tester is a good method to measure the green and final bond strength. Figure 6.17 shows adhesive strength (load) versus peel time for uncoated and coated papers glued at 1 MPa pressure, 1 second time, and 55% solids. The loads were high for the uncoated followed by the 40 pph and then the 10 pph samples. This test also showed that the maximum loads can be achieved within the first 60 seconds of run for the uncoated and 10 pph samples while it took around 110 seconds to reach that for the 40 pph samples. During the first 60 seconds of peeling, the green bond strengths were 8 N, 4 N, and 4 N for the uncoated, 10 pph, and 40 pph samples, respectively.

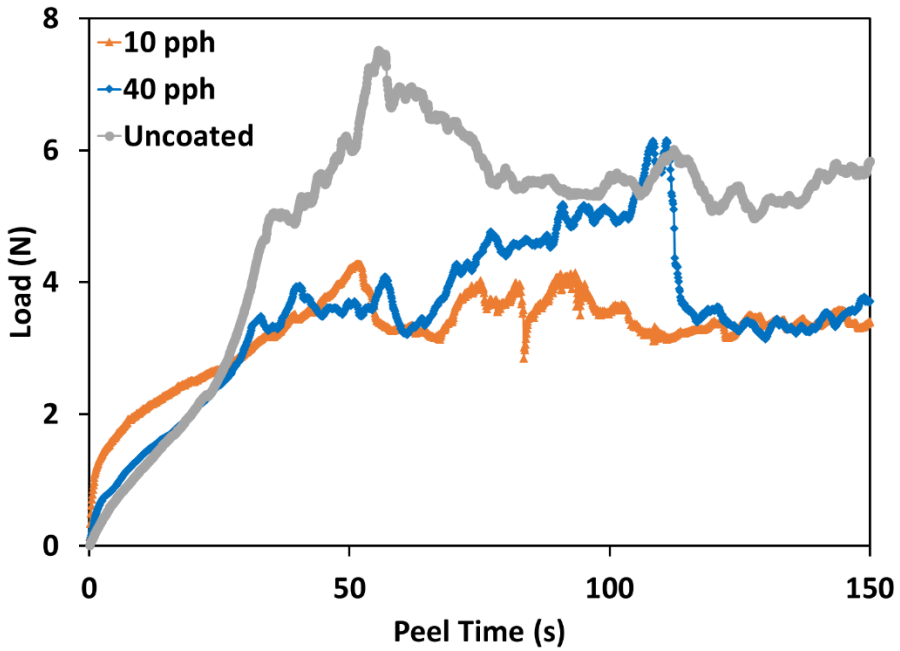

Figure 6.17. Peeling test results for 55% adhesive solids, 1 MPa press pressure, and 1 second press time, for the coated and uncoated samples.

Tensile tests were also performed on samples glued with 45% solids adhesive. Figure 6.18 shows adhesive strength (load) versus peel time for uncoated and coated papers glued at 1 MPa

pressure, 1 second time, and 45% solids. Similar to the 55% results, the loads were high for the uncoated followed by the 40 pph and then the 10 pph samples. More interestingly is that the maximum loads were achieved for all samples during the first 60 seconds of peeling time then they shifted to fiber tear only for the remaining time. So, in this case the green bond strength is equal to the final bond strength if we only take the results from the first 60 seconds of run.

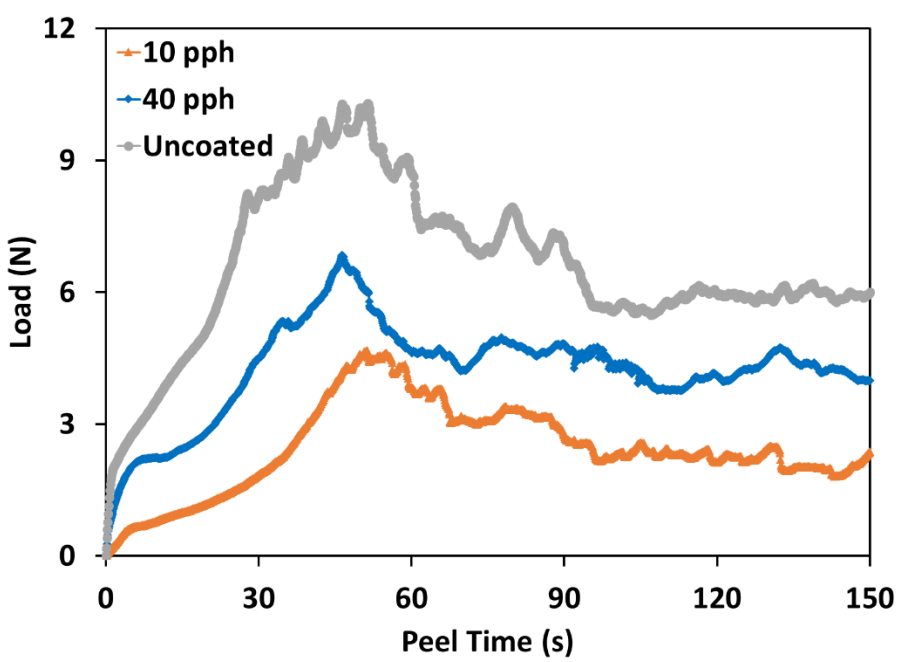

Figure 6.18. Peeling test results for 45% adhesive solids, 1 MPa press pressure, and 1 second press time, for the coated and uncoated samples.

6.5.3 Theories of Adhesion

Several theories of adhesion have been proposed to describe adhesive bonding. These theories are mechanical (microscopic scale), electrostatic (macroscopic scale), diffusion (molecular scale), wettability (molecular scale), chemical bonding (atomic scale), and weak boundary layer (molecular scale). The mechanical theory illustrates that the adhesive should

penetrate the pores of the substrate to perform “mechanical interlocking ” between the adhesive and the adherends. Electrostatic theory on the other hand states that the electrostatic effects are responsible for the adhesion between the adhesive and the adherend. The adhesion occurs due to the interdiffusion of molecules in between the adhesive and the adherend (both polymers) as suggested by the diffusion theory. The wetting theory suggests that adhesion occurs due to the surface forces that generate due to molecular contact between two substrates. The chemical bonding theory suggests that adhesion is formed due to surface chemical forces (chemical bonding at the interface). Finally, the weak boundary layer theory proposes that a bond failure happens at the interface due to either a cohesive break or a weak boundary layer (Ebnesajjad 2008).

For the scale of experiments in this thesis and based on the tensile test results, the mechanical interlocking theory seems to describe the formation of bonds for all glued samples. Besides, for the low latex level coated surfaces, the weak boundary layer theory seems to represent the bond failure seen at the interface.

6.5.4 Controlling Mechanisms for Water-Based Adhesive Setting

In some other tests, three different experimental approaches were studied to explain some of the previous results. The first approach included starting with a wet paper before adhesion tests began plus varying dry techniques after adhesion tests. The constant paper that has been used for all previous adhesions was used in this approach as well. The second approach included cutting the amount of adhesive in half and using both the constant paper as well as a new paper. The third approach was to look at the influence of changing paper on the results with varying press pressures and times.

Table 6.9 shows the experimental adhesive penetration depths for the uncoated samples glued at 55 and 45% solids, 0.15 and 1 MPa pressure, and 10 seconds time using the carver press tester. In this table, “start dry” means that the sample was dry during the adhesion events while “start wet” means that the sample was wet during adhesion events. On the other hand, “controlled dry” means that the sample dried in a controlled room of 23 ^{o}C and 50% RH immediately after adhesion tests, “oven dry” means that the sample dried in an oven of 105 ^{o}C immediately after adhesion tests, and finally “air dry” means that the sample dried using a hot air of 120 ^{o}C immediately after adhesion tests. For the 55% solids and 10 seconds time, the depths increased as we go from “start dry, controlled dry” towards “start wet, controlled dry” with about an 11 μm increase for the 0.15 MPa and a 22 μm increase for the 1 MPa. For the 45% of solids, the results were similar independent of pressure and dry differences. The results of the start wet approach can be a clear indication that the clogging mechanism is the key mechanism in the setting of water-based adhesive because starting wet increased the penetration to some degree. When the paper starts wet, it does not have the ability to pull water from the adhesive into the fibers, increasing the viscosity or cause clogging. While the increase is not drastic for the “start wet” experiments, it does indicate increased penetration that may be caused by less of a buildup of solids in the pore and the resulting clogging. In the case of wetted paper, when we used the original viscosity in the model, the model predicted more penetration than what was measured as shown in the last column of Table 6.9. This result indicates a "clogging" mechanism because dewatering is eliminated for this condition because the fibers are already saturated. It may also be that the dewatering helps the clogging occur faster with starting dry samples.

Table 6.9. Average penetration depths and their 95% confidence intervals for the uncoated paper glued at 55 and 45% solids, 0.15 and 1 MPa pressure, and 10 s time.

Solids %	ΔP (MPa)	Experiment, Start Dry, Controlled Dry (μm)	Experiment, Start Dry, Oven Dry (μm)	Experiment, Start Dry, Air Dry (μm)	Experiment, Start Wet, Controlled Dry (μm)	One-Layer Model, Start Wet, (μm)	One-Layer Model (μm), Start Wet, No change in viscosity ($S_{new}=S_o$)
55	0.15	32±6	35±10	38±16	43±11	36	75
55	1	34±11	45±9	44±7	56±28	61	69
45	0.15	42±5	49±20	–	–	–	–
45	1	42±16	43±18	–	–	–	–

The paper that was held constant for all previous results was compared with a new paper that is uncoated and has different properties (basis weight=580 g/m^2, thickness=383 μm, void fraction=0.49, permeability=2.18×10^{-14} m^2, surface tension=0.07 N/m, and contact angle=44.81 degree). The new paper is shown next to the constant paper in Figure 6.19 with a water droplet on top of each.

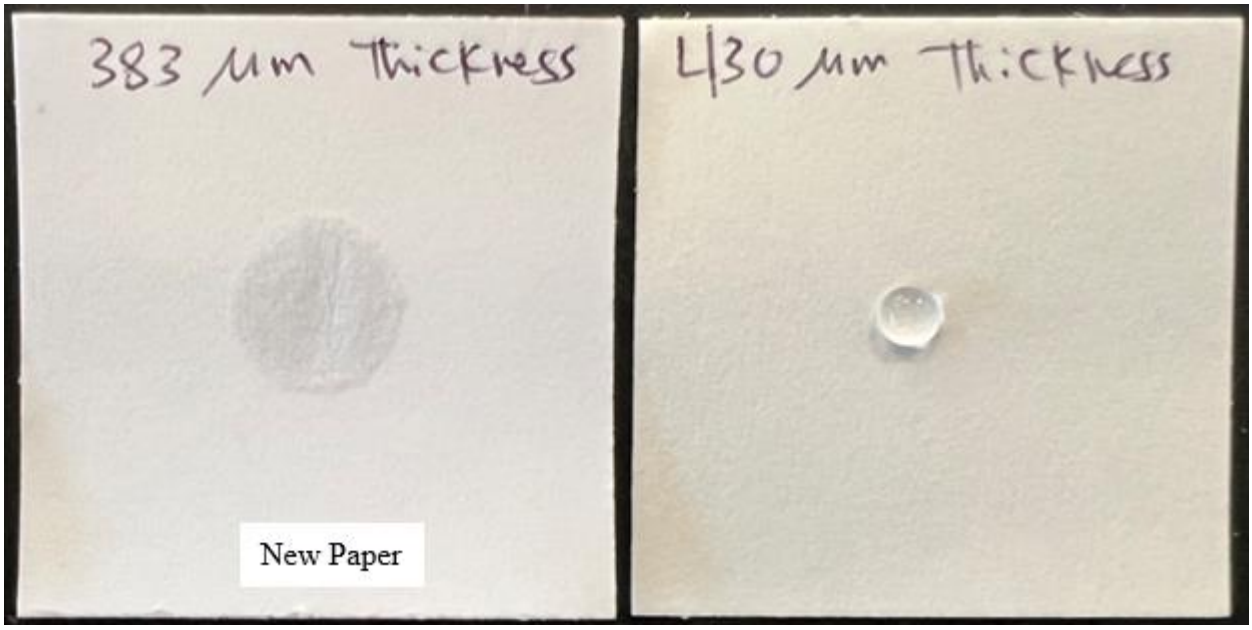

Figure 6.19. New paper (left) and the paper that was used for all previous adhesion tests (right).

The amount of adhesive was reduced to 0.2 ml after was 0.4 ml for all previous runs. Table 6.10 show the experimental adhesive penetration depths for both uncoated papers glued at 55% solids, 0.15 and 1 MPa pressure, and 1 and 10 seconds time using the carver press tester. Cutting the adhesive amount in half did not change the penetration depths for all conditions and both papers despite the differences in both paper properties. In this situation, the results are independent of any further decrease in the adhesive amounts. As a result, it is worth mentioning that low amounts of adhesive are enough to bond the sample and reach the same penetration depth as higher amounts. Considering this interesting finding, if a wise usage of adhesive is considered, then issues around adhesive cost and storage should be minimized. This finding is another confirmation of dewatering and clogging mechanisms seen with the higher adhesive amounts since reducing adhesive amounts did not change penetration depths. This situation is further approved by Table 6.11 which shows the experimental adhesive penetration depths for both uncoated papers glued at 55% solids, 0.15 and 1 MPa pressure, and 1, 10, and 60 seconds time using the carver press tester. In this table, the adhesive amount was restored to normal (0.4 ml) but the penetration depths were still similar to the case of 0.2 ml adhesive regardless of the paper used and the press pressure or time applied.

Table 6.10. Average penetration depths and their 95% confidence intervals for the uncoated paper glued at 55% solids, 0.15 and 1 MPa pressure, 1 and 10 s time, and 0.2 ml adhesive.

Paper Type	ΔP (MPa)	Time (sec)	Experiment (μm)	Lmax (μm)	One-Layer Model (μm)	One-Layer Model (μm), No change in viscosity ($S_{new}=S_o$)
Constant Paper	0.15	1	33±28	42	12	34
Constant Paper	1	10	34±10	34	34	34
New Paper	0.15	1	30±19	41	–	–
New Paper	1	10	35±8	36	–	–

Table 6.11. Average penetration depths and their 95% confidence intervals for the uncoated paper glued at 55% solids, 0.15 and 1 MPa pressure, 1 and 10, 60 s time, and 0.4 ml adhesive.

Paper Type	ΔP (MPa)	Time (sec)	Experiment (μm)	Lmax (μm)
Constant Paper	0.15	1	31±5	85
Constant Paper	0.15	60	34±17	81
New Paper	0.15	1	26±14	87
New Paper	0.15	60	38±22	75
Constant Paper	1	10	34±11	58
Constant Paper	1	60	43±14	53
New Paper	1	10	32±26	63
New Paper	1	60	46±14	53

To further confirm the clogging mechanism, the adhesive was diluted down to low concentrations (10% and 1% solids) and then filtered using the paper of interest (uncoated, 10 pph, and 40 pph papers) for five minutes each as shown in Figure 6.20. The vacuum pressure in the aspirator was around 95.3 KPa measured using a digital pressure gauge (RuchundeBu, 202200194) with an accuracy of ±0.3%. It turned out that these adhesives, even at low concentrations, seem to "clog" up the paper. It may be because the latex is deformable and when pulled into a pore, can deform and clog it. These filtration tests prove the idea of clogging as well.

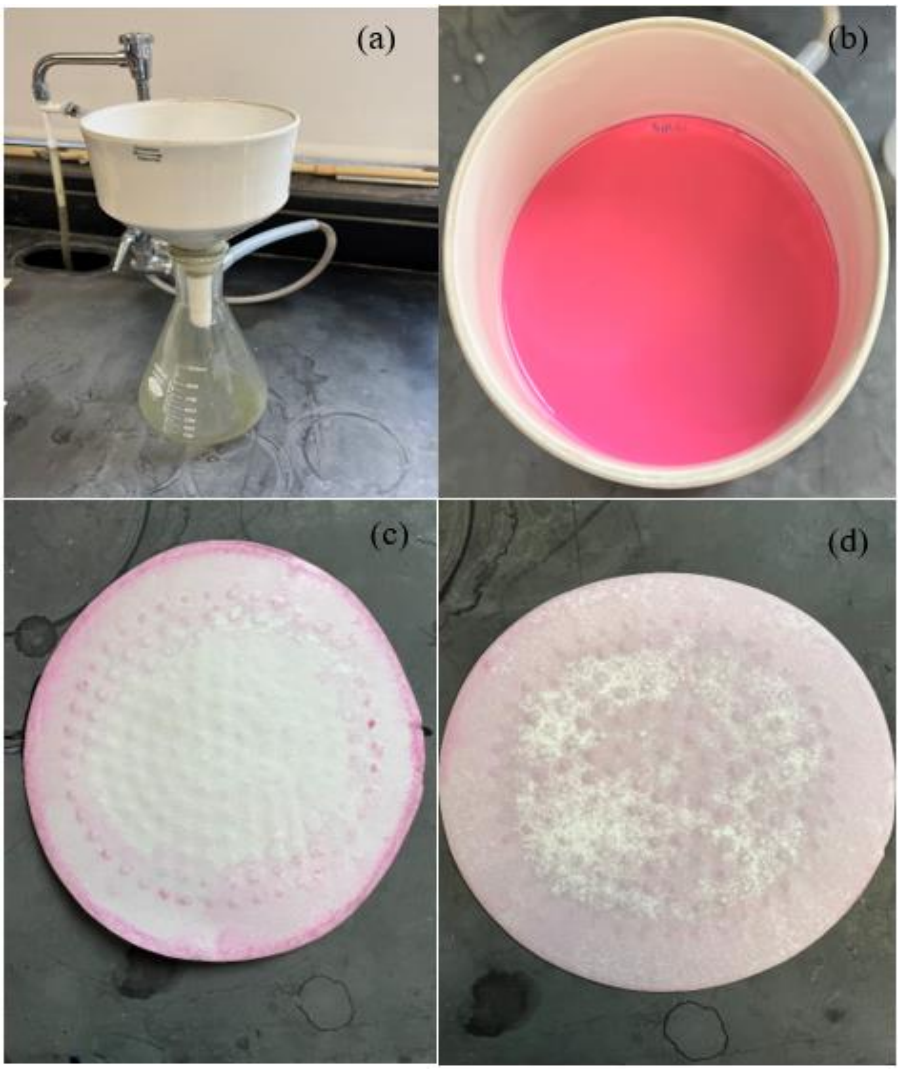

Figure 6.20. Filtration method. Water aspirator (a), paper sample in aspirator with adhesive on top (b), back side of sample with no sign of adhesive (10% solids) at the center (c), and back side of sample with some spots of adhesive (1% solids) at the center (d).

Table 6.12 shows that even with 10% adhesive solids, the penetration depths were 24, 23, and 7 μm for the uncoated, 10 pph, and 40 pph samples, respectively. These values are low but quite close to the previous values obtained from the adhesion tests done at different conditions which further explains that the penetration depth results are independent of the adhesive concentrations or amounts because of the clogging. The one-layer model also confirmed clogging by showing increased penetration depths when using the original viscosity but was limited by the maximum penetration depth for all cases.

Table 6.12. Average penetration depths for coated and uncoated papers. Adhesive with 10% solids was filtered under vacuum through each paper for five minutes using water aspirator.

Sample	Experiment (μm)	Lmax (μm)	One-Layer Model (μm), No change in viscosity (S_{new}=S_o)
Uncoated	24	40	40
10 pph SA+Medium	23	75	75
40 pph SA+Medium	7	51	51

Figure 6.21 depicts the three mechanisms that are 1) dewatering, 2) clogging, and 3) squeezing. For the dewatering mechanism, the particles of the adhesive will get closer to each other as the water leaves into the fibers increasing adhesive solids, concentration, and finally viscosity. The clogging mechanism on the other hand is controlled by the size of the particles flowing into the pores. Finally, the squeezing mechanism is based on a simple squeezing of the adhesive out from the region of interest with more time or pressure leaving the same amount available for penetration, and in this case, the penetration is limited by the Lmax.

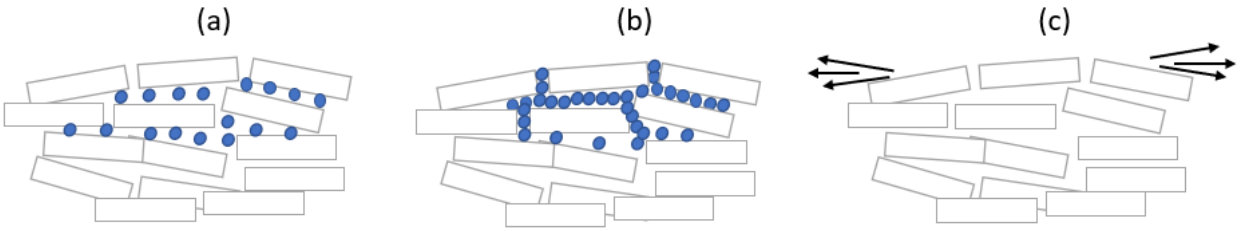

Figure 6.21. Adhesive particles in pores surrounded by few fibers for dewatering (a) and clogging (b), while squeezing (c).

Table 6.13 shows the filtercake resistance values calculated for samples glued using the roll press tester while Table 6.14 shows the filtercake resistance values calculated for samples glued using the carver press tester, applying Equation (6.17). The filtercake resistance values were mostly in the range of 10^{16}-10^{17} for all solids, papers, times, and pressures which can be related to the "clogging" mechanism as well.

Table 6.13. Filtercake resistance values for samples glued using the roll press tester.

Sample	Solids %	ΔP (MPa)	Time (sec)	Filtercake Resistance α (m/Kg)
Uncoated	55	1	1	1.3×10^{16}
10 pph SA+Medium				1.2×10^{16}
40 pph SA+Medium				4.2×10^{16}
Uncoated	45	1	1	2.1×10^{16}
10 pph SA+Medium				1.4×10^{16}
40 pph SA+Medium				6.1×10^{17}

Table 6.14. Filtercake resistance values for samples glued using the carver press tester.

Sample	Solids %	ΔP (MPa)	Time (sec)	Filtercake Resistance α (m/Kg)
Uncoated	55	0.15	1	2.4×10^{15}
			10	2.2×10^{16}
			30	4.5×10^{16}
			60	1.2×10^{17}
		1	1	1.1×10^{16}
			10	1.3×10^{17}
			30	2.8×10^{17}
			60	4.9×10^{17}
Uncoated	45	0.15	1	1.2×10^{15}
			10	1.5×10^{16}
			30	5.7×10^{16}
			60	1.2×10^{17}
		1	1	9.5×10^{15}
			10	1.1×10^{17}
			30	2.3×10^{17}
			60	4.3×10^{17}
10 pph SA+Medium	55	0.15	1	4.9×10^{14}
			10	2.3×10^{16}
			30	5.5×10^{16}
			60	1.4×10^{17}
		1	1	1.5×10^{16}
			10	1.3×10^{17}
			30	2.5×10^{17}
			60	9.7×10^{17}
40 pph SA+Medium	55	0.15	1	3.9×10^{16}
			10	4.1×10^{17}
			30	3.3×10^{17}
			60	4.4×10^{21}
		1	1	3.4×10^{17}
			10	3.5×10^{18}
			30	7.6×10^{18}
			60	4.2×10^{18}

6.6 Concluding Remarks

The results of the setting of the water-base adhesive in an uncoated substrate and substrates coated with two latex levels and one pigment size were discussed using two different setting methods and two press pressures, two adhesive solids, and four press times. The penetration depth decreased as the latex level increased in the coating layer. The penetration depth results were independent of press times and pressures and solids. Mechanical testing confirmed this situation as well by showing similar loads for various conditions. Mechanical testing also showed that as the latex level increased in the coating layer the load increased as well.

An attempt was made to characterize the dynamic setting or the green bond strength as well as the final bond strength using the roll press tester. The force needed to peel the glued samples apart at different peeling times was measured with dynamic data being recorded. The green bond strength and final strength were measured by different adhesives applied at different solids as well as for different substrates. The roll press tester is a nice method to predict the green bond strength where it in a repeatable way provides the shortest time between spreading the adhesive on a substrate and measuring the green bond strength.

The experimental results were also compared to Darcy's model which accounts for the change of viscosity of the fluid as it enters the pore, a multi-layer system, and a finite adhesive quantity. Good agreement is seen for the uncoated paper and low predictions for the coated substrates. Out of the three mechanisms that influence water-based adhesive setting systems which are dewatering, clogging, and simple squeezing, the dewatering and clogging mechanisms seem to describe the results best.

6.7 Model of Penetration into a Single Capillary Accounting for Unsteady Diffusion Through Capillary Wall

6.7.1 Introduction

The setting of water-based adhesives was modeled similarly to the hot melt adhesives, but now, the viscosity is a function of concentration, not temperature. Two-phase flow with the level-set method and transport of diluted species are used to simulate solvent loss to capillary walls; this loss should be related to water uptake into the cellulose structure of the fiber, leaving the polymer behind at the boundary. The unsteady-state flow was simulated in which the viscosity is a function of the amount of solvent (water) that diffuses through paper or board walls where both water and adhesive diffusion coefficients play a major role. The viscosity function was represented in Equation (6.8) above.

The penetration as a function of time is predicted similarly to the temperature dependent case described earlier. At the internal boundary of the capillary, the concentration of the polymer was specified. This concentration should be the value that represents a saturated solution of the polymer. If the polymer is latex, then the concentration at the wall will be taken as the maximum packing of the latex particles. The inlet concentration of the polymer is well known from the solids.

As fluid penetrates the pore, the polymer concentration at the wall will be high compared to the polymer concentration of the incoming fluid. Therefore, the polymer will diffuse from the wall into the fluid. This increase in concentration will increase the viscosity of the fluid, decreasing the rate of polymer penetration. It is expected that the rate of penetration will likely come to a stop after some point in the simulation.

This model assumes that the pore boundary is able to take up water quickly and transport it away from the pore. The water retention value of the fibers is known, but the time scale for this

transport is not clear. If the model under predicts the penetration, it may be caused by a limited rate of water transport from the pore wall to the fiber bulk. If this is the case, a concentration boundary condition that increases in time could be imposed in the model.

When the water-based adhesive penetrates the coating layer, water is not expected to be absorbed by the boundaries of the coating layer. To model this effect, the coating layer thickness could be represented by a pore that has a no flux condition imposed. This pore would be followed by a pore that would represent the paper structure, with the boundary condition found for the uncoated samples.

6.7.2 Model Set-Up

The model set-up used here is similar to the one used for the isothermal, Chapter 2, and non-isothermal, Chapter 3, cases described earlier except that the transport of diluted species physics was added instead of the heat transfer in fluids physics. Also, instead of the non-isothermal flow that was added to the Multiphysics tree to couple fluid flow with heat transfer, the reacting flow, diluted species was added where both fluid flow and transport of diluted species were coupled. The meshed geometry is depicted in Chapter 2 in Figure 2.1.

In the transport of diluted species section, we added the initial concentration boundary for the capillary (1500 mol/m^3) as well as for the adhesive (1500 mol/m^3). Two other boundaries have been added also, one was used to set the wall concentration (Boundary 6) to be at C_w (3000 mol/m^3) and the other was used to let the inlet region (Boundaries 2 and 8) be at C_{Ao} (1500 mol/m^3). The diffusion coefficient of the fluid that is flowing into the pore can be inserted into the parameter section. For the full range of parameters, the normal mesh at small times and the slip length factor (f =1) were used.

6.7.3 Results and Discussion

The parameters that control the importance of solvent diffusion into the pore walls can be combined into several dimensionless groups. The wall concentration can be scaled with the initial concentration C_{Ao}. Therefore, the first dimensionless parameter to develop is $C_w^* = C_w/C_{Ao}$. The parameter E is also scaled with the initial concentration $E^* = E/C_{Ao}$. The Schmidt number which is defined as the ratio of molecular momentum transfer to molecular mass transfer is used to relate the diffusion coefficient with viscosity and density $Sc= A/D_f \rho$. The last parameter group that is important to test is $M^*= \rho R^2 \Delta P/A^2$. The latter group is important in specifying the key influencing parameters that control the flow in the porous media and can be practically important when compared with the experimental data. The Schmidt number depends on viscosity, density, and diffusion coefficient, and the difference between it and the M* group is that it does not account for the changes in pressure pulse and pore radii. These groups were tested to determine the limits that control the diffusion of solvent away from adhesive through pore walls during the modeling of concentration changes.

The goal of this section is to quantify how concentration dependency of viscosity can affect the penetration depth and amount when concentration changes viscosity. The highest and lowest values of the viscosity based on Equation (6.8) are equal to 0.01 Pa s and 10 Pa s when using A is equal to 0.01 Pa s, E is equal to 20723 mol/m^3, and C_A is going from 1500 mol/m^3 to 3000 mol/m^3.

Figure 6.22 shows the results of the modeling of various values of C_w^*. When the applied pressure was increased into $\Delta P^*=50$, the increase in the L* was about 96% for the modeling of $C_w^*=2$ at the t* value of 2000. The C_w^* value of 2 represents the results when the inlet fluid concentration is set to the high concentration and the fluid viscosity is uniformly high (following the case when the viscosity is of the higher value). However, the C_w^* value of 1 represents the

results when the wall is set to the same concentration as the inlet C_{Ao}, to recover the case with no diffusion effects (following the case when the viscosity is of the lower value). The modified Lucas-Washburn equation has been perfectly recovered for the C_w* of 1 at ΔP*=0, while the C_w* of 1.1 was the value that gave an excellent agreement with the theory at ΔP*=50.

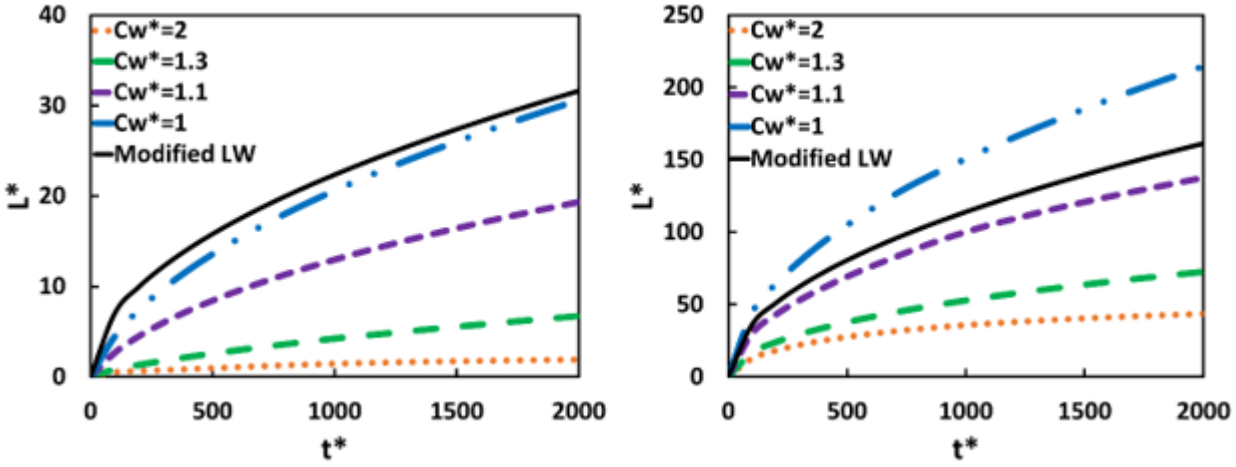

Figure 6.22. Effect of C_w* changes on the penetration depth for E* of 13.8, Sc of 37227, and M* of 139, for ΔP*=0 (Left) and ΔP*=50 (Right).

Figures 6.23 and 6.24 show the modeling results of various values of Sc and M*, respectively. The Sc values of 0.372 and 3,722,731 represent the minimum and maximum values that any other values above or below these limits will give the same L*. The penetration depths were low for the modeling of Sc and M* where the decrease in the L* was about 94% at ΔP*=0 and about 70% at ΔP*=50 when comparing the results of the modeling of Sc value of 3,722,731 with the results of the modeling of C_w* value of 1, both at t*=2000. This is a clear indication that the solvent diffusion coefficient can play a major role during the setting of water-based adhesives. Increasing C_w* will increase adhesive viscosity, slowing adhesive penetration into the pore. On the other hand, the opposite behavior was seen when increasing Sc and/or M*.

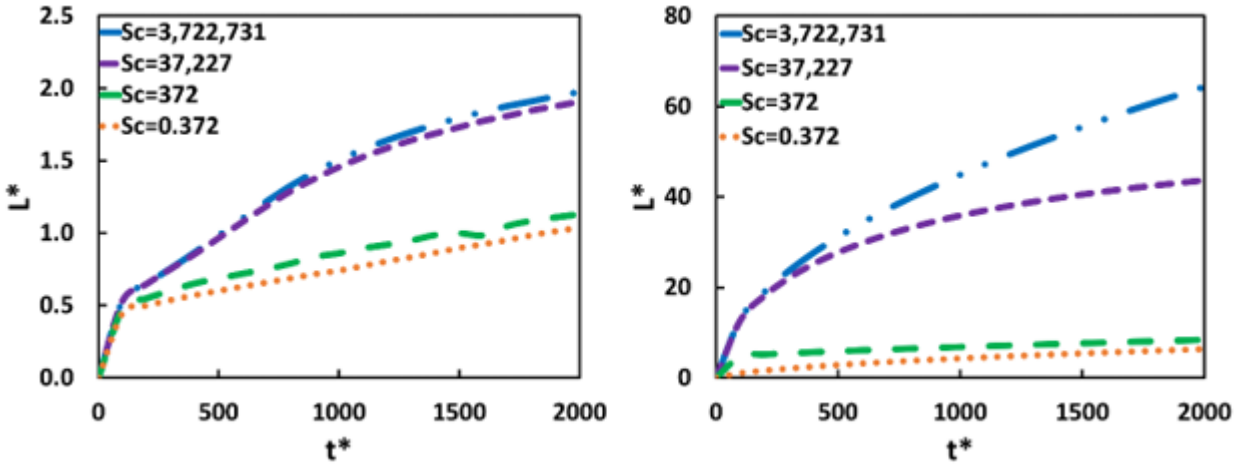

Figure 6.23. Effect of Sc changes on the penetration depth for C_w* of 2, E* of 13.8, and M* of 139, for ΔP*=0 (Left) and ΔP*=50 (Right).

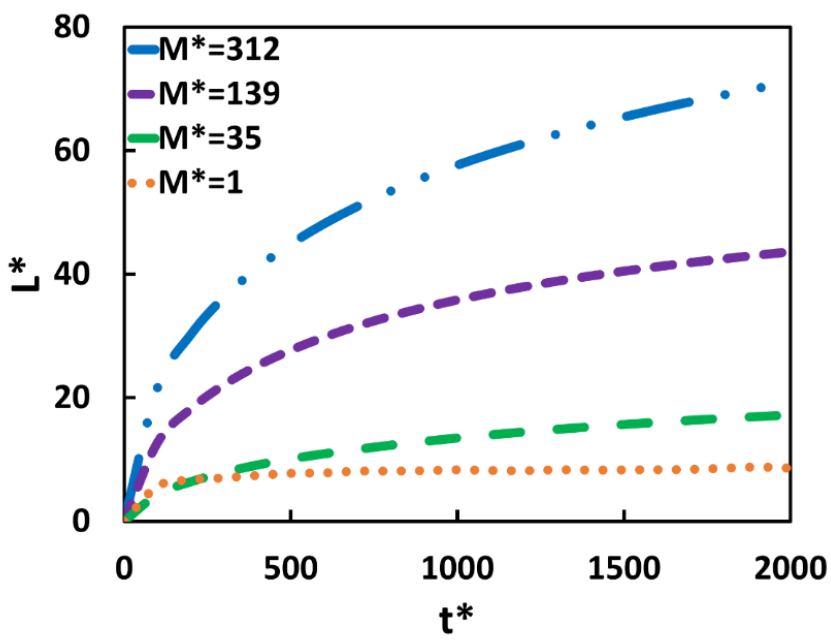

Figure 6.24. Effect of M* changes on the penetration depth for C_w* of 2, E* of 13.8, and Sc of 37227.

A clear scene of the results can be seen through the 2D surface plots that are depicted in Figures 6.25 and 6.26 where the concentration and viscosity fields are shown for various values of Sc and M* in which three different diffusion coefficients and pore radii were modeled. It is

interesting to notice when these groups are large (low diffusion coefficient and/or large pore radius), the viscosity only increases along with the layer near the pore boundary, but as they decrease, the viscosity is high throughout the pore region. This may contribute to the fact that at a low value of solvent diffusion coefficient, the solvent will slowly diffuse through the pore walls and the change in the adhesive concentration throughout the pore region will remain almost the same leading to a uniform adhesive viscosity distribution inside the pore. On the other hand, as the pore radius increases, the concentration that builds up at the pore wall will need more time to diffuse back into the pore region due to the large pore radius and in this case, the change in adhesive viscosity inside the pore region is going to be less compared to the case with the lower pore radius.

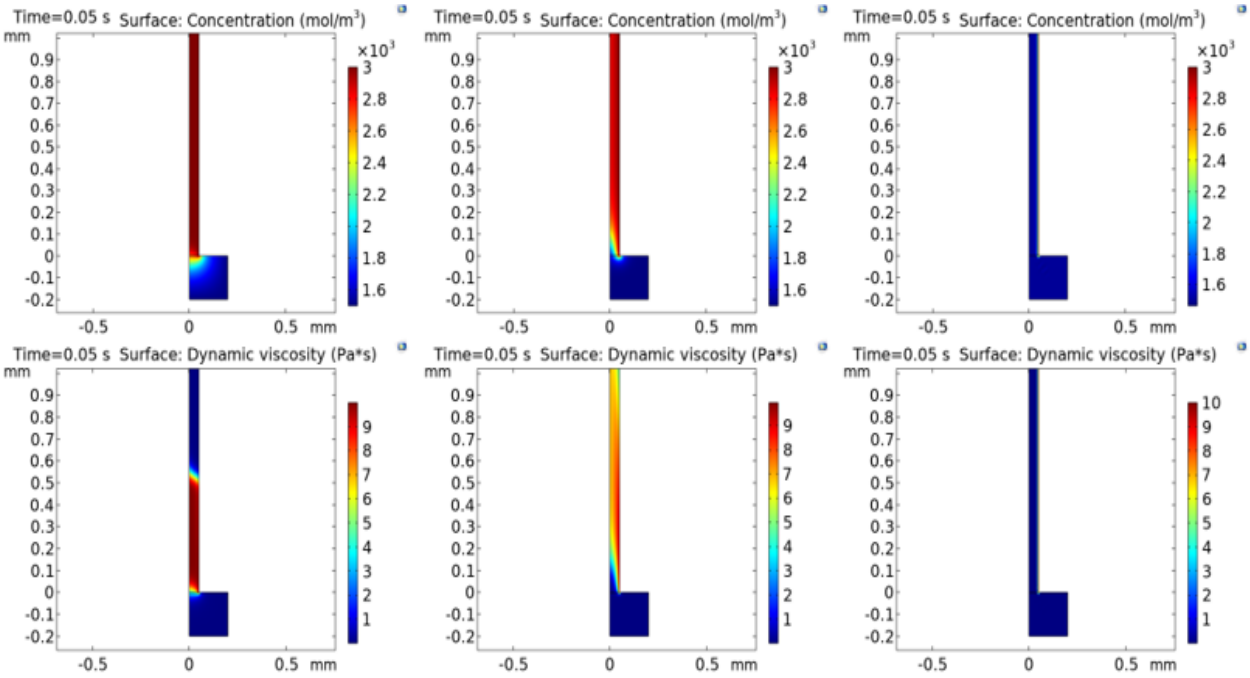

Figure 6.25. Concentration (top row) and viscosity (bottom row) distribution in the pore region for $\Delta P^*=50$, $E^*=13.8$, $C_w^*=2$, $M^*=1388$ for values of Sc of 0.0372, 372, and 3722731 from left to right respectively. Blue is a low value and red is a high value.

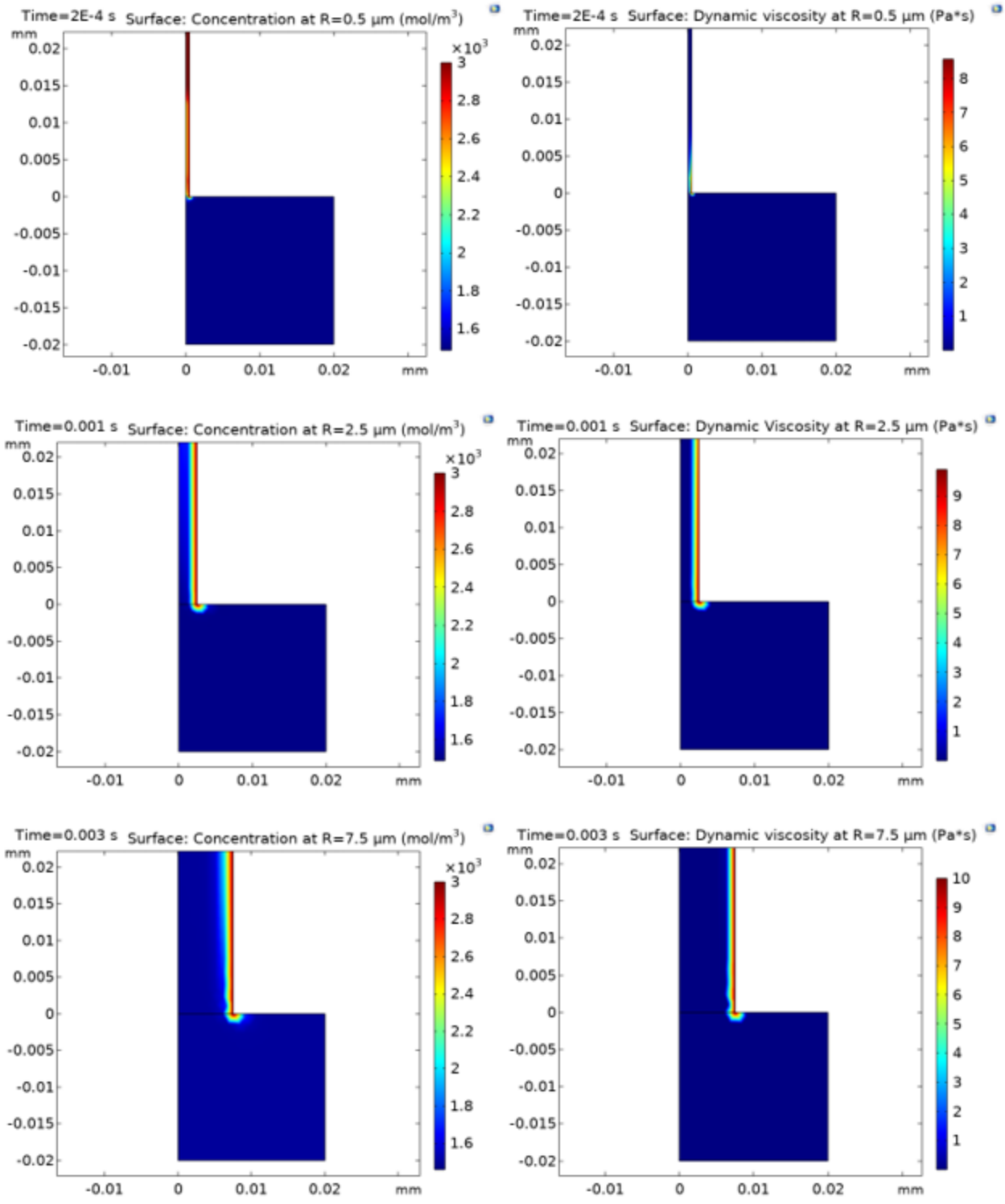

Figure 6.26. Concentration (left column) and viscosity (right column) distribution in the pore region for E*=13.8, C_w*=2, Sc=37227 for values of M* of 1 (top row), 35 (middle row), and 312 (bottom row). Blue is a low value and red is a high value.

Just like for the non-isothermal case, the dimensionless group that causes to switch from "no concentration change" to "concentration change important" is predicted that we call Z*

$$Z^* = Sc\ M^* = \frac{R^2\ \Delta P}{D_f\ A} \qquad (6.18)$$

In this group, different parameters determine if solvent diffusion is important or not. When this group is large, over 5×10^6, diffusion is minimal and large penetration happens. When it is small, less than 5×10^6, as in most normal values of parameters, diffusion is important and little penetration happens. This makes sense since if A is large, Z* is small, the flow is slow, and more chance for more diffusion through the pore walls. If the pore is small, you get less flow and less distance for mass transfer, more chance for more diffusion. If ΔP is large, the flow is large, and solvent diffusion through walls is minimal.

This new dimensionless group is interesting in that it combines the fluid flow and mass transfer parameters into a single group. This group can be useful in a practical situation in that if this combination of parameters is less than 5×10^6, it can be assumed that the solvent diffusion is important, and the penetration should be minimized. For most reasonable estimates for material parameters for adhesive, this group is often small. For example, for a pore radius of 5 μm, density of 1110 kg/m^3, a diffusion coefficient of 2.42×10^{-10} m^2/s, pressure pulse of 500 kPa, and a viscosity of 100 Pa s, and surface tension of 0.05 N/m, the group Z* = 516. If the pore size is 1 μm, the value drops to 21 while it drops to 0.05 when using a diffusion coefficient value of 2.42×10^{-6} m^2/s. For this range of parameters, the viscosity increases everywhere in the pore region as represented by Figures 6.25 and 6.26. For low values of diffusion coefficients and/or large pore sizes, the concentration and viscosity increase only along the side of the pore as shown in Figures 6.25 and 6.26.

6.7.4 Concluding Remarks

In a conclusion, the model predictions shown above were expected since when the solvent diffuses through the pore walls, the adhesive particles will accumulate near the pore walls, leading to an increase in its concentration. This increase in concentration will lead to an increase in the viscosity of the adhesive, decreasing the rate of adhesive penetration. The results of the modeling of the wall concentration C_w* showed high penetration depths. On the other hand, the penetration depths were low for the modeling of Sc and M*. Small values of viscosity or diffusion coefficient link to high flow rates into the pore or low mass transfer leading to less diffusion through the pore wall. Small pore sizes generate slow flow into the pore and small mass transfer distances are required to increase adhesive concentration. Large values of pressure increase the flow and decrease the chance of solvent diffusion. The Z* dimensionless group is interesting in that it combines the fluid flow and mass transfer parameters into a single group. This group can be useful in a practical situation in that if this combination of parameters is less than 5×10^6, it can be assumed that the solvent diffusion is important, and the penetration should be minimized.

CHAPTER 7: CONCLUSIONS AND RECOMMENDATIONS

7.1 Conclusions

The general goal of this work is to overcome the failure of the bonded joints in which fluid flow and temperature and concentration changes play a major role. The failure mechanisms are hard to predict especially when there are multiple parameters that control the fluid flow in an unsteady-state case. However, these mechanisms can be understood well when these parameters are divided into a series of groups that have a dependency on each other. In the current research study, these parameters were studied both experimentally and theoretically, as well as simulations using COMSOL were performed to cover the whole range of parameters that affect setting processes.

The first part of this research involved several lab experiments in efforts to understand the extent of penetration of hot melt and water-based adhesives into several porous coated and uncoated substrates and to reach the best technique that results in the strongest green and final bonds between adhesives and substrates. The significant finding in this research study is that the penetration depth of hot melt and water-based adhesives was successfully measured experimentally on a microscale level using four novel experimental techniques developed in the laboratory. These methods were internally consistent and showed similar results for different adhesion conditions. Out of these four methods, the silicone oil method was less complex, had high accuracy, and was repeatable to characterize the adhesive penetration depth.

The process of bonding two papers using the hot melt adhesive was done in the carver press tester in which two paper temperatures and press pressures were varied. The samples were coated with styrene acrylate latex at four levels (10, 20, 30, and 40 pph) and three pigment sizes (Premier, Astra-glaze, Astra-plate) at 60% solids using the rod draw-down coater. For the uncoated surfaces,

the results showed that the paper temperature is the key parameter in the setting of hot melt adhesive where little penetration and peeling force were associated with the samples glued at the ambient temperatures and high penetration and peeling force were achieved for the high paper temperature glued samples. For the coated surfaces, the results showed that the permeability of the sample is the key parameter as the latex level increases in the sample, the penetration depth decreases due to the reduced permeability. The three pigment sizes used in this study had a minor impact on the results.

For the water-based adhesive, the samples were bonded using the carver press test as well as the roll press test at two press pressures and four press times, and two adhesive solids contents. Besides uncoated surfaces, coated surfaces were generated using two latex levels (10 and 40 pph) and one pigment size (Premier). The results here showed more penetration when the paper is uncoated and less penetration when the latex level increased in the coating layer. However, the various press pressures, times, and adhesive solids showed similar penetration depths. This could be related to a filtercake formation that happens when the fluid penetrates the paper filling out some pores but then the particles clog and stop flowing. This is supported by the mechanical tester that showed similar peeling forces for all conditions as well. The dewatering mechanism also played a role during the water-based adhesive setting where water diffuses through the fibers leaving the adhesive at increased viscosity. In a conclusion, both dewatering and clogging mechanisms are important for practical operation where smaller pore size or bigger adhesive particle can prevent adhesive penetration, increases its viscosity due to dewatering to the point at which the adhesive stops flowing, and solidifies inside the pore. If the paper substrate has a bigger pore size compared to adhesive particles, then better penetration and adhesion are expected. In

addition, the green bond strengths were measured for all conditions using the roll press tester where they were low compared to the final bond strengths measured for the same samples.

The second part of this research involved several modeling to support the experimental work. The first model used was based on Darcy's law which was used to predict the adhesive penetration depth in a porous media as a function of fundamental parameters accounting for different layers of pore space and the limited supply of adhesive. The second model used to compare with experiments was based on the Lucas-Washburn equation modified for the inlet pressure accounting for fluid flow in a single pore. COMSOL modeling was the third option used in this research. The reason for using COMSOL modeling is to cover most of the parameters that have the potential to influence the process of penetration. All model predictions were compared to the experimental results and good agreement for all conditions was obtained. The validation of the model predictions with the experimental data will constitute a novel contribution to science and engineering. In addition, two dimensionless groups (D^* for the hot melt adhesive model) and (Z^* for the water-based adhesive model) were generated based on COMSOL to test if cooling and diffusion are important. The results concluded that if $D^* > 1000$, cooling is not expected to occur and large penetration happens, while if $Z^* > 5\times10^6$, diffusion is minimal and large penetration happens as well.

Modeling can bring more knowledge and understanding to this area since it is going to be the first-time investment of this software in the setting of adhesives. Modeling can become a predictive tool that provides a more rapid diagnosis ahead of the adhesion failure and solves the more complicated penetration situations. Moreover, modeling can help in reducing lab efforts, time, and cost. The investment in modeling techniques to predict the setting rate and the bond strength should balance the ease of use with a good description of the gluing event.

The outcome of the theoretical and experimental works will provide insight into the key parameters that affect the process of penetration of adhesives into a porous media and will give insight into the importance of different mechanisms on penetration. Understanding the key influencing parameters that control the dynamic behavior during the setting of adhesives will help in getting useful dynamic data, finding appropriate scenarios to prevent adhesion failure in the early stages, as well as contribute to providing the literature with a new and novel study that involves heat and mass changes in the setting of adhesive applications. The net outcome of this project can be utilized in understanding different other areas such as the flow in the blood vessels and oil pipelines, the penetration of drugs into the tissues, the membrane separations, and many other systems besides wood staining and gluing.

7.2 Recommendations for Future Studies

Failure modes are strongly related to the adhesive penetration depth. The amount and penetration depth are controlled by many factors. For example, the depth of adhesive is strongly controlled by how viscous the adhesive is. The viscosity in turn is a function of temperature, time, and position for hot melt adhesives and concentration, time, and position and solid and solvent percentages for water-based adhesives. Temperature can in turn affect the thermal conductivity, heat capacity, and density of the adhesive. The concentration of adhesive depends on other parameters such as the solvent diffusion through pores walls. Controlling the viscosity of the adhesive will lead in the end to good penetration and overcome failure modes that exist in the bonded joints. Nip pressure is another factor that affects both viscosity and penetration. Increasing pressure will force more adhesive to penetrate the porous medium where in this case capillary effects are negligible.

Although there were many parameters addressed in this research, there are still other parameters that need more attention in the future. The first recommendation for future works for the hot melt adhesive system would be to investigate different press times and paper temperatures and see how that could impact the penetration depth and eventually bond strength. The influence of thermal conductivity and heat capacity of both paper and polymer could be a separate study. Another recommendation would be to further study the diffusion of water inside pores and how that could impact the process of setting water-based adhesives. It would be beneficial to pay more attention to the impact of different adhesive solids contents on the penetration depth and the green and final bond strengths.

Another study could look at the effect of the types and amounts of adhesives applied and the types and sizes of the papers used on both hot melt and water-based adhesive systems. This study can help in understanding the clogging mechanism which is controlled by the pore size distribution of the paper and the particle size of the water-based adhesive. A great study would be to investigate the effect of various types and amounts of latexes and types and amounts of pigments on the penetration depth and the bond strength.

The penetration depths of adhesives were measured using four novel techniques developed in this study, however, developing other techniques could advance the knowledge presented here and limit the use of cross-sectional images for depth determinations. In yet another study, the effect of pore size distribution, pore volume, permeability, surface tension, and contact angle on adhesives settings requires more investigation. In addition, both the carver press and roll press methods were great techniques to press two papers together, however, more novel techniques are required especially for the water-based adhesive setting that needs short times to measure green bond strengths.

Incorporating temperature and concentration changes during the penetration of liquid adhesives into a porous media using modeling techniques must contribute to providing new and unique dynamic details where there is an obvious lack of articles in both modeling and setting of adhesives that have discussed these types of problems. Solving and understanding the dynamic details of adhesives penetration have not been covered yet to the extent that can be understood well, especially when having parameters dependent on each other such as the temperature and concentration dependency of viscosity. These dynamic details play a major role in the setting of adhesives.

REFERENCES

A. Chiminelli, C. Valero, M. Lizaranzu, C. I. López & M. Canales, “Modelling of Bonded Joints with Flexible Adhesives.” The Journal of Adhesion 95(5–7): 369–84. (2019).

A.O. Rapp, H. Bestgen, W. Adam and R.-D. Peek, ”Electron Energy Loss Spectroscopy (EELS) for Quantification of Cell-Wall Penetration of a Melamine Resin”. Holzforschung Vol. 53, No. 2, (1999).

Ahmed, Sharf U., “Hot Melt Adhesives Comprising Crystalline and Amorphous Polymers.” TAPPI Journal 89–93 (2001).

Alexander F. Routh, William B. Zimmerman, “Distribution of particles during solvent evaporation from films.” Chemical Engineering Science 59, 2961–2968 (2004).

Alleborn, Norbert, and Hans Raszillier, “Dynamics of Films and Droplets Spreading on Porous Substrates.” TAPPI Journal 6(3): 16–23 (2007).

Alshare, A. A., P. J. Strykowski, and T. W. Simon, “Modeling of Unsteady and Steady Fluid Flow, Heat Transfer and Dispersion in Porous Media Using Unit Cell Scale.” International Journal of Heat and Mass Transfer 53(9–10): 2294–2310 (2010).

Avni, E, Salama, S, Turi, E, Union Camp Corp, ‘‘Method of Making High Quality Extrusion Coated Paper for Quality Printing.’’ US Patent 4,929,474 (1990).

Awasthi, Mukesh Kumar, and Rishi Asthana, “Viscous Potential Flow Analysis of Capillary Instability with Heat and Mass Transfer through Porous Media☆.” International Communications in Heat and Mass Transfer 40: 7–11 (2013).

Babaelahi M., D. D. Ganji, and A. A. Joneidi, “Analysis of Velocity Equation of Steady Flow of a Viscous Incompressible Fluid in Channel with Porous Walls.” International Journal for Numerical Methods in Fluids 63: 1048–59 (2010).

Baggio, P., C. Bonacina, and B. A. Schrefler, “Some Considerations on Modeling Heat and Mass Transfer in Porous Media.” Transport in Porous Media 28(3): 233–51 (1997).

Bashford, Richard, “Water Borne Adhesives.” Polymers, Laminations & Coatings Conference 373–75 (1993).

Blunt, Martin J., and Harvey Scher, “Pore-Level Modeling of Wetting.” Physical Review E 52(6): 6387–6403 (1995).

Bousfield, Douglas W, and George Karles, “Penetration into Three-Dimensional Complex Porous Structures.” Journal of Colloid and Interface Science 270(2): 396–405 (2004).

Bousri, A., Nebbali, R., Bennacer, R., Bouhadef, K. and Beji, H., “Numerical investigation of forced convection nonequilibrium effects on heat and mass transfer in porous media.” Heat Transfer Engineering 38(1), pp. 122-136 (2017).

Bulcke, J Van Den, V Rijckaert, J Van Acker, and M Stevens, “Quantitative Measurement of the Penetration of Water-Borne Coatings in Wood with Confocal Lasermicroscopy and Image Analysis.” Holz als Roh- und Werkstoff 61: 304–10 (2003).

C. J. Buckley, C. Phanopoulos, N. Khaleque, A. Engelen, M. E. J. Holwill and A. G. Michette, “Examination of the Penetration of Polymeric Methylene Di-Phenyl-Di-Isocyanate (pMDI) into Wood Structure Using Chemical-State X-Ray Microscopy.” Holzforschung 56 215–222 (2002).

C. J. van Oss, R. J. Good, and M. K. Chaudhury, “Additive and Nonadditive Surface Tension Components and the Interpretation of Contact Angles.” Langmuir 4: 884–91 (1988).

Carl Houtman, Steve Severtson, Jihui Guo and Helen Xu, Larry Gwin , “Properties of Water-Based Acrylic Pressure Sensitive Adhesive Films in Aqueous Environments.” TAPPI 8th Researcb Forum on Recyling: 1–6 (2007).

Charles C. Han and A. Ziya Akcasu, “Concentration dependence of diffusion coefficient at various molecular weights and temperatures.” POLYMER Vol 22 (1981).

Charles R. Frihart, “Adhesive Groups and How They Relate to the Durability of Bonded Wood.” Journal of Adhesion Science and Technology 23:4, 601-617 (2009).

Chen, Qingyan (Yan), Zhiqiang (John) Zhai, and Liangzhu (Leon) Wang, “Computer Modeling of Multiscale Fluid Flow and Heat and Mass Transfer in Engineered Spaces.” Chemical Engineering Science 62(13): 3580–88 (2007).

Cheng Xing, Bernard Riedl, Alain Cloutier, Stephen M. Shaler, “Characterization of urea–formaldehyde resin penetration into medium density fiberboard fibers.” Wood Sci Technol 39: 374–384 (2005).

Cheng, HY, Yang, YJ, Li, SC, Hong, JY, Jang, GW, ‘‘Modification and Extrusion Coating of Polylactic Acid Films.’’ Journal of Applied Polymer Science 132 (35) (2015).

Cooper, L.J., Daly, K.R., Hallett, P.D., Naveed, M., Koebernick, N., Bengough, A.G., George, T.S. and Roose, T., “Fluid flow in porous media using image-based modelling to parametrize Richards' equation.” Proceedings of the Royal Society A: Mathematical, Physical and Engineering Sciences 473(2207), p. 20170178 (2017).

Dadvar, Shima, Sanjeev Chandra, and Nasser Ashgriz, “Adhesion of Wax Droplets to Porous Polymer Surfaces.” The Journal of Adhesion 91(7): 538–555 (2015).

Dahlstrom, Christina, and Tetsu Uesaka, “Microstructure Variations in Paper Coating : Direct Observations.” American Chemical Society 51(24): 8246−8252 (2012).

Daub, E, U Hoeke, and L Goettsching, “Gluing Corrugating Medium and Linerboard Together on the Corrugator.” TAPPI Journal 73(6): 171–178 (1990).

Davit, Y. and Quintard, M., “One-phase and two-phase flow in highly permeable porous media.” Heat Transfer Engineering 40(5-6), pp. 391-409 (2019).

Ding, X. and Harris, T.A., “Review on penetration and transport phenomena in porous media during slot die coating.” Journal of Polymer Science Part B: Polymer Physics 55(22), pp. 1669-1680 (2017).

Ding, X., Fuller, T.F. and Harris, T.A., “Predicting fluid penetration during slot die coating onto porous substrates.” Chemical Engineering Science 99, pp. 67-75 (2013).

Dogan Tutak, Bekir Keskin, Said Abubakr, and Paul D. Fleming III, “Investigation of the Effect of Rubber Based Offset Ink printed on packaging Cardboard on the Strength Properties of Packing Cartons.” International Journal of Applied Science and Technology Vol. 9, No. 3, (2019).

Doug Bousfield, Harrison Gates, Jay Shands, Vaughn Wildfong, and Phil Smith, “Prediction of Starch Penetration during Sizing and Drying.” PaperCon (2016).

Douglas J. Gardner, “Application of The Lifshitz-van Der Waals Acid-base Approach To Determine Wood Surface Tension Components.” Wood and Fiber Science 28(4): 422–28 (1996).

E.G. Koricho, E. Verna, G. Belingardi, B. Martorana, V. Brunella, “Parametric Study of Hot-Melt Adhesive under Accelerated Ageing for Automotive Applications.” International Journal of Adhesion and Adhesives 68: 169–81 (2016).

Elhalwagy, Mahmoud Mohamed, and Anthony Gerald Straatman, “Dynamic Coupling of Phase-Heat and Mass Transfer in Porous Media and Conjugate Fluid/Porous Domains.” International Journal of Heat and Mass Transfer 106: 1270–86 (2017).

Erik V. Bachtiar, Gaspard Clerc, Andreas J. Brunner, Michael Kaliske and Peter Niemz, “Static and Dynamic Tensile Shear Test of Glued Lap Wooden Joint with Four Different Types of Adhesives.” Holzforschung 71(5): 391–396 (2017).

Espín, L. and Kumar, S., “Droplet spreading and absorption on rough, permeable substrates.” Journal of Fluid Mechanics 784, pp. 465-486 (2015).

Farwaha, Rajeev, and Chris Lazaroff, “Recent Advancements in Vinyl Acetate Ethylene Copolymers (VAE) for Use in Paperboard and Paper Coating.” PaperCon 196–203 (2012).

Forsyth, Robert S., “Waterborne Adhesives for Bottle Labeling.” PLACE Conference 381–89 (2004).

Fries, N, and M Dreyer, “An Analytic Solution of Capillary Rise Restrained by Gravity.” Journal of Colloid and Interface Science 320(1): 259–63 (2008a).

Fries, N, and M Dreyer, “The Transition from Inertial to Viscous Flow in Capillary Rise.” Journal of Colloid and Interface Science 327(1): 125–28 (2008b).

Gadhave, Ravindra V, Prakash A Mahanwar, and Pradeep T Gadekar, “Starch-Based Adhesives for Wood / Wood Composite Bonding : Review.” Open Journal of Polymer Chemistry 7 19–32 (2017).

Gane, P., Matthews, G., Schoelkopf, J., Ridgway, C., Spielmann, D., “Fluid transport into porous coating structures: Some novel findings.” TAPPI Journal Vol. 83(5) (2000).

Gaur, U, Wunderlich, B, ‘‘Heat Capacity and Other Thermodynamic Properties of Linear Macromolecules. II. Polyethylene.’’ Journal of Physical and Chemical Reference Data 10 (1) 119–152 (1981).

Ghassemzadeh, J. and Sahimi, M., “Pore network simulation of fluid imbibition into paper during coating—III: modelling of the two-phase flow.” Chemical engineering science 59(11), pp. 2281-2296 (2004).

Ghassemzadeh, J., Hashemi, M., Sartor, L. and Sahimi, M., “Pore network simulation of imbibition into paper during coating: I. Model development.” AIChE Journal 47(3), pp. 519-535 (2001).

Gindl, M, A Reiterer, G Sinn, and E Stanzl-tschegg, “Effects of Surface Ageing on Wettability, Surface Chemistry, and Adhesion of Wood.” Holz Roh Werkst 62: 273–80 (2004).

Gindl, M, and Stefanie Tschegg, “Significance of the Acidity of Wood to the Surface Free Energy Components of Different Wood Species.” Langmuir 18(29): 3209–12 (2002).

Godfrey, D.A. and Ardemagni, L.A., “New generation of low-density hot-melt packaging adhesives.” TAPPI Journal 77(8), pp. 88-91 (1994).

Gunnells, David W, Douglas J Gardner, and Michael P Wolcott, “Temperature Dependence of Wood Surface Energy.” Wood and Fiber Science 26(4): 447–55 (1994).

Hammerquist, Chad C., and John A. Nairn, “Numerical Simulation of Pressure-Driven Adhesive Penetration into Realistic Wood Structures.” Wood Science and Technology 52 1271–88 (2018).

Hamraoui, Ahmed, and Tommy Nylander, “Analytical Approach for the Lucas-Washburn Equation.” Journal of Colloid and Interface Science 250: 415–21 (2002).

Hansen, D, Bernier, GA, ‘‘Thermal Conductivity of Polyethylene: The Effects of Crystal Size, Density and Orientation on the Thermal Conductivity.’’ Polymer Engineering & Science 12 (3) 204–208 (1972).

Hashim, Rokiah, Siti Noorbaini Sarmin, Othman Sulaiman, and Lili Hanum Md Yusof, “Effects of Cold Setting Adhesives on Properties of Laminated Veneer Lumber from Oil Palm Trunks in Comparison with Rubberwood.” European Journal of Wood and Wood Products 69: 53–61 (2011).

Hiroshi Fujita, Akira Kishimoto, and Kinya Matsumoto, “Concentration and temperature dependence of diffusion coefficients for systems polymethyl acrylate and n-alkyl acetates.” Trans. Faraday Soc. 56, 424-437 (1960).

Hosseinalipour, S.M. and Namazi, M., “Pore-scale numerical study of flow and conduction heat transfer in fibrous porous media.” Journal of Mechanical Science and Technology 33(5), pp. 2307-2317 (2019).

Husnain, S., A. Mehmood, and A. Ali, “Heat and Mass Transfer Analysis in Unsteady Boundary Layer Flow through Porous Media with Variable Viscosity and Thermal Diffusivity.” Journal of Applied Mechanics and Technical Physics 53(5): 722–32 (2012).

J. Komornicki, G. Marin, and I. Leclere, “Rheological Behavior and Adhesion Properties of EVA-Based Hot-Melt Adhesives : Use of Computation Tools.” TAPPI Journal 185–91 (1991).

Jäder, J. and Järnström, L., “The influence of thickener addition on filter cake formation during dewatering of mineral suspensions.” Applied Rheology 13(3), pp.125-131 (2003).

Jennings, Jessica D, Audrey Zink-sharp, Charles E Frazier, and A Kamke Frederick, “Properties of Compression-Densified Wood , Part II : Surface Energy.” Journal of Adhesion Science and Technology 20(4): 335–44 (2006).

Jingxin Na, Yisa Fan, Wei Tan, Shouwu Guo & Wenlong Mu, “Mechanical Behavior of Polyurethane Adhesive Bonded Joints as a Function of Temperature and Humidity.” Journal of Adhesion Science and Technology 32(5): 457–72 (2018).

John L. Gainer, “Concentration and Temperature Dependence of Liquid Diffusion Coefficients.” Ind. Eng. Chem. Fundam. Vol. 9, No. 3, (1970).

Johnson, D, Paradis, M, Tajvidi, M, Walker, C, Bousfield, D ‘‘Surface Application of Cellulose Microfibrils on Paper—Effects of Basis Weight and Surface Coverage Levels.’’ Proc. TAPPI PAPERCON Conference (2019).

Jun Yao, Wenhui Song, Dongying Wang, Hai Sun, Yang Li, “Multi-scale pore network modelling of fluid mass transfer in nano-micro porous media.” International Journal of Heat and Mass Transfer 141, 156–167 (2019).

K. Ramachandra Manohar, Yakkala M K Raghunadh, B. Kiran Kumar, L Ranganath, B.Koteswararao, “Experiment Analysis to Examine the Effects of Adhesive and Adherent Type of Geometrical Configuration on Joint Failure Loads.” The American Physical Society, Materials Today: Proceedings 18 4665–4674 (2019).

Kamke, Frederick A., and Jong N. Lee, “Adhesive Penetration in Wood - A Review.” Wood and Fiber Science 39(2): 205–220 (2007).

Karsten E. Thompson, Gordon A. and Mary Cain, “Pore-Scale Modeling of Fluid Transport in Disordered Fibrous Materials.” AIChE Journal 48(7): 1369–89 (2002).

Kasaeian, A., Daneshazarian, R., Mahian, O., Kolsi, L., Chamkha, A.J., Wongwises, S. and Pop, I., "Nanofluid flow and heat transfer in porous media: a review of the latest developments." International Journal of Heat and Mass Transfer 107, pp. 778-791 (2017).

Kettle, J., Lamminmäki, T. and Gane, P., "A review of modified surfaces for high speed inkjet coating." Surface and coatings Technology 204 (12-13), pp.2103-2109 (2010).

Kewen Li, Danfeng Zhang, Huiyuan Bian, Chao Meng & Yanan Yang, "Criteria for Applying the Lucas-Washburn Law." Scientific Reports 5:14085 (2015).

Khlewee, M., Al-Gharrawi, M. and Bousfield, D., "Modeling the penetration of polymer into paper during extrusion coating." Journal of Coatings Technology and Research 19(1), pp. 25-34 (2021).

Khlewee, M., DeSisto, W. and Bousfield, D., "Comparison of methods to characterize the penetration of hot melt adhesive into paper." Nordic Pulp & Paper Research Journal (2022).

Koppolu, R, Lahti, J, Abitbol, T, Swerin, A, Kuusipalo, J, Toivakka, M, ''Continuous Processing of Nanocellulose and Polylactic Acid into Multilayer Barrier Coatings.'' ACS Applied Materials & Interfaces 11 (12) 11920–11927 (2019).

Kornev, K.G. and Neimark, A.V., "Spontaneous penetration of liquids into capillaries and porous membranes revisited." Journal of colloid and interface science 235(1), pp. 101-113 (2001).

Kúdela, Jozef, "Wetting of wood surface by a liquids of a different polarity1)." Wood Research 59(1): 11–24 (2014).

Kumar, V, Elfving, A, Koivula, H, Bousfield, D, Toivakka, M, ''Roll-to-Roll Processed Cellulose Nanofiber Coatings.'' Industrial & Engineering Chemistry Research 55 (12) 3603–3613 (2016).

Kumar, V, Koppolu, VR, Bousfield, D, Toivakka, M, ''Substrate Role in Coating of Microfibrillated Cellulose Suspensions.'' Cellulose 24 (3) 1247–1260 (2017).

Kuusipalo, J, ''PHB/V in Extrusion Coating of Paper and Paperboard—Study of Functional Properties. Part II.'' Journal of Polymers and the Environment 8 (2) 49–57 (2000).

Kuusipalo, J, ''PHB/V in Extrusion Coating of Paper and Paperboard: Part I: Study of Functional Properties.'' Journal of Polymers and the Environment 8 (1) 39–47 (2000).

Kuusipalo, J, Savolainen, A, ''Adhesion Phenomena in (Co)extrusion Coating of Paper and Paperboard.'' Journal of Adhesion Science and Technology 11 (8) 1119–1135 (1997).

L. Nilsson and S. Stenstrom, "A Study of the Permeability of Pulp and Paper." Int. J. Multiphase Flow Vol. 23, No. 1, pp. 131-153, (1997).

Lavoine, N, Desloges, I, Dufresne, A, Bras, J, ‘‘Microfibrillated Cellulose–Its Barrier Properties and Applications in Cellulosic Materials: A Review.’’ Carbohydrate Polymers 90 (2) 735–764 (2012).

Lee, J.G. and Shaikevitch, A., “Blended EVAs Compared to Reactor Grade EVAs in Hot Melt Adhesives.” In Hot Melt Symposium, pp. 123-146, (2000).

Lepoutre, P., “The Structure of Paper Coatings: An Update.” Progress in Organic Coatings 17(2): 89–106 (1989).

Lokendra Pal, Margaret K. Joyce, and Paul D. Fleming, “A Simple Method for Calculation of the Permeability Coefficient of Porous Media.” TAPPI Journal vol. 5: no. 9, pp. 10-16, (2006).

M. de Meijer, K. Thurich & H. Militz, “Comparative study on penetration characteristics of modern wood coatings.” Wood Science and Technology volume 32, pages 347–365 (1998).

M. Rasi, A. Koponen, U. Aaltosalmi, J. Timonen, M. Kataja, and K. J. Niskanen, “Permeability of paper: experiments and numerical simulations.” TAPPI International Paper Physics Conference 297-306, (1999).

M.A. Rodrı ´guez-Valverde, M.A. Cabrerizo-Vı ´lchez, P. Rosales-Lo´pez, A. Pa´ez-Duen˜as, R. Hidalgo-A´ lvarez, “Contact Angle Measurements on Two (Wood and Stone) Non-Ideal Surfaces.” Colloids and Surfaces. A: Physicochemical and Engineering Aspects 206: 485–495 (2002).

Mahesh Tirumkudulu, William B. Russel and T. J. Huang, “Measuring the “tack” of waterborne adhesives.” Journal of Rheology Vol. 47, No. 1399, (2003).

Mahesh Tirumkudulu, William B. Russel and T. J. Huang, “On the measurement of ‘‘tack’’ for adhesives.” Phys. Fluids Vol. 15, No. 6, (2003).

Mario Zauer, Simone Hempel, Alexander Pfriem, Viktor Mechtcherine, Andre´ Wagenfu¨hr, “Investigations of the Pore-Size Distribution of Wood in the Dry and Wet State by Means of Mercury Intrusion Porosimetry.” Wood Sci Technol 48: 1229–40 (2014).

Mariola M. Błaszczyk, Jerzy P. Sęk, Łukasz Przybysz, “Modeling and experimental data of the flow of highly concentrated emulsions in porous media.” Engineering Science and Technology, an International Journal. Volume 23, Issue 6, Pages 1444-1454 (2020).

McBride, E., “Consistent Viscosity in EVA Based Hot Melt Adhesives.” TAPPI Journal 23–27 (1994).

Meijer, Mari De, “A Review of Interfacial Aspects in Wood Coatings : Wetting , Surface Energy , Substrate Penetration and Adhesion.” Conference: COST E18 Final Seminar (2005).

Meijer, Mari De, Sander Haemers, Wiro Cobben, and Holger Militz, “Surface Energy Determinations of Wood : Comparison of Methods and Wood Species.” Langmuir 16(44): 9352–59 (2000).

Mika Vähä-Nissi, KCL, “Influence of Paperboard on Bond Formation and Strength of Adhesive Joint.” 12th TAPPI European PLACE Conference (2009).

Miller Mendoza, Philipp Hass, Falk K. Witte, Peter Niemz, Hans J. Herrmann, “Adhesive Penetration of Hardwood: A Generic Penetration Model.” Wood Science and Technology 46(1–3): 529–49 (2012).

Milojka Gindl, Gerhard Sinn, Wolfgang Gindl, Alexander Reiterer, and Stefanie Tschegg “A Comparison of Different Methods to Calculate the Surface Free Energy of Wood Using Contact Angle Measurements.” Colloids and Surfaces. A: Physicochemical and Engineering Aspects 181: 279–287 (2001).

Moura, M J, P J Ferreira, and M M Figueiredo, “Mercury Intrusion Porosimetry in Pulp and Paper Technology.” Powder Technology 160: 61–66 (2005).

Mousavi, SMM, Afra, E, Tajvidi, M, Bousfield, DW, Dehghani-Firouzabadi, M, ‘‘Application of Cellulose Nanofibril (CNF) as Coating on Paperboard at Moderate Solids Content and High Coating Speed Using Blade Coater.’’ Progress in Organic Coatings 122 207–218 (2018).

Myo T. Tyn and Waclaw F. Calus, “Temperature and Concentration Dependence of Mutual Diffusion Coefficients of Some Binary Liquid Systems.” Journal of Chemical and Engineering Data Vol. 20, No. 3, (1975).

Nasir, Muhammad, Sufian Munawar, Ahmer Mehmood, and Asif Ali, “Unsteady Flow and Heat Transfer in a Composite Porous Annulus with Time-Dependent Injection.” Zeitschrift für Naturforschung A 67a: 657–64 (2012).

Ninness, Brian, Greg Welsch, Don Ventresca, and Dave Williams, “Aqueous Glue Setting in Double-Coated Paperboard Systems: The Impact of Application System and Individual Coating Layer Thickness on Glue Bond Formation.” PaperCon 1751-1769 (2011).

P. Shallhorn and N. Gurnagul, “A simple model of the air permeability of paper.” In Advances in Pulp and Paper Research, Oxford 2009, Trans. of the XIVth Fund. Res. Symp. Oxford, 2009, (S.J. I’Anson, ed.), pp 475–490, FRC, Manchester, 2018.

Paris, Jesse L., and Frederick A. Kamke, “Quantitative Wood-Adhesive Penetration with X-Ray Computed Tomography.” International Journal of Adhesion and Adhesives 61: 71–80 (2015).

Philipp Hass, Falk K. Wittel, Miller Mendoza, Hans J. Herrmann, Peter Niemz, “Adhesive Penetration in Beech Wood: Experiments.” Wood Science and Technology 46(1–3): 243–56 (2012).

Piao, Cheng, Jerrold E Winandy, and Todd F Shupe, “From Hydrophilicity to Hydrophobicity: A Critical Review: Part I. Wettability and Surface Behavior.” Wood and Fiber Science 42(4): 490–510 (2010).

Putkisto, K, Maijala, J, Gron, J, Rigdahl, M, ‘‘Polymer Coating of Paper Using Dry Surface Treatment: Coating Structure and Performance.’’ TAPPI Journal 3 16–23 (2004).

Quintin Parker, BASF Corp, “Aqueous Gluing of Coated Paperboard Packaging Products in North America.” Solutions!, Online Exclusives (2004).

Raghunath, K, M Obulesu, and R Sivaprasad, “Heat and Mass Transfer on an Unsteady MHD Flow through Porous Medium between Two Porous Vertical Plates.” AIP Conference Proceedings 2220, 130003 (2020).

Rhim, JW, Lee, JH, Hong, SI, ‘‘Increase in Water Resistance of Paperboard by Coating with Poly(lactide).’’ Packaging Technology and Science: An International Journal 20 (6) 393–402 (2007).

Ribeiro, Helena Aguilar, and Carlos A.V. Costa, “Modeling and Simulation of the Hot-Pressing Process in Paper Production: A Heat- and Mass-Transfer Analysis.” Industrial and Engineering Chemistry Research 46(24): 8205–19 (2007).

S. Budhe, M.D. Banea, S. de Barros, L.F.M. da Silva, “An updated review of adhesively bonded joints in composite materials.” International Journal of Adhesion & Adhesives 72 30–42 (2017).

Sernek, Milan, Joze Resnik, and Frederick A. Kamke, “Penetration of Liquid Urea-Formaldehyde Adhesive into Beech Wood.” Wood and Fiber Science 31(1): 41–48 (1999).

Sheridan, J., Williams, A. and Close, D.J., “An experimental study of natural convection with coupled heat and mass transfer in porous media.” International journal of heat and mass transfer 35(9), pp. 2131-2143 (1992).

Shi, Y., Tang, G.H., Lin, H.F., Zhao, P.X. and Cheng, L.H., “Dynamics of droplet and liquid layer penetration in three-dimensional porous media: A lattice Boltzmann study.” Physics of Fluids 31(4), p. 042106 (2019).

Simons, John, “A New Method For The Characterization and Selection of Resins in EVA, EBA, and APAO Based Hot Melt Adhesives.” TAPPI Journal 205–18 (1996).

Sina Ebnesajjad, “Adhesives Technology Handbook.” 2nd Edition, ISBN: 978-0-8155-1533-3 (2008).

Songok, Joel, Douglas W. Bousfield, Patrick A.C. Gane, and Martti Toivakka, “Heat and Mass Transfer Models to Understand the Drying Mechanisms of a Porous Substrate.” The European Physical Journal E 39: 25: 1–8 (2016).

Spence, KL, Venditti, RA, Rojas, OJ, Pawlak, JJ, Hubbe, MA, ‘‘Water Vapor Barrier Properties of Coated and Filled Microfibrillated Cellulose Composite Films.’’ BioResources 6 (4) 4370–4388 (2011).

Tannert, Thomas, Till Vallée, and Simon Hehl, “Experimental and Numerical Investigations on Adhesively Bonded Timber Joints.” Wood Science and Technology 46(1–3): 579–90 (2012).

Tayeb, AH, Tajvidi, M, Bousfield, D, ‘‘Based Oil Barrier Packaging Using Lignin-Containing Cellulose Nanofibrils.’’ Molecules 25 (6) 1344 (2020).

Tayeb, AH, Tajvidi, M, Bousfield, D, ‘‘Enhancing the Oxygen Barrier Properties of Nanocellulose at High Humidity: Numerical and Experimental Assessment.’’ Sustainable Chemistry 1 (3) 198–208 (2020).

U Aaltosalmi, Markku Kataja, Antti Ilmari Koponen, J. Timonen, A Goel, and G Lee, Shri Ramaswamy, “Numerical analysis of fluid flow through fibrous porous materials.” Journal of Pulp and Paper Science (2004).

V. Muralidharan, Anil Tihminlioglu, Olivia Antelmann, J. Larry Duda, Ronald P. Danner, Andre De Haan, “Temperature and Concentration Dependence of Diffusion Coefficients in Ethylene–Propylene-Diene Copolymers.” Journal of Polymer Science: Part B: Polymer Physics Vol. 36, 1713–1719 (1998).

Ventresca, D, Welch, G, ‘‘Comparison of Coating Strength of Four Binder Chemistries Used in Paperboard coatings.’’ Proc. 2019 PAPERCON Conference, TAPPI Journal, Atlanta, GA.

Wang, J, Gardner, DJ, Stark, NM, Bousfield, DW, Tajvidi, M, Cai, Z, ‘‘Moisture and Oxygen Barrier Properties of Cellulose Nanomaterial-Based Films.’’ ACS Sustainable Chemistry & Engineering 6 (1) 49–70 (2018).

Wolfgang Gindl, Eugenia Dessipri, Rupert Wimmer, “Using UV-Microscopy to Study Diffusion of Melamine-Urea Formaldehyde Resin in Cell Walls of Spruce Wood.” Holzforschung 56 103–107 (2002).

Xiang, Y., Bousfield, D.W., Hayes, P.C. and Kettle, J., “A model to predict ink-setting rates based on pore-size distributions.” Journal of pulp and paper science 30(5), pp. 117-120 (2004).

Xiang, Yang, and Doug W Bousfield, “Influence of Coating Ink Setting Rate on Ink Transfer.” In Proceedings of the Technical Association of the Graphic Arts, TAGA, 66–68 (2003).

Yanhua Zhang, Longlong Ding, Jiyou Gu, Haiyan Tan, Libin Zhu, “Preparation and Properties of a Starch-Based Wood Adhesive with High Bonding Strength and Water Resistance.” Carbohydrate Polymers 115: 32–37 (2015).

Younes, A., “On modelling the multidimensional coupled fluid flow and heat or mass transport in porous media.” International Journal of Heat and Mass Transfer 46(2), pp. 367-379 (2003).

Zatloukal, M, ‘‘Measurements and Modeling of Temperature-Strain Rate Dependent Uniaxial and Planar Extensional Viscosities for Branched LDPE Polymer Melt.’’ Polymer 104 258–267 (2016).

Zhang, G., Quetzeri-Santiago, M.A., Stone, C.A., Botto, L. and Castrejón-Pita, J.R., “Droplet impact dynamics on textiles.” Soft matter 14(40), pp. 8182-8190 (2018).

Zhenjiong Wang, Zhengbiao Gu, Yan Hong, Li Cheng, Zhaofeng Li, “Bonding Strength and Water Resistance of Starch-Based Wood Adhesive Improved by Silica Nanoparticles.” Carbohydrate Polymers 86(1): 72–76 (2011).

APPENDIX A: UNCERTANITY ANAYLSIS FOR DEPTH TECHNIQUES

The uncertainty analysis was performed using MATHCAD Prime 8.0.0.0. The results showed that the uncertainty is less than 1% for all of the methods used for penetration depth determination as shown below.

$$eRel_{PenetrationDepth1} := \frac{e_{PenetrationDepth1}}{PenetrationDepth_1} = 0.084$$ Less than 1% for this method

Contribution of variables

$$frac_a := \frac{de2_a}{de2_{PenetrationDepth1}} = 0.138$$ 13.8%

$$frac_{\delta p} := \frac{de2_{\delta p}}{de2_{PenetrationDepth1}} = 0.021$$ 2.1%

$$frac_{W1} := \frac{de2_{W1}}{de2_{PenetrationDepth1}} = 0.022$$ 2.2%

$$frac_{W2} := \frac{de2_{W2}}{de2_{PenetrationDepth1}} = 0.022$$ 2.2%

$$frac_{\rho so} := \frac{de2_{\rho so}}{de2_{PenetrationDepth1}} = 0.003$$ 0.3%

$$frac_{\varepsilon p} := \frac{de2_{\varepsilon p}}{de2_{PenetrationDepth1}} = 0.794$$ 97.4% Largest contribution of input variable

$$frac_a + frac_{\delta p} + frac_{W1} + frac_{W2} + frac_{\rho so} + frac_{\varepsilon p} = 1$$

Figure A. 1. Uncertainty analysis and contribution of input variables for the silicone oil method.

$$eRel_{PenetrationDepth1} := \frac{e_{PenetrationDepth1}}{PenetrationDepth_1} = 0.104$$ Less than 1% for this method

Contribution of variables

$$frac_{Vp} := \frac{de2_{Vp}}{de2_{PenetrationDepth1}} = 0.497$$ 49.7%, Largest Contribution of Input Variable

$$frac_{Vs} := \frac{de2_{Vs}}{de2_{PenetrationDepth1}} = 0.497$$ 49.7%, Largest Contribution of Input Variable

$$frac_{WB} := \frac{de2_{WB}}{de2_{PenetrationDepth1}} = 0.005$$ 0.5%

$$frac_{Vp} + frac_{Vs} + frac_{WB} = 1$$

Figure A. 2. Uncertainty analysis and contribution of input variables for the mercury porosimetry method.

$$eRel_{PenetrationDepth1} := \frac{e_{PenetrationDepth1}}{PenetrationDepth_1} = 0.018$$ Less than 1% for this method

Contribution of variables

$$frac_{\delta rl} := \frac{de2_{\delta rl}}{de2_{PenetrationDepth1}} = 0.56$$ 56.0%, Largest Contribution of Input Variable

$$frac_{Wa} := \frac{de2_{Wa}}{de2_{PenetrationDepth1}} = 0.14$$ 14.0%

$$frac_{\rho} := \frac{de2_{\rho}}{de2_{PenetrationDepth1}} = 0.007$$ 0.7%

$$frac_{a} := \frac{de2_{a}}{de2_{PenetrationDepth1}} = 0.294$$ 29.4%

$$frac_{\delta rl} + frac_{Wa} + frac_{\rho} + frac_{a} = 1$$

Figure A. 3. Uncertainty analysis and contribution of input variables for the thickness method.

$$eRel_{PenetrationDepth1} := \frac{e_{PenetrationDepth1}}{PenetrationDepth_1} = 0.132$$ Less than 1% for this method

Contribution of variables

$$frac_{Wrl} := \frac{de2_{Wrl}}{de2_{PenetrationDepth1}} = 0.009$$ 0.9%

$$frac_{Ws} := \frac{de2_{Ws}}{de2_{PenetrationDepth1}} = 0.009$$ 0.9%

$$frac_{WB} := \frac{de2_{WB}}{de2_{PenetrationDepth1}} = 0.81$$ 81.0%, Largest Contribution of Input Variable

$$frac_{Wh} := \frac{de2_{Wh}}{de2_{PenetrationDepth1}} = 0.009$$ 0.9%

$$frac_{a} := \frac{de2_{a}}{de2_{PenetrationDepth1}} = 0.163$$ 16.3%

$$frac_{\delta p} := \frac{de2_{\delta p}}{de2_{PenetrationDepth1}} = 7.733 \cdot 10^{-5}$$ 0.0%

$$frac_{Wrl} + frac_{Ws} + frac_{WB} + frac_{Wh} + frac_{a} + frac_{\delta p} = 1$$

Figure A. 4. Uncertainty analysis and contribution of input variables for the weight method.

APPENDIX B: EFFECT OF SLIP LENGTHS AND MESH SIZES ON THE PENETRATION DEPTH DURING ISOTHERMAL FLOW

The slip length parameter (β) of the wetted walls has a large impact on the penetration depth, but a middle range of values all match the modified Lucas-Washburn equation in an excellent agreement. Figure B.1 shows that high and low values of this parameter can give results quite different than theory, but values in the range of 3×10^{-3} to 2×10^{-3} for $\Delta P^*=0$ and 2.5×10^{-4} to 2.5×10^{-7} for $\Delta P^*=50$ give excellent results.

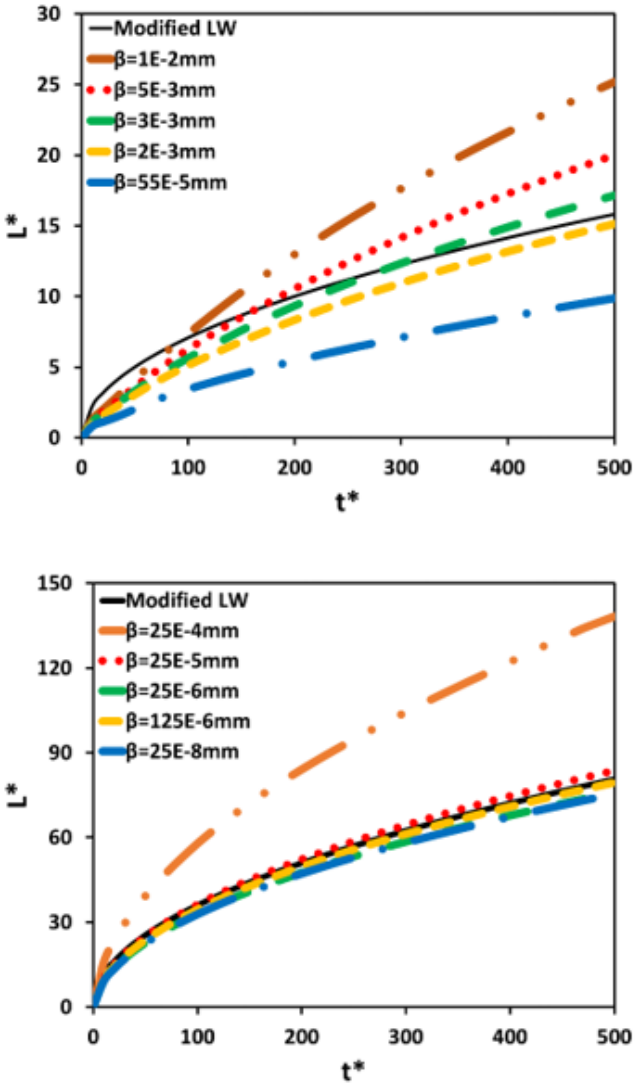

Figure B. 1. Effect of various slip lengths on the penetration depth for a viscosity of 0.01 Pa s and $\Delta P^*=0$ (Top) and $\Delta P^*=50$ (Bottom).

Using the normal mesh, the predictions of the model can approach the theory by adjusting the slip length (β). Figure B.2 shows, for various dimensionless pressures, a close comparison can be obtained by using different values of the slip length. Therefore, depending on the pressure difference, a slip length can be selected to obtain good comparison to the theory. As a summary, the modified Lucas-Washburn equation is recovered for the isothermal flow using a normal mesh and a slip length of 1.25×10^{-4} mm for ΔP*=50 and 2×10^{-3} mm for ΔP*=0.

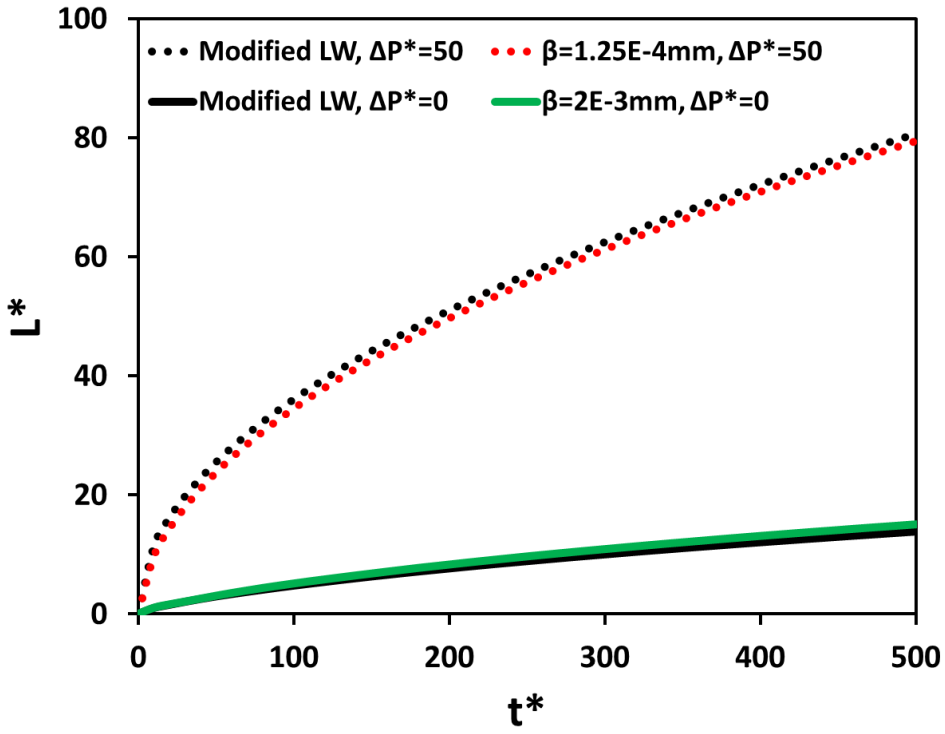

Figure B. 2. Comparison of model predictions to the modified Lucas-Washburn equation using best matched slip lengths for a liquid viscosity of 0.01 Pa s.

APPENDIX C: EFFECT OF SURFACE TENSION AND CONTACT ANGLE ON THE PENETRATION DEPTH DURING ISOTHERMAL AND NON-ISOTHERMAL FLOW

The setting of adhesives between two porous substrates involves chemical, mechanical, and physical changes that strongly affect green and final bond strengths. These changes can be controlled to achieve better adhesion if a proper selection is made regards substrate and adhesive properties, pretreatment process, press time, press pressure, process temperature, etc. Proper selection of these parameters will result in better wettability, better penetration, and finally strong bond strength. The wettability is influenced also by surface hydrophilicity ($\theta<90^o$) or hydrophobicity ($\theta>90^o$) which is related to the chemical composition of the surface as well as by surface free energy components. The surface free energy and its components can be determined from contact angle measurements in which different approaches are used such as Zisman's critical surface tension, geometric-mean, harmonic-mean, and acid-base. These approaches are compared using different test liquids. The lower the contact angle, the greater the wettability. It is believed that the degree of penetration of adhesive into a porous substrate will determine the green and final bond strengths. So, as the adhesive penetrates deeper into the pores, then a high improvement will be seen in the bond strength. A pore level model was developed to describe penetration during isothermal and non-isothermal situations that take into account the change of viscosity of the fluid as it enters a pore. The model indicates that the surface tension and/or contact angle are critical parameters in the penetration of adhesive if there is no pressure. The model results confirm the previously published outcomes in which low surface tension and/or high contact angle values will result in no penetration where a 90^o and 0.0001 N/m resulted in no penetration. However, a 0^o and 1 N/m gave the largest penetration depth. All modeling predictions shown below were based on neglecting gravity and inertial terms.

Unsteady Isothermal Flow into a Capillary

To validate the finite element model, the isothermal flow into a capillary was described. Both inertia and gravity terms were neglected. For cases that do not depend on temperature, where the viscosity is fixed, the model can give a good comparison to the Lucas-Washburn equation (Equation 2.1).

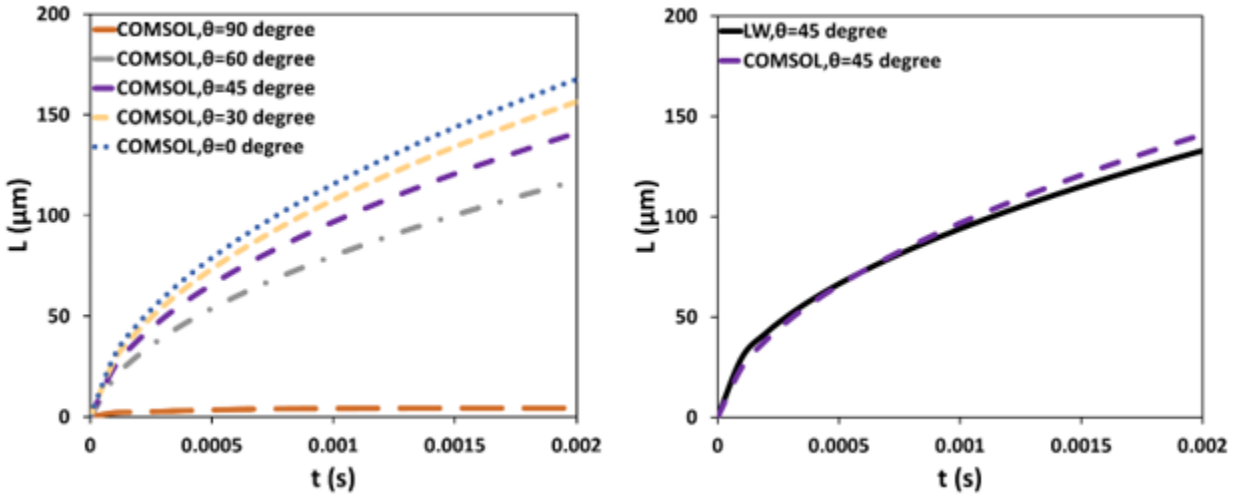

Figure C. 1. Influence of various contact angles on the penetration depth (left) and compare with the Lucas-Washburn equation (right) for adhesive viscosity of 0.01 Pa s, ΔP=0.

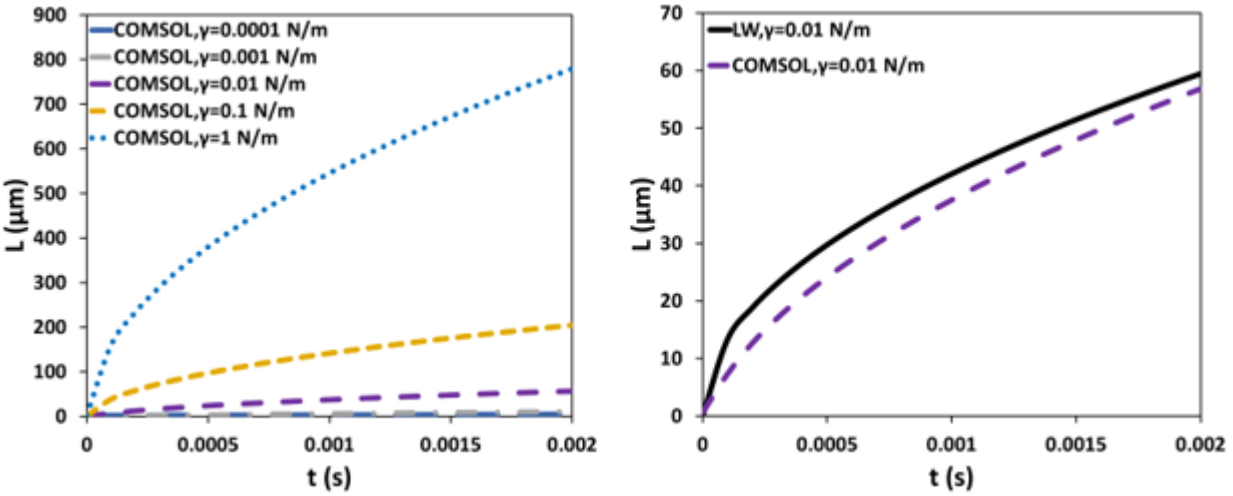

Figure C. 2. Influence of various surface tensions on the penetration depth (left) and compare with the Lucas-Washburn equation (right) for adhesive viscosity of 0.01 Pa s, ΔP=0.

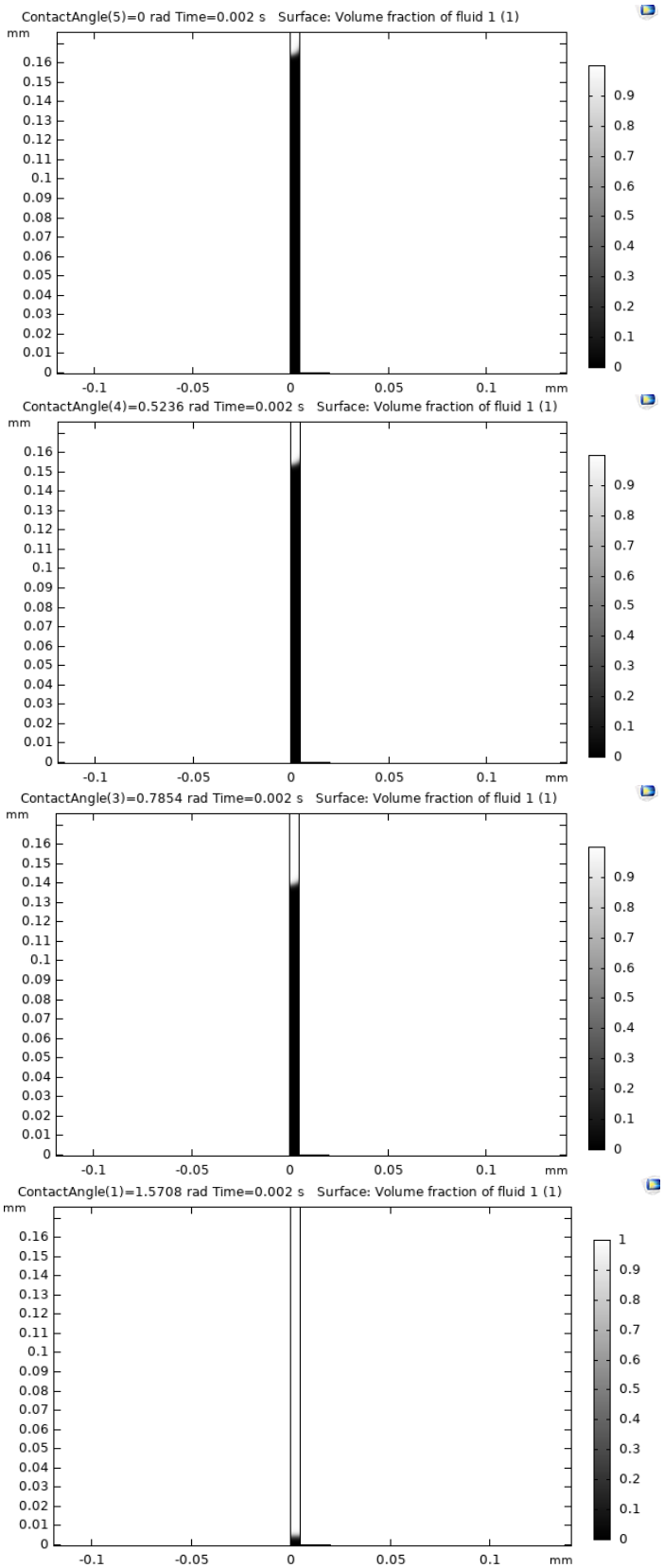

Figure C. 3. Penetration depth distribution in the pore region for adhesive viscosity of 0.01 Pa s and values of θ of 0, 30, 45 and 90^{o} from top to bottom respectively, ΔP=0.

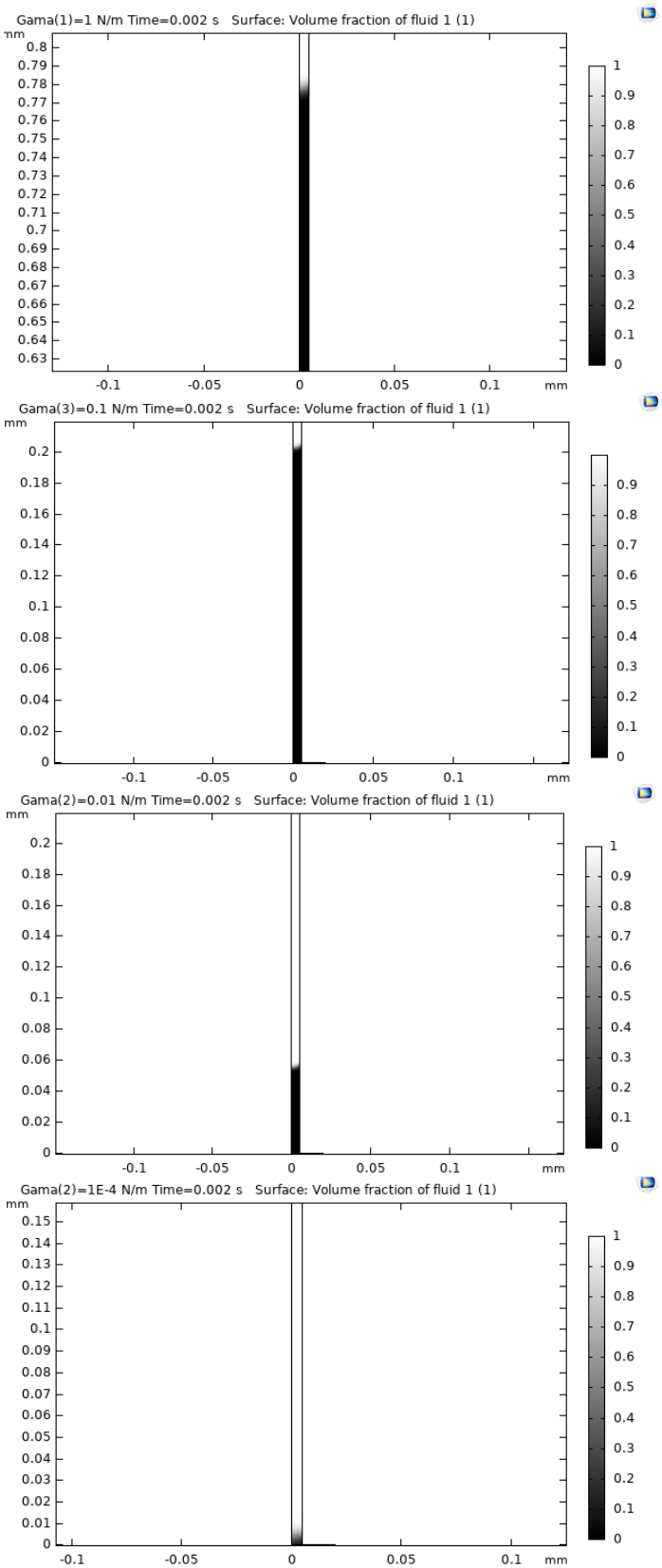

Figure C. 4. Penetration depth distribution in the pore region for adhesive viscosity of 0.01 Pa s and values of γ of 1, 0.1, 0.01 and 0.0001 N/m from top to bottom respectively, ΔP=0.

Unsteady Non-isothermal Flow into a Capillary

To account for the influence of temperature, the unsteady-state heat transfer problem must be solved. For cases that depend on temperature, where the viscosity is a function of temperature, the model underpredicted the Lucas-Washburn equation (Equation 2.1).

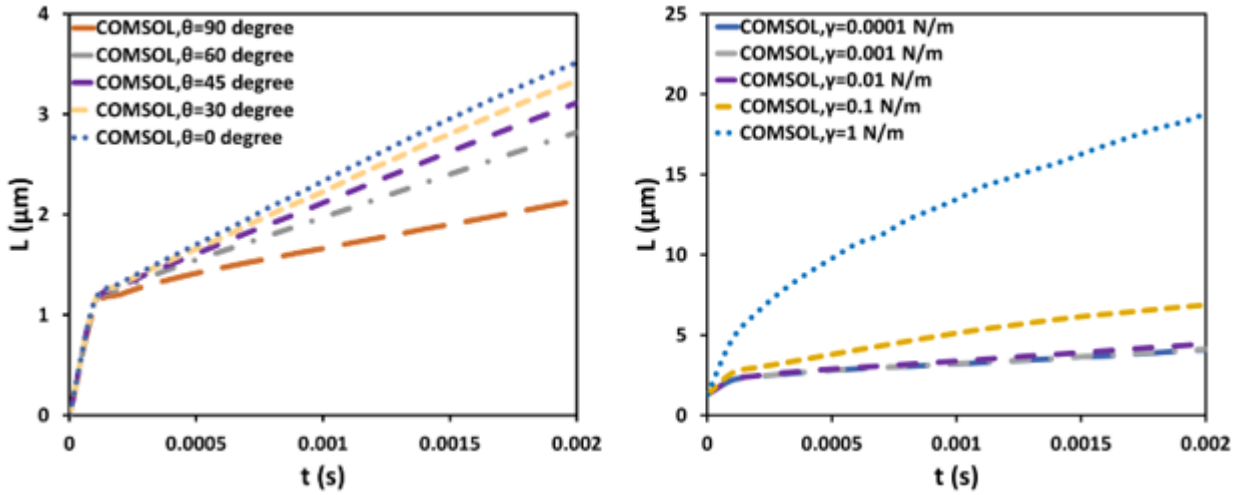

Figure C. 5. Influence of various contact angles (left) and various surface tensions (right) on the penetration depth, $\Delta P=0$.

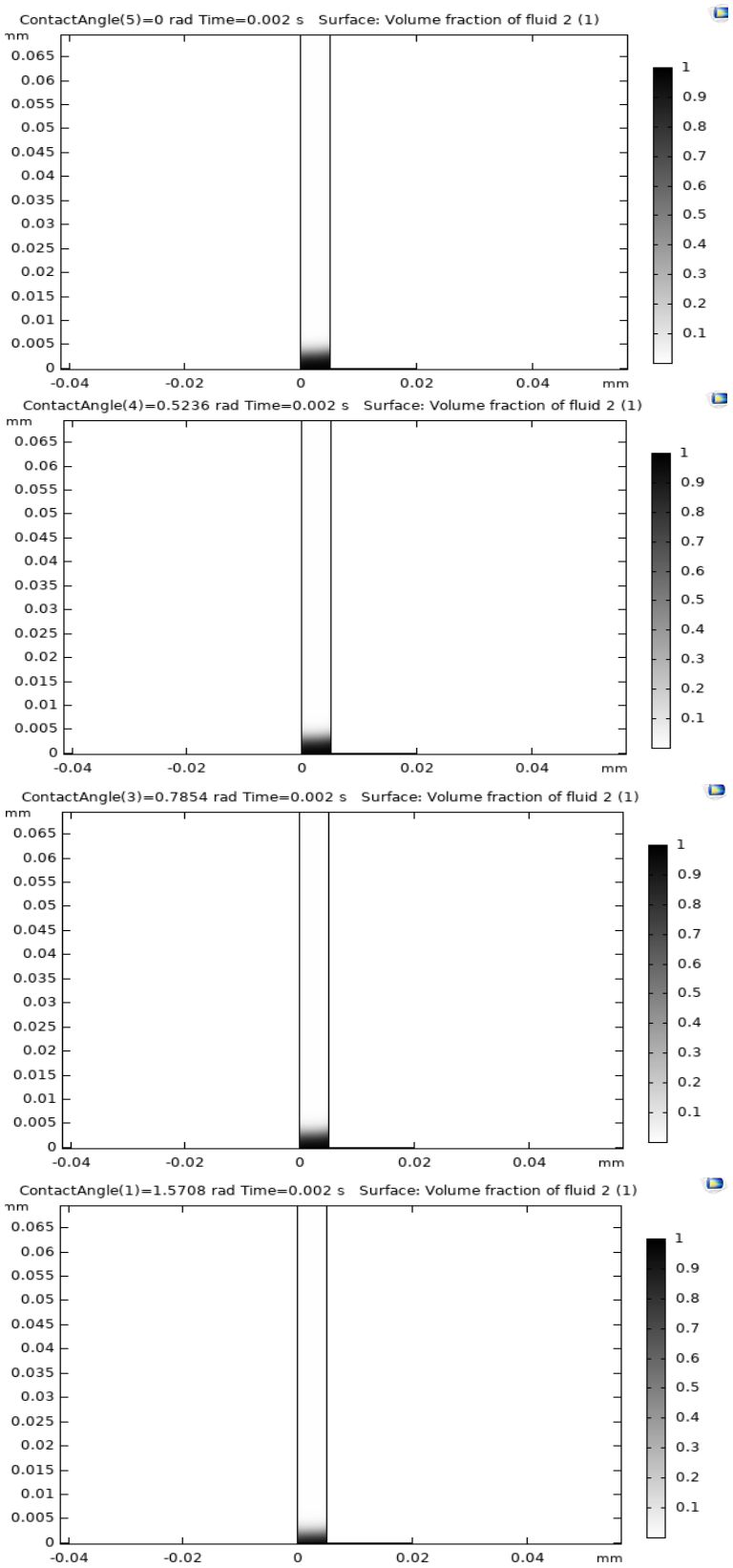

Figure C. 6. Penetration depth distribution in the pore region for values of θ of 0, 30, 45 and 90º from top to bottom respectively, ΔP=0.

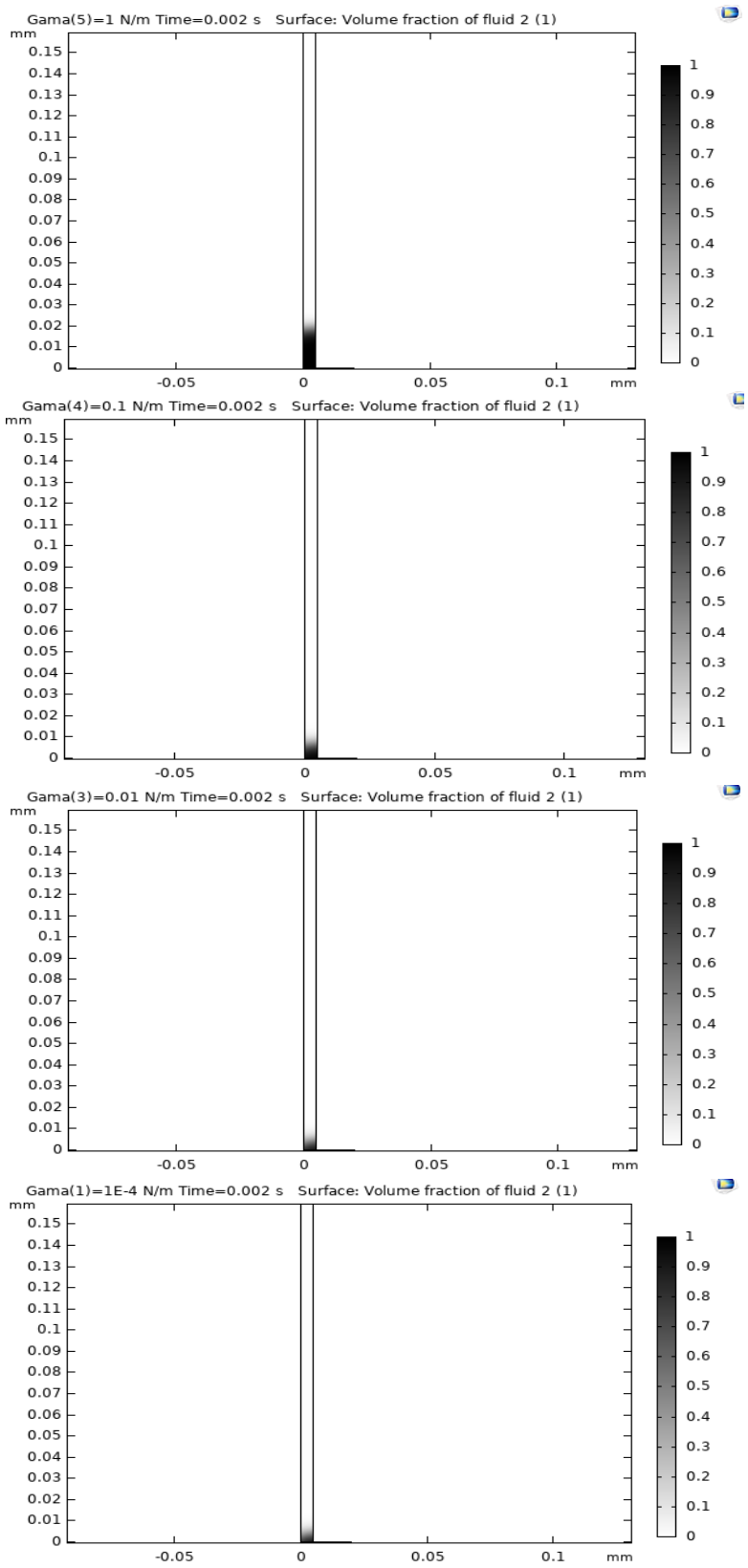

Figure C. 7. Penetration depth distribution in the pore region for values of γ of 1, 0.1, 0.01 and 0.0001 N/m from top to bottom respectively, ΔP=0.

Adhesive penetration into a porous media with surface tension and contact angle changes are measured as time progresses. Firstly, for the isothermal flow, a contact angle of 90^{o}, a surface tension of 0.0001 N/m, and a viscosity of 10 Pa s gave the lowest penetration depth. On the other hand, a contact angle of 0^{o}, a surface tension of 1 N/m, and a viscosity of 0.01 Pa s gave the highest penetration depth. Secondly, for the non-isothermal flow, a contact angle ranges from 0^{o} to 60^{o}, and a surface tension ranges from 0.1 to 0.0001 N/m gave almost similar results. Similar to the isothermal case, a contact angle of 0^{o} and a surface tension of 1 N/m resulted in the highest penetration depth among other modeled values.

The Lucas-Washburn equation was well predicted during the isothermal flow where values of 45^{o} of contact angle, 0.01 N/m of surface tension, and 0.01 Pa s of adhesive viscosity gave an excellent match between modeling results and the theory. However, for the non-isothermal flow, the model underpredicted the Lucas-Washburn equation. As adhesive penetrates deeper into the pores, the bond strength increases as a result of that. Therefore, it is important to improve adhesive penetration into the pores by increasing surface tension and/or decreasing contact angle.

APPENDIX D: PROCEDURES TO RUN BROOKFIELD, WATER RETENTION VALUE, CONTACT ANGLE AND SURFACE ENERGY, AND SEM

Brookfield:

1. Put your 400 ml solution in a 600 ml glass beaker.
2. Write down:
    a. Solution Temperature
    b. Solution Concentration
    c. Solution Solid Content
    d. Speed (rpm)
        i. For a high viscous solution choose a higher rpm (100)
        ii. For low viscous solution choose a lower rpm (0.5)
    e. Spindle number
        i. For a high viscous solution choose a higher number (7)
        ii. For low viscous solution choose a lower number (1)
3. Turn the equipment on from the button at the back side of the equipment.
4. Do not install the spindle on the equipment at this point.
5. Press any key on the screen.
6. Install the spindle to the equipment.
7. Press any key on the screen.
8. Press on a select spindle and put the spindle number by pressing the arrow buttons.
9. When done press select spindle.
10. Press the select speed and put the speed number (rpm 0.5 - 100) by pressing the arrow buttons.
11. When done press select speed.
12. Make sure that the rpm and spindle on the screen are right.
13. Press the motor on/off. At the same time have a timer of up to 30 seconds.
14. Record the cp and % values. Cp is the centipoise unit.
15. Repeat that five times and take the average.
16. If % is less than 10 then:

a. Choose a lower spindle number (1)
b. Choose a lower rpm (0.5)

17. If cp and % = EEEE (error), then:
    a. Choose a higher spindle number (7)
    b. Choose a higher rpm (100)
18. Spindle and rpm should give:
    a. Cp is not too high and not too low.
    b. % between 10-30.
19. Wash spindles in the water very well.
20. Restore the beaker to its place.
21. Close the spindles box.
22. Turn the equipment off.

Water Retention Value:

1. Soak 30 g of paper pieces that should be torn by hand and not by using a scissor in 2 liter water overnight or until paper pieces dissolve in water. For the soaking use a 2000 ml beaker.
2. Put the total suspension after soaking in the disintegrator for mixing for 3 minutes and 6 seconds at 10,000 rpm for one time only.
3. Take a crucible and record its number.
    a. In TAPPI standard, we have to put an empty and clean crucible in the oven for 1 hr and then put it in the desiccator for another hour. After that start your procedure.
4. Weigh the empty and clean crucible.
5. The crucible has two mesh sizes inside that are fine and coarse. The fine mesh is going to be on top of the coarse mesh.
6. The solution consistency should be (1.2% to 1.5%). So, (30 g fiber/2000 ml water) = 1.5%. This 1.5% is the range we need.
7. We need 1.8 g dry fiber from the solution, so 1.8±0.2 g fiber/X ml water =1.5% >>>> X=120 g meaning that in this 120 g, we have 1.8 g dry fiber and 118.2 g water.
8. Fix the crucible to the water aspirator.

9. You need to start at a low vacuum rate (low water flow in the tap) to suck little water into the aspirator, then when there is almost no water in the fibers, you can increase the vacuum rate (high water flow in the tap) to suck the remaining water from the fibers.
10. Pour the 120±0.2 g solution into the crucible. You have to use the spatula to press fiber down nicely to arrange its shape at its surface. You can also add more water if you want to arrange the fiber shape inside the crucible. The excess water is not affecting the weight because it will be lost in the water aspirator.
11. Close the crucible immediately using a metal lid after finishing preparing it.
12. Weigh a centrifugal cup first. If you are using two cups for two samples, then their weights should be the same.
13. Weigh the crucible with the fiber inside it. If you are using two crucibles for two samples, then their weights should be the same. If their weights are not the same, then either decrease the weight of one crucible by using the water aspirator or add water into the crucible that has a low weight to bring its weight close to the other crucible but you have to add some cotton underneath the crucible.
14. Close the crucible using a metal lid.
15. Arrange the crucibles to be fitted inside the centrifugal cups.
16. Put the crucible and the cotton underneath it together inside the centrifugal cup.
17. Open the centrifugal lid.
18. Put the cups inside the centrifugal.
19. There should be at least two cups inside the centrifugal to make a balance. We have to put cups of equal weight in front of each other.
20. Close the centrifugal lid.
21. Adjust the rpm to 2 which is equal to 2000 rpm.
22. Adjust time to 30 minutes.
23. Take the sample out of the centrifugal when done and put it in the oven for at least 12 hr at 105 ^{o}C.
24. The next day, cool the sample in the desiccator that is under vacuum for at least 1 hr.
25. Record the weight of the sample after it cools down.
26. Clean the crucible, and all other tools used.

Contact Angle and Surface Energy:

1. Young's Equation:
    a. $\gamma_{sg} = \gamma_{sL} + \gamma_{Lg} \cos(\theta)$
    b. γ_{sg}= Surface tension at the solid and gas interface (N/m).
    c. γ_{sL}= Surface tension at the solid and liquid interface (N/m).
    d. γ_{Lg}= Surface tension at the liquid and gas interface (N/m).
    e. θ_{young}=contact angle at which the liquid-gas interface meets the solid-liquid interface.
    f. $\theta > 90$=hydrophobic.
    g. $\theta < 90$=hydrophilic.
2. Water is polar.
3. Diiodomethane MD is non polar (disperse).
4. Remove the pump and the black cover.
5. Check water and DM nozzles.
6. Put water and DM tubes in the KRUSS upside down.
7. Reinstall the pump and the black cover.
8. Run software
    a. When connected the KRUSS into the laptop, there will be a clicking sound in the KRUSS that needs to go away before starting the test.
    b. Click on advance software.
    c. Choose double sessile drop.
    d. Clean the paper surface using KimTech before starting testing.
    e. Adjust the resolution from the setting option to see the sample.
    f. Press the run button on the KRUSS for one second then release when you see the droplet shape appears on the laptop screen. Then clean the paper using KimTech tissue and press again on another spot in the paper.
    g. If you still do not see data on the laptop then adjust the resolution in the software and repeat.
    h. Click on the peak that is an error or out of the range then uncheck its box.
    i. Scroll down to see the results and droplet shapes.
    j. Print the results in a pdf form.

9. When done:
    a. Release water and DM tubes using a special tool.
    b. Remove water and DM tubes upside down.
    c. Turn off the KRUSS and put it with the tubes in its specific storage box.
    d. Shut down the laptop.

Scanning Electron Microscopy:

Sample Preparation and Holder

1. Bring your sample a day before the analysis.
2. Take one empty box located on the shelf just before you enter the SEM room.
3. Take some sample holders located on the shelf just above the desktop in the hallway.
4. Take double carbon adhesive tapes (small carbon adhesive tape circles to hold your sample on the holder) located on the shelf just above the desktop in the hallway.
5. Take one of the paper notes (has number, date, etc.) located on the shelf that is in the opposite direction of the shelf above the desktop in the hallway.
6. Put the paper note underneath the sample holder after writing sample info in it.
7. Stick your sample into the double carbon adhesive tape that is stuck into the holder from the other side.
8. Put your sample in the desiccator overnight.

Log Sheet:

1. Write everything in the lab book next to the machine like the date, your name, start and end reading of the filament. The reading of the filament is close to the SEM column.

Vent Stage:

1. Press vent.
2. Turn the N_2 gas on (the valve that closes to the SEM Machine).
3. Turn the N_2 gas off (the valve that closes to the SEM Machine) when you hear hissing.

Load Sample:

1. Slide the chamber door out to reveal the stage.
2. Hold the stub inside the hole of the stage using the forceps where the stub stem should hit the forceps pin, then use the Allen key to tight smoothly.
3. Use the Z-axis button to let the stub (sample) is below the top of the box (the small sliver box located after the sample immediately).
4. Slide the chamber door closed, hold it in place and press evacuate, then release once the pump starts.

Wait for Evacuation:

1. Wait till have a reading of 6 to 8 on the top gauge or 19 on the bottom.
2. Check if all sensors are working properly using the meter select button.

Run Software:

1. Turn Pc on.
2. Login using a username and password.
3. Open Iridium Ultra Software.
4. Pull open the column chamber valve. You need to pull it with some force. And when you are done you need to push it back with some force so you hear a clicking sound.

Adjust things before image optimization starts:

1. Turn the console on.
2. Acceleration potential to be 10 Kv.
3. Emission to be 90. Do not turn this on until the evacuation of 6 to 8 on the top gauge or 19 on the bottom has been reached.

Image Optimization:

1. Select the sample position of interest to be in the middle by using the X and Y buttons located on the front of the stage. Make sure that the T button has zero on its top reading.
2. Adjust magnification to 100x.
3. Focus to get a clear image.

4. Adjust the working distance to 6 mm by (adjusting the Z axis located on the stage and then adjusting the focus switch located on the console, both Z and focus should move in the same direction, at each Z turn you need to focus to get a better and clear image).
5. Flip the switch back from working distance reading to magnification reading.
6. Adjust magnification to 500x.
7. Focus to get a clear image.
8. Use the partial field button with higher magnification values.
9. Adjust magnification to 1000x.
10. Focus to get a clear image.
11. Adjust magnification to 5000x.
12. Focus to get a clear image.
13. Adjust magnification to 10,000x.
14. Focus to get a clear image.
15. Adjust magnification to 20,000x.
16. Focus to get a clear image.
17. When we have unstable images as we use the focus button (even with the partial field button on) and then adjust stigmation knobs (one at a time, X then Y, located on the console).
18. If still have unstable images as you use the focus button and adjusting stigmation knobs does not help (even with the partial field button on), then turn the wobber button on and adjust aperture knobs (one at a time, X then Y, located on SEM machine right side).
19. Remember that stigmation knobs and aperture knobs will not enhance the image resolution and it will only make it more stable.
20. When you get a stable image, turn the wobber and the partial field buttons off.
21. Now at this step do not touch the focus button anymore.
22. If you want for example a magnification to be 10,000x for your publication then adjust the magnification to be first 12,000 and focus and do all of the partial field, stigmation knobs, and wobber works, then when you get a clear image turn the partial field and wobber buttons off and go back to a magnification of 10,000x and take an image.
23. Adjust brightness and contrast located on the console.

Image Analysis:

1. Select work with digital images.
2. Enter the acceleration potential and the magnification.
3. Click acquire an image.
4. Right mouse button>>process>>convolute>>press smooth once.
5. Right mouse button>>properties>>display>>adjust brightness and contrast.
6. File>>save as>>your name>>information like magnification value, working distance, make and model of SEM, type of sample, etc.

Shut Down:

1. Exit the software
2. Lower the acceleration potential to zero
3. Lower Magnification to 20 using arrows
4. Close the column chamber valve
5. Press the vent button
6. Turn the N2 gas on
7. When hearing a hissing sound from the chamber door, turn the N2 gas off
8. Pull the chamber out and remove the sample from the stage using the allen key and forceps
9. Closed the chamber door and hold it closed and press evacuate until engages
10. Retrieve all necessary documents from the computer.
11. Turn off
    a. The computer
    b. The console
    c. The iXRF system box
    d. The master switch

BIOGRAPHY OF THE AUTHOR

Mubarak Mohammed Khlewee was born in Thiqar Province, Iraq. He graduated from Al Markaziyah High School in Thiqar in June 2006. In June 2011, Mubarak graduated from Southern Technical University (Engineering Technical College) in Basra Province, Iraq, with a Bachelor of Science degree in Fuel and Energy Engineering. After graduation, he worked for the geophysical company BGP located in Basra, Iraq for one year as a supervisor engineer, which specializes in seismic surveys. After that, he got employed by the Thiqar Oil Company, Iraq, in the production division, then in the custody transfer measurement department as a senior engineer where he has been working there physically and then remotely since April 2012. Mubarak traveled to Orono City, Maine State, USA, and received a Master of Science degree in chemical engineering from the University of Maine in December 2017. Mubarak joined the Chemical Engineering graduate program at the University of Maine again to pursue his Ph.D. study in September 2019. During his Master's and Ph.D. programs, Mubarak attended many symposiums and conferences and published many papers in different disciplines. Mubarak is a candidate for the Doctor of Philosophy degree in Chemical Engineering from the University of Maine in May 2023.